UNIVERSITY OF OKLAHOMA

GRADUATE COLLEGE

LIPID-BASED NANOPARTICLES FOR TISSUE REGENERATION AND CANCER PHOTOTHERMAL THERAPY

A DISSERTATION SUBMITTED TO THE GRADUATE FACULTY

In partial fulfillment of the requirements for the

Degree of

DOCTOR OF PHILOSOPHY

BY

MENGMENG ZHAI

Norman, Oklahoma

2020

Downloaded from SHAREOK. Persistent Handle URL: https://hdl.handle.net/11244/324412

LIPID-BASED NANOPARTICLES FOR TISSUE REGENERATION AND CANCER PHOTOTHERMAL THERAPY

A DISSERTATION APPROVED FOR THE

DEPARTMENT OF CHEMISTRY AND BIOCHEMISTRY

BY THE COMMITTEE CONSISTING OF

Dr. Rakhi Rajan

Dr. Wai Tak Yip

Dr. Si Wu

Dr. Roger Harrison

© Copyright by MENGMENG ZHAI 2020
All Rights Reserved.

Acknowledgment

I am so happy that I could pursue my Ph.D. degree at the best age. It seems like a movie that appears in my brain. In the past six years, I met a lot of challenges and hardness both in my research work and personal life. However, I was not alone and have been accompanied by many kind-hearted people who have supported and encouraged me to date. These experiences in the past a few years made me stronger, not only in academia but also in mind.

Firstly, I would like to thank my supervisor, Dr. Chuanbin Mao, for his guidance and support for my research work. Under his advice, I could overcome the obstacles either in my research or life to complete my projects and this dissertation. He has a big impact on me not only on the research work but also for the enthusiasm for science in my future career.

Secondly, I would like to give special thanks to my advisory committee members, Dr. Rakhi Rajan, Dr. Roger Harrison, Dr. Wai Tak Yip, and Dr. Si Wu. I am grateful for your time and valuable suggestions in my research and career. I also thank Dr. Rakhi Rajan for my new committee chair during Dr.Mao's medical leave. I also would like to thank Dr. Wai Tak Yip for his kindly help when I was working as a teaching assistant.

I also appreciate my current and former lab members in Dr.Mao's research group. They are very friendly and helpful in both my research and life. I would like to thank Dr. Binrui Cao and Dr. Penghe Qiu for their valuable research suggestions. They are very nice, patient, and knowledgeable. I also thank my former lab members, Kegan Sunderland, Lin Wang, Xuewei Qu, Wen Yang, Yan Li, and Jing Guo and current lab members, Ningyun Zhou, Liwei Zhang, Yueyi Sun, Tongmeng Jiang, Chenxin Ou, Nanzhong Deng and Haojie Xu for their help of research work.

Finally, I am extremely grateful to my parents for their continuous understanding, supports, and sacrifice during my Ph.D. years. I also thank my younger sister to help me relax from my work stress and support me to go further. She is so energetic and actively to influence me a lot by her energetics. I also thank my best friends, Mei Sun, Wentao Dai, and Pingmei Wang for their kindly help and good suggestions in my life.

Table of contents

Acknowledgment iv

Table of contents vi

List of tables ix

List of figures x

List of abbreviations xii

Abstract xiv

Chapter 1 Introduction 1

1.1 General background 1

1.2 Filamentous M13 bacteriophage 1

1.2.1 Biology and structure of phage 1

1.2.2 Phage display 3

1.2.3 Potential of the as-selected peptides in nanotechnology 4

1.3 Mesenchymal stem cells (MSCs) derived exosomes 5

1.3.1 Biology and structure of the exosomes 5

1.3.2 Exosome engineering 7

1.3.3 Applications of the engineering exosomes for delivery of therapeutic molecules 9

1.4 Fabrication of the 3D printing scaffold 12

1.4.1 3D biomaterials scaffold and properties 12

1.4.2 Applications of the 3D templated scaffold in tissue regeneration 14

1.5 Fabrication of photothermal therapy (PTT) materials 16

1.5.1 The PTT material and properties 16

1.5.2 Applications of PTT materials 18

Chapter 2: Human mesenchymal stem cell-derived exosomes enhance cell-free bone regeneration by altering the exosomal miRNAs profiles 22

2.1 Introduction 22

2.2 Materials and experiments 24

2.2.1 Cell culture, exosome isolation, identification and quantification 24

2.2.2 The osteogenesis of the hMSCs induced by the osteogenic exosomes 25

2.2.3 Immunofluorescence staining 26

2.2.4 Real-Time PCR 26

2.2.5 Alkaline phosphatase (ALP) activity and Alizarin red staining 27

2.2.6 Colocalization of the exosomes and clathrin or caveolin-1 membrane protein 27

2.2.7 Exosome next-generation sequencing (EXONGS) 28

2.2.8 Construction of the osteogenic 3D Ti-scaffold 28

2.2.9 The exosome loading and releasing behaviors of the 3D Ti-scaffold 29

2.2.10 *In vivo* evaluation of the osteogenic 3D Ti-scaffold 29

2.2.11 Statistical analysis 30

2.3 results and discussion 31

2.3.1 The identification and quantification of the exosomes derived from the hMSCs 31

2.3.2 The exosomes derived from the pre-differentiated stem cells induce the osteogenic differentiation of hMSCs *in vitro* 32

2.3.3 The cell-free 3D Ti-scaffolds with the exosomes derived from the stem cells induced the bone tissue regeneration *in vivo* 36

2.4 Mechanism for osteogenesis of hMSCs induced by osteogenic exosomes 42

2.5 Conclusion 48

2.6 Author contribution statement 51

Chapter 3: Discovery of exosome-internalizing peptides for targeted breast cancer therapy 52

3.1 Instruction 52

3.2 Methods and materials 54

3.2.1 MCF-7 cell culture 54

3.2.2 Cell culture and exosome isolation 54

3.2.3 Selection of the exosome-internalizing peptides from a Ph.D.-12 phage library 54

3.2.4 Phage capture ELISA 55

3.2.5 Phage affinity and specificity to exosome by the atomic force microscopy (AFM) 55

3.2.6 Platinum nanoparticles synthesis 56

3.2.7 Construction of the Exo-PtNPs nano complex 56

3.2.8 Characterization of PtNPs and Exo-PtNPs nano complex by Transmission electron microscopy (TEM) 56

3.2.9 Photothermal properties of the PtNPs and Exo-PtNPs nano complex by an infrared camera 57

3.2.10 Photothermal killing of the MCF-7 cell using the Exo-PtNPs nano complex 57

3.2.11 Cell viability of the MCF-7 breast cancer cells 57

3.2.12 *In vivo* study of the photothermal therapy 58

3.2.13 Organ biodistribution of the Exo-PtNPs nano complex 58

3.2.14 Statistical analysis 59

3.3 Results 61

3.3.1 Identification of exosome-internalizing peptides from a Ph.D-12 phage library by biopanning 61

3.3.2 Prepare the platinum nanoparticles loaded into tumor-homing exosome and characterize the photothermal properties of Exo-PtNPs nano complex 63

3.3.3 *In vivo* study Photothermal therapy (PTT) using the EAPW 66

3.4 Discussion and Conclusion 70

3.5 Author contribution statement 75

Reference: 76

Appendix: List of Copyrights and Permission 103

List of tables

Table 1.1: Summary of engineering exosomes for cargo delivery…….9

List of figures

Figure 1.1: The structure of the M13 bacteriophage particles……2

Figure 1.2: TEM image of M13 phage……3

Figure 1.3: The exosome biogenesis. ……6

Figure 1.4: Exosome-based drug delivery system. ……...11

Figure 1.5: Various types of 3D scaffold and their applications in tissue regeneration. ……..14

Figure 2.1: The characterization of the stem cell-derived exosomes. ……...32

Figure 2.2: Osteogenic differentiation of hMSCs by the osteogenic exosomes. ……..35

Figure 2.3: The quantitation of the Immunofluorescence staining, Gene expression, and ALP activity. ……36

Figure 2.4: SEM images of the Ti-scaffolds, hMSCs-Ti-scaffolds, and exosome-Ti-scaffolds. ..40

Figure 2.5: H&E staining and Masson's trichrome staining confirmed the new bone formation *in vivo* after 4 and 12 weeks. ……41

Figure 2.6: Toluidine Blue staining and Van Gienson staining confirmed the new bone formation *in vivo* after 4 and 12 weeks. ……42

Figure 2.7: Histological analysis of the hMSCs decorated Ti-scaffolds (a, b, e, and f) and EXO-D15 decorated Ti-scaffolds (c, d, g, and h). ……..43

Figure 2.8: Mechanism for the osteogenesis of hMSCs induced by the osteogenic exosomes….46

Figure 3.1: Identification of exosome-internalizing phage from a Ph.D.-12 phage library by biopanning. ……...…….63

Figure 3.2: Characterization of the EXO-PtNPs nano complex. ……66

Figure 3.3: Cell viability of the MCF-7 breast cancer cells before and after NIR laser irradiation.……..……69

Figure 3.4: MCF-7 breast cancer mice model constructions and organ biodistribution of EAPW…….....70

Figure 3.5: *in vivo* PTT by using EAPW. ……71

Scheme 2.1: Cell-free bone tissue regeneration by the stem cell-derived exosomes. ……31

Scheme 2.2: The possible signaling pathways for the exosome-induced osteogenic differentiation of hMSCs *in vitro* and in *vivo*. ……. 47

Scheme 3.1: The overall idea of the photothermal therapy……54

Scheme 3.2: Exosome-internalized peptide selection ……...……61

List of abbreviations

3D	three dimension
AFM	atomic force microscopy
Ag	silver
ALP	alkaline phosphatase
Au	gold
CNT	Carbon nanotubes
COL	collagen I-α1
EAPW	Exo-PtNPs nano complex
ECM	extracellular matrix
ELISA	Enzyme-linked Immune Sorbent Assay
EXO-D0	exosome derive from 0-day predifferentiated stem cells
EXO-D10	exosome derive from 10-day predifferentiated stem cells
EXO-D15	exosome derive from 15-day predifferentiated stem cells
EXO-D20	exosome derive from 20-day predifferentiated stem cells
EXO-D4	exosome derive from 4-day predifferentiated stem cells
EXONGS	Exosome next-generation sequencing
Exo-PtNPs	Exosome-platinum nanoparticles
FePt	iron Platinum
GAPDH	Glyceraldehyde 3-phosphate dehydrogenase
GO	graphene oxide
hMSCs	human mesenchymal stem cells

MHC	major histocompatibility complex
miRNA	microRNA
MVE	multivesicular endosome
MWNTs	multi-walled nanotubes
NIR	near-infrared
NP	nanoparticles
OPN	osteopontin
PBS	phosphate-buffered saline
PCR	polymerase chain reaction
Pt	platinum
PTT	photothermal therapy
QD	quantum dots
RFU	relative fluorescence intensity
Runx2	Runt related transcription factor 2
SD	Sprague Dawley
SEM	scanning electron microscope
siRNAs	small interfering RNA
ss DNA	single-strand DNA
SWNTs	single-walled nanotubes
TEM	transmission electron microscope
Ti	titanium

Abstract

Exosome, a cell budded nanovesicle in diameter around 30 nm to 200 nm, has been found useful for the gene and drug delivery in bone tissue regeneration and cancer therapy. Exosome derived from donor cells has some specific physical properties, such as stability, permeability, low toxicity, lower immune response, and biocompatibility for gene and drug delivery. In this dissertation, stem cell-derived exosomes were used to induce bone tissue regeneration *in vitro* and *in vivo*. In addition, exosomes were modified with tumor-homing peptide for target breast cancer therapy.

In chapter 2, this study confirmed that exosomes could be employed to induce osteogenic differentiation of human mesenchymal stem cells (hMSCs) and decorate 3D-printed titanium alloy scaffolds to achieve cell-free bone regeneration on a bone radial defect rat model. Specifically, the exosomes secreted by hMSCs osteogenically pre-differentiated for different periods were applied to induce the osteogenesis of hMSCs. It was discovered that pre-differentiation for 10 and 15 days led to the production of osteogenic exosomes. Then purified exosomes were loaded into the scaffolds and the current researchers found that the cell-free exosome-coated scaffolds regenerated bone tissue as efficiently as the well-reorganized hMSC-seeded exosome-free scaffolds within 12 weeks. RNA-sequencing results suggested that these osteogenic exosomes induced the osteogenic differentiation by using their upregulated osteogenic miRNA cargos (such as Hsa-miR-146a-5p, Hsa-miR-503-5p, Hsa-miR-483-3p, and Hsa-miR-129-5p) or downregulated osteogenic miRNAs cargos (such as Hsa-miR-32-5p, Hsa-miR-133a-3p, and Hsa-miR-204-5p) to activate the PI3K/Akt and MAPK signaling pathways. Consequently, identification of osteogenic exosomes secreted by pre-differentiated stem cells and the use of them to replace stem cells represent a novel cell-free bone regeneration strategy.

In Chapter 3, phage display and nanotechnology were integrated to develop novel exosome-based nanoparticles for delivering platinum nanoparticles (PtNPs), a photothermal reagent, for targeted breast cancer therapy. An exosome-internalizing peptide was first identified through a phage display technique. Then a novel nano complex (defined as the EAPW- nano complex) was developed by loading the peptide modified PtNPs into exosomes, of which the surface has been engineered to display breast cancer tumor-homing peptides. The tumor-homing peptides on exosomes led to enhanced delivery of PtNPs to the breast cancer cells *in vitro* and the tumors *in vivo,* resulting in significantly improved cancer-killing efficiency and inhibition of tumor growth.

Chapter 1 Introduction

1.1 General background

Exosomes as lipid-based nanovesicles budded from donor cells can mediate the local or intercellular communication by releasing the proteins, nucleic acids (DNAs and RNAs), and lipids into the target cells to alter the cell fate. Exosomes play a vital role in the biological and biomedicine area, such as cell proliferation and differentiation, immune regulation, tissue (cardiac, kidney, nerve, fat, bone, etc.) regeneration,[1] cancer therapy, [2] etc. Currently, hMSCs are widely applied in cell therapy and tissue regeneration due to their multipotent and abundant unique characters. HMSCs can continuously produce and secrete exosomes, which carry some of the biological cues of hMSCs, such as low immunity, multiple differentiation ability, etc. Owing to their unique properties, exosomes have been considered as a strong candidate for the diagnosis and therapy of many diseases, especially in tissue regeneration and cancer treatment.[3, 4] In this dissertation, hMSCs-derived exosomes decorated Ti-scaffolds were used for cell-free bone tissue regeneration. Besides, tumor-homing exosomes loaded with platinum nanoparticles were also developed for targeted breast cancer therapy.

1.2 Filamentous M13 bacteriophage

1.2.1 Biology and structure of phage

M13 bacteriophage is a nanofiber, which is composed of a single strand DNA (ss DNA) and wrapped with 2700 copies of the major protein, pVIII and capped with 5 copies of four minor proteins (pIII, pX, pVI, and pVII) at two ends (Figure 1.1). The pIII protein could combine with F pilus during phage infection of the bacteria. The wild type phage is about 900 nm in length and 10

nm in diameter. Inside of the phage, there is a 6407-6408 nucleotide single-strand DNA (ssDNA). The ssDNA can encode all the coating proteins, of which there are 2700 copies of major protein (pVIII) and 5 copies of each minor protein (pIII, pVI, pVII, and pIX). M13 phage belongs to non-lytic bacteriophage, so the host was not be lysed after infection, instead, the cell growth rate and division decreased. [5] Bacteriophage only infect bacteria and does not have any toxicity issue or cause an immune response to humans.[6]

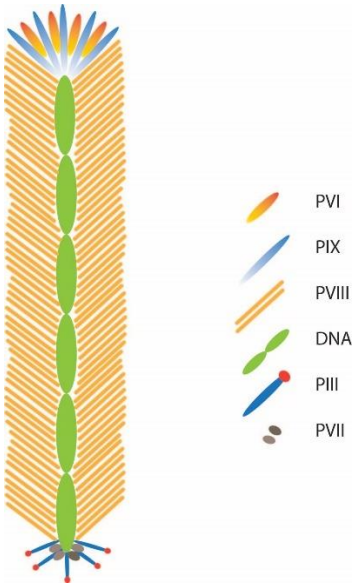


Figure 1.1 The structure of the M13 bacteriophage particles. The ssDNA is encapsulated by five different types of coating proteins (one major coating protein pVIII, and four minor coating proteins including pIII, pVI, pVII, and pIX).

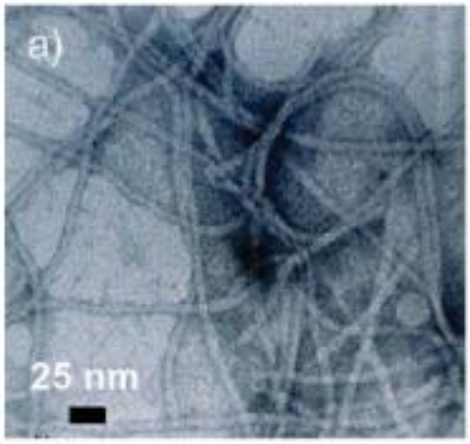


Figure1. 2 TEM image of M13 phage.[7]

1.2.2 Phage display

Phage display was invented by Gorge Smith in 1985 to display polypeptide on the surface of filamentous bacteriophage.[8] All the five coating proteins can be genetically modified through the ssDNA inside.[9] Normally, the pIII and pVIII proteins could be modified individually or together, the latter is called double display.[10] This technique allows the phage to carry out dual biological functions.

Given this specific technique, the phage display can be applied to construct the peptide displayed phage library. A phage library is composed of phage colonies, which are randomly carrying various foreign DNA on the appropriate sites of phage genome and also coated by various peptides on the outside.[11] The phage display system can be categorized into different systems by the recombinant proteins outside. It is more popular to display the foreign peptide on the pIII or pVIII proteins. For the pIII protein displayed libraries, they are widely used and commercially available in the market. Moreover, the foreign protein can be fused on all the five pIII proteins copies at the tip of the phage fiber. Similarly, the foreign protein can also be modified on the pVIII major coat

proteins. However, not all foreign peptides could be displayed on all 2700 copies of the pVIII proteins. The foreign 15-mer peptide could be displayed on up to ~300 copies of pVIII. So far, the most popular application of the phage-displayed library is the affinity selection against the target ligands or receptors. After several rounds of the affinity selection (biopanning), an as-selected peptide with the highest binding affinity were identified. [12] The selection can be conducted against many different types of targets, such as metals, semiconductors, magnetics, carbon materials, polymers, and organic compounds etc.[13-16] For the above reasons, the selected peptides can be further modified on the phage surface as a bio-template in research in the future.

1.2.3 Potential of the as-selected peptides in nanotechnology

The as-selected peptides could be conjugated with protein, polymer, and antibodies in the bioconjugate chemistry, especially in the biomedical field. It reported that the peptide could be conjugated to targets by ester chemistries, thiol-maleimide conjugation, and click methods. Currently, an updated overview indicated that the as-selected therapeutic peptide and protein can be conjugated to organic reagents and polymers by a novel molecular tool in a bioconjugation toolbox.[17] Besides, the amphiphiles based peptide was confirmed to conjugate to a biopolymer to enhance self-assemble function in the biological study. [18] The as-selected soluble peptide was also conjugated to poor water-soluble drugs for drug delivery.[19] Based on those studies, the as-selected peptide from biopanning has a high potential for conjugated chemistry and could be used for the modification of inorganic, organic and biological materials (protein and antibodies) with the active group (-NH_2, -COOH) for targeted drug delivery, tissue regeneration, etc. in the future.

1.3 Mesenchymal stem cells (MSCs) derived exosomes

1.3.1 Biology and structure of the exosomes

MSCs can be collected from various tissues, such as adipose tissue, bone marrow, cord blood, liver, etc. and have a high possibility to self-renew and multipotent differentiation capability into different cell lineage, such as mesenchymal (bone, cartilage, fat, and muscle, etc.) and non-mesenchymal cells (neuron, hepatocytes).[20-22] The MSCs are widely studied in clinical trials due to its multi-directional differentiation ability, promotion of tissue repair, and immunosuppression. Normally, the MSCs are widely used in tissue injury to replace damaged cells for tissue repair. However, the lower efficiency in differentiation and transition limits tissue regeneration. So exosomes derived from MSC are considered as a new vector to carry the biomarkers to repair the tissue, such as repairing the cardiac and kidney injuries, modulating the immune response, and tumor growth. [23]

Exosome derived from the cells is a kind of microvesicle (MV) and is about 30-200 nm in size (Figure 1.3). Exosomes are inward budded from the endosomal membranes, intracellular multivesicular body, and exocytotic released to the surroundings [24, 25]. The exosomes released into the extracellular environments contain a range of genetic information[26], including proteins, mRNA, microRNA, and DNA. Exosomes play a vital role in immune modulation and cell-to-cell communication[27]. Exosomes released from stem cells could deliver the proteins, lipid, and nucleic acid (RNAs, DNAs) to the surrounding cells and change the fate of the recipient cells[28]. When released from the cells, exosomes may interact with the recipient cells by adhering to the cell surface. Exosomes and cells communicate with each other by the lipid-ligand receptor interaction, endocytosis, or fusion of vesicles and cell membrane[29]. The genetic information, including proteins,

lipids, and nucleic acids (DNAs and RNAs) carried by the exosomes might determine the cells' fate[30]. It reported that intravenous and intracoronary MSC-conditioned medium reduce the infarct size by approximately 50% in a porcine model of myocardial ischemia and reperfusion injury[31]. It also showed that MSC-conditioned medium induces the migration and proliferation of kidney-derived epithelial cells. Under this condition, the tubule cell death diminished *in vitro*, and tubular

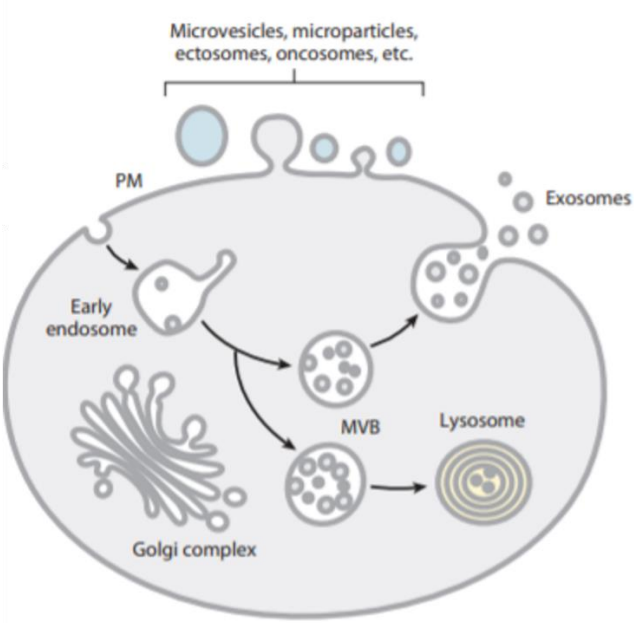


Figure 1.3 The exosome biogenesis.[32] The multivesicular body (MVBs) are formed firstly, which is includes the exosomes. The MVB further fused with the plasma membrane and release the exosome into the extracellular matrix (ECM). Exosomes contain the protein, RNAs, and lipids from the original cells.

cell survival increases *in vivo*[33]. It is said that the intravenous injection of MSC-derived exosomes increases the axonal density along the ischemic boundary cortex zone, further confirming that exosomes from MSCs could improve and contribute to neurovascular remodeling[34]. So the

biochemical cues encapsulated in the exosomes could also induce the osteogenesis of the MSC *in vitro* and bone tissue formation *in vivo*. [35]

Exosomes can be harvested from the conditioned medium of stem cells like hMSCs[36]. They can be distinguished from the microvesicles (100 nm-1 μm) by size and morphology by transmission electron microscopy (TEM) or atomic force microscopy (AFM)[37]. Stem cell-derived exosomes are less immunogenic than the cells because of the low content of membrane proteins, such as major histocompatibility complex (MHC) molecules[38]. Exosomes, as the cells' products, can be standardized and detected in terms of dose and biological activity. They keep their biological activities for a long time[39]. Small soluble molecules in the exosomes, such as lipids, proteins (cytokines, transcription factors, growth factors), nucleic acid (DNA and RNAs), are protected by the bilayer lipid and released exactly to target tissues[40].

1.3.2 Exosome engineering

A variety of cells derived from exosomes have been applied to the clinical therapeutics due to its stability, permeability, biocompatibility, and low immune reaction to the targets. Meanwhile, the study of the lipid and surface proteins are more popular and important recently. The surface marker of the exosomes, depending on the origin of the cells, plays an important role in the exosomal therapy and communication with the target cells. Moreover, it is necessary to understand the composition of the exosomes for the modification of exosome surface or cargo packaging exosomes. Normally, there are two approaches to exosome engineering: active and passive encapsulation. The different approaches lead to different loading efficiencies of the drugs inside the exosome.

For the passive loading approach, it is very simple and does not need extra chemicals or equipment to help improve this process, such as incubation with exosomes or donor cells. It proved that hydrophobic drugs can directly fuse into the exosomes by simple coincubation. [41] The main drawback of this approach is lower loading efficiency. In another approach, drugs could be incubated with the donor cells to enable the loading of the drugs in the secreted exosomes. It also reported that a low dosage of paclitaxel incubated with the SR4978 Mesenchymal stromal cells for 24 hours caused the secreted exosomes to have obvious anti-proliferative activities against the pancreatic cells.[42]

For the active loading approach, it indirectly loads the drugs by a probe, mechanical force, freezing and thaw cycles, electroporation, clicks chemistry and antibody conjugation, etc. It was reported that the mechanical force by the sonification probe could let the drugs diffuse into exosomes by deformation of the exosome membrane.[43] Fuhrmann et al. loaded the porphyrin into MDA-MB231 breast cancer cells derived exosomes by a syringe-based extruder. [44] Besides, drugs were also successfully loaded into RAW264.7 macrophages derived exosomes by freezing in liquid nitrogen and thaw at room temperature triple times.[45] However, the drug loading efficiency into exosomes by this method is low. Another research group also found that siRNAs can be loaded into exosomes by electroporation. The small siRNAs or miRNAs could be efficiently loaded into exosomes by this method companying the possibility of RNA aggregation. [46] Interesting research illustrated that hydrophilic drugs incubated with saponin can help increase the loading efficiency into exosomes up to 11-fold compared to passive loading without saponin. This means that saponin can grab the drug and communicate with the cholesterol in the exosome membrane, and then penetrate exosomes.[47] The chemical reaction, such as the click chemistry, can also help conjugate small molecules on the surface of the exosomes for drug delivery.[48] The exosome surface modification

could also be achieved by antibody combination. Higginbotham et al. had confirmed that the CD9 conjugated with Alex-647 could combine to the DiFi cells-derived exosomes because the exosomes could carry the biomarker (CD9 receptor) from the original cells.[49] Table 1 summarizes the various approaches to engineer exosomes for cargo delivery. [50]

Table 1. Summary of engineering exosomes for cargo delivery.[50]

		Advantages	Disadvantages
I) Passive loading	a) Incubation of exosomes and free drugs	Simple Do not compromise membrane integrity	Low drug loading efficiency
	b) Incubation of the donor cells with free drugs	Simple Do not compromise membrane integrity	Low drug loading efficiency Drugs may cause cytotoxicity to the donor cells
II) Active loading	a) Sonication	High drug loading efficiency	Compromise membrane integrity
	b) Extrusion	High drug loading efficiency	Compromise membrane integrity
	c) Freeze/thaw	Medium drug loading efficiency Liposome-exosome fusion	Aggregations
	d) Electroporation	Loading with large molecules such as siRNA, miRNA	Aggregations
	e) Incubation with saponin	Enhanced drug loading	Toxicity
	f) Click chemistry	Quick and efficient Better control over the conjugation site	
	g) Antibody binding	Specific and easy to operate	

1.3.3 Applications of the engineering exosomes for delivery of therapeutic molecules

Based on the good biocompatibility of exosomes, engineered exosome loaded with small therapeutic molecules, RNA, proteins, and imaging nanoparticles could be used for the therapies *in vitro* and *in vivo*.

Munagala et al. loaded chemotherapeutic and chemopreventive chemicals, such as pacilitaxel, withaferin, and doxorubicin into exosomes derived from the bovine milk by passive loading. These drugs combined or went inside the exosome by their specific hydrophobic or hydrophilic

characters (Figure 1.1). [50] It showed that the inhibitory concentration ($IC_{50}S$) of the paclitaxel-loading exosome was much lower compared to the free paclitaxel and Taxol. [51]

RNA delivery to the target, especially in the *in vivo* study, is very challenging now. It reported that RNA could be wrapped by liposomes,[52] [53] dendrimers,[54] and cationic-polymers [55] for target delivery or therapy. However, these vectors are not good candidates for the clinical application because of their safety concerns and instabilities.[56] To date, siRNAs or miRNAs could be loaded into the exosomes by electroporation. Alvarez-Erviti et al. combined the Lamp2b protein targeting and murine derived exosomes to deliver the GAPDH siRNA and BACE1 siRNA to the blood-brain barrier in mice. After these exosome treatments, the mRNA expression and beta-amyloid in the brain were suppressed significantly, compared to the lipofectamine delivery.[57] This study showed that exosomes had provided a promising method for gene and drug deliveries due to its biosafety and biocompatibility compared to the viral vector, liposomes, and other polymers.

The protein loading into exosomes was already achieved by genetic modification of the donor cells. Then the isolated exosomes were further applied onto the targets. In another way, proteins could also be loaded into exosomes either by active or passive methods as described above. It reported that the catalase loaded exosomes can efficiently inhibit the microgliosis and astrocytosis in a mouse brain. These results indicated that exosome can carry foreign proteins, such as the catalase to the brain for neuron protection *in vivo*. [41]

For the delivery of imaging molecules by exosomes, Lai et al. have engineered the exosomes derived from the human embryonic kidney 293T so that exosomes can express the Gaussian luciferase, which was integrated to a biotin receptor domain. This fluorescently conjugated exosome was also employed to track exosomes *in vivo*. [58] Recently, Oshra et al. demonstrate that Au loaded exosomes, were employed to an *in vivo* neuroimaging study to diagnose various brain

disorders. [59] In this study, AuNPs was coated by the glucose and mediated to MSCs by the glucose transporter GLUT-1.

Base on the above studies, the exosomes were modified or engineered by passive or active methods to deliver the therapeutics molecules, including RNA, proteins, and imaging nanoparticles (dye or inorganic nanoparticles, such as AuNP or PtNP), etc. Therefore, the modified and engineered exosomes or macrovesicle is more popular on cancer therapy, tissue regenerations (cardiac, kidney, and bone tissue repairing) due to its good properties.

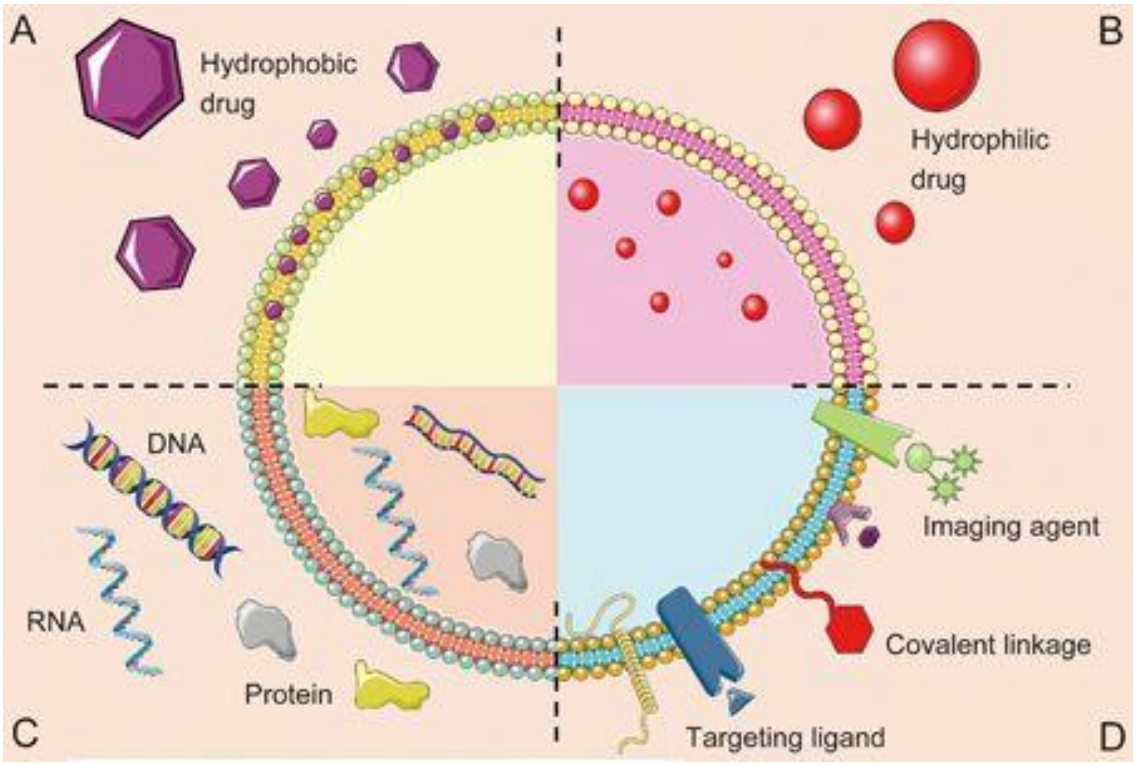


Figure 1.4. Exosome-based drug delivery system. [50] Exosomes are composed of a bilayer lipid phosphate with an aqueous core. The hydrophobic (A) or hydrophilic (B) regents could either combine to the surface or go inside the exosomes. (C) DNA, RNA, protein delivery by exosomes. (D) Imaging molecules can also be linked through targeting receptors on the exosome membrane.

1.4 Fabrication of the 3D printing scaffold

1.4.1 3D biomaterials scaffold and properties

3D biomaterials are popular to serve as scaffolds for cell attachment, proliferation, ECM regeneration and vessels, muscles, and bone tissue regeneration. The common 3D biomaterials include ceramics, polymers, metals & alloys, and their composites. According to their geometry or materials sources, they can be classified as porous scaffolds, fibrous scaffolds, microsphere/microparticles scaffolds etc.[60]

Porous scaffold

Porous scaffolds, such as a sponge, and foam could provide the pore structure for bone tissue regeneration, vessel formation, and ECM deposition. The porous structure can allow gas, cells, and nutrients to migrate thorough the channel. Ideally, the porous structure should contain 90% pores to reach up to the optimal mechanical properties. In fact, the scaffold pore size depends on the requirement of the various cells and tissue regenerations. For bone tissue regeneration, a pore size of about 200-400 μm is more effective for bone formation.[61] And a pore size around 50 - 200 μm is suitable for smooth muscle cell growth as well.[62] For the fibrous tissue regeneration, a pore size around 10 -75 μm is ideal for their migration and proliferation .[63] So the pore size can be controlled according to the requirement of tissue regeneration.

Fibrous scaffold

Fibrous scaffold, such as the Polycaprolactone (PCL),[64] polyelectrolytes (PLA),[65] poly L-lactic-co-glycolic acid (PLGA),[66] gelatin,[67] cellulose,[68] and silk fibroin,[69] are a kind of biodegradable polymers used for the tissue regeneration of skin, cartilage, bone, muscle, vein and can also be employed as vectors for DNA, protein and gene delivery.[70] It is discovered that the aligned poly-

L-lactide (PLLA) scaffold can enhance the endogenic differentiation of the MSCs, compared to the osteogenic induction of the random fibers.[71] However, these fibrous scaffold lacks some mechanical and physicochemical properties for tissue regeneration.

Microsphere scaffold

Microsphere scaffolds are usually used to deliver the drug, gene, and growth factors in the advanced biomedical applications. It is found that the polyurethane scaffold loaded with lovastatin microparticles can release the lovastatin to enhance the BMP-2 expression in the osteoblast cells for two weeks.[72] Another research group loaded BMP-2 growth factors on the PLGA scaffold and VEGF (vascular endothelial growth factors) onto a poly(propylene fumarate) (PPF) scaffold to induce bone tissue formation and blood vessel formation in a rat bone model *in vivo*.[73] Normally, this kind of scaffold was used in the advanced application and site-specific targeting therapies by delivering the gene, proteins, growth factors, etc. bone therapeutic molecules.

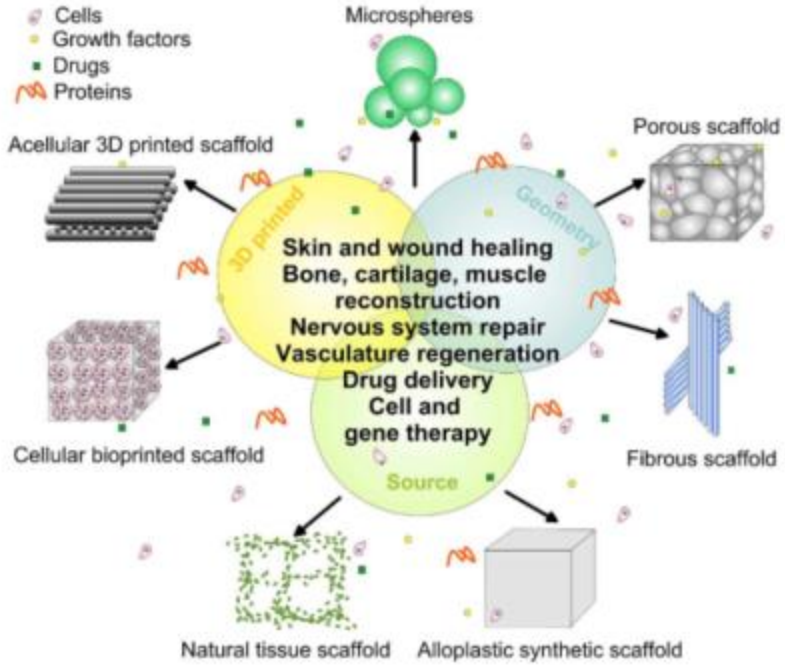


Figure 1.5 Various types of 3D scaffold and their applications in tissue regeneration.[74]

1.4.2 Applications of the 3D templated scaffold in tissue regeneration

Recently, more and more patients with bone defects in the US require bone grafts, and most of them receive surgical implantation due to various clinical diseases such as bone infections, bone tumors, and bone trauma[75]. Traditional therapies for bone defects include autografts, allografts, and xenografts[76]. However, these therapies have their limitations. For the autografts, the donor source is always limited and mismatches with the defect sites. For the allografts and xenografts, they have the risks of disease transmission and immune rejection[77]. Therefore, bone tissue engineering is considered a promising method where a 3D scaffold including the biochemical and physical cues is implanted into the bone defective to induce bone tissue regeneration. The metallic 3D scaffold is the most popular candidate for the loading-bearing bone tissue regeneration compared to the ceramics, or polymers owing to their high mechanical strength, resistance, and

printing possibilities. Titanium foam mimics the bone structure to induce bone formation successfully by their permeabilities and porosity properties.[78] Meanwhile, using variable pore size polymer materials could help to create the optimal scaffold stiffness from 4 kN/mm to 7.1 kN/mm.[67] Furthermore, 3D printed titanium scaffold is confirmed to have good biocompatibility and osteointegration capability and it has the similar induction performance of the polyester ether ketone materials.[79] The porous Mg scaffolds are also promising for bone formation because of its good mechanical properties and biodegradability.[80]

For ceramic biomaterials, it is composed of calcium and phosphate salts that can promote bone tissue formation and induce osteogenic differentiation. All the non-absorbable, bioactive, and resorbable ceramics are brittle but also has good compression and corrosion resistance. β-tricalcium phosphate, hydroxyapatite, and bioactive glass are also common biomaterials for a 3D scaffold for bone tissue formation.[81] Interestingly, the mesoporous silica-based particle treated ceramic bone could help improve the biodegradation of the materials and induce bone formation at the same time.[82]

Polymer materials are also widely employed for tissue regeneration due to their good biocompatibility, reproducibility, physical properties, and low price. Some acrylic polymers such as Polymethylmethacrylate (PMMA), *N*-(2-Hydroxypropyl) methacrylamide (PHPMA),[83 84] and conductive polymer,[85] are considered as good candidates for implantation due to the biodegradability. It reported that a two-part self-polymerizing PMMA was the most popular material in orthopedic surgery, such as joint replacement.[86]

In conclusion, the requirements for tissue engineering scaffolds are dependent on their specific purposes and applications. Moreover, some general characters and properties are needed to be considered to fulfill a serious of the requirement's as followed. i) materials are biocompatible; ii)

scaffold is biodegradable. The degradation rates are adjustable, and non-toxic or harmful after implantation. iii) scaffolds own good mechanical and strength to support the bone with the highly resistant and loading properties. iv) optimal porosity for cell migration and proliferation; v) high surface/volume for cell attachment. The scaffolds with the above properties would be a considerable candidate for the implanted bone defect tissue regeneration in the next.

1.5 Fabrication of photothermal therapy (PTT) materials

Photothermal therapy is a kind of photo-based therapy, which concert near-infrared light (NIR) (800-1000 nm) to heat (42 ^{o}C) to induce cell apoptosis or tissue necrosis by increasing ROS response in cells without any damage of the skin and organs in the subject.[87] Therefore, an optimal PTT material is the key for a succeeded PTT on cancer therapy. Also, PTT is an ideal therapy for the ablation of tumors by decreasing the skin and organ damage in the future.

1.5.1 The PTT material and properties

Hyperthermia is a kind of disease that is caused by a virus or bacterial infection. Hyperthermia has been employed as a treatment for diseases for a long time. Currently, hyperthermia is applied for wound healing, analgesic, drug delivery, or tumor removal by light ablation. Hyperthermia therapy can be classified as two types: 1) mild hyperthermia, the temperature is lower than 44 ^{o}C and no necrosis happens. 2) thermal ablation, cell apoptosis will happen under this condition since the temperature will rise above 45 ^{o}C. Usually, the heat can be generated by radiology, ultrasound, and near-infrared light. [88, 89] NIR light (800-1000nm) has much greater tissue transparency without causing damage to normal tissue. Therefore, PTT materials inside of tumors or tissues can absorb the NIR light to generate heat to induce cell apoptosis and tumor inhibition locally. There are

several PTT materials for photothermal therapies, such as metal nanoparticles, inorganic, and organic nanomaterials, etc.

Inorganic materials: including metal nanoparticles and carbon tubes

The noble metal materials, such as silver (Ag), gold (Au), quantum dots (QDs), and platinum (Pt) nanoparticles are considered as good PTT materials because of their good absorption, which is about 4-5 fold higher compared to other conventional molecular PTT materials. [90] Jena et al. had confirmed that chitosan-coated AgNPs have antibacterial properties by PTT but cause cell toxicity as well.[91] Therefore, the toxicity of the AgNPs to cells has limited their application. Furthermore, Ag was also combined with Au and constructed as nanoshell, nanorod, nanocages, and bimetallic particles. [92-96] Cheng et al. confirmed that silica-Au nanoshell was more efficient among three Au related nanomaterials, such as silica-Au nanoshell, hollow Au/Ag nanosphere and Au nanorods, during the photothermal therapies.[95] [95] Gold nanoparticles, such as nanospheres, [97] hollow and solid nanoshells, [98] nanorods,[99] nanostars,[100] nanocubes[101], etc., were the most popularly studied metallic nanoparticles for PTT. It was confirmed that cytoplasm targeting the Au nanosphere was more efficient in PTT compared to the nuclear targeting Au nanosphere by laser irradiation.[102] It was also proven that Pd nanoparticles have a significantly higher photothermal stability compared to Ag and Au because of its higher melting point.[103] However, the optical absorption of Pd nanoparticles mainly falls around the UV/visible region instead of the NIR. Chen et al. have reported that the Folic coated FePt nanoparticles can enhance the photothermal therapy efficacy in the EMT-6 breast cancer cells.[104] Recently, it was confirmed that the QDs could generate free charges by surface plasmon resonance (SPR) and could be also be applied to the PTT.[105] Besides, graphene oxide (GO) was also another good candidate for the PTT since GO had absorbance from UV to the NIR region. And GO had been applied to an *in vivo* study for the ablation of the tumor.[106]

Carbon nanotubes (CNT), such as single-walled nanotubes (SWNTs) and multi-walled nanotubes (MWNTs), have strong optical absorption and heat energy conversion around the NIR region when applied for PTT. It also reported that the specifically modified CNT could load drugs, like Dox, and deliver drugs to the tumor for PTT.[107]

Organ materials

The organic-based nanomaterials, such as the organic dye-based or polymer-based materials, can be utilized to convert NIR to heat kill cancer cells *in vitro* and *in vivo*. [108] The cyanine derives as a kind of organic compound are widely employed for fluorescent imaging and PTT recently by the irradiation of the NIR.[109, 110] Other organic material, porphyrin, and its derivatives were also employed in the PTT in cancer therapy.[111] Zheng et al. constructed a lipid-based nanoparticle called "porphysomes" by the porphyrin lipids. These materials can absorb and convert NIR to heat efficiently. Tumor inhibition was also confirmed by using porphysomes with the irradiation of NIR.[112]Also, the polymer-based nanomaterials conjugated with other molecules were widely employed in biomedicine, like cancer therapy. Yang et al. reported a novel conjugated polymer nanoparticle for photothermal cancer therapy. In their study, polyaniline based nanoparticles were applied for tumor inhibition *in vitro* and *in vivo*. [113]

1.5.2 Applications of PTT materials

Tumor imaging

The organic dye-based nanomaterials are the most common and promising clinical agents for tumor imaging. The organic dyes can be conjugated with tumor-targeting agents (such as small molecular, peptides, proteins, and antibodies) for targeted tumor imaging with NIR irradiation. The newly developed NIR dyes like the Cyanine dyes,[114] squaranine derivatives,[115]

Phthalocyanines and porphyrin derivatives,[116] borondipyrromethane dyes, [117] were more active in the NIR light region and have been applied in the biomedical application for tumor detection and imaging. For these dyes, they have intensive fluorescence intensity and half lifetime. Some of them have been improved to disperse into the water to avoid aggregation in tissue. These organic materials are promising agents for biomedical imaging.

Photothermal therapy

Metal nanoparticles, including gold nanoparticles, gold nanorods, gold nanoshells, [118] gold nanocages,[119] platinum nanoparticles[120, 121] and organic nanoparticles, including graphene oxide,[118] carbon-based nanotubes, SWNT[122] can be directly introduced into cancer tissues for PTT through enhanced permeability and retention (EPR) effect. Alternatively, they could be modified by tumor-targeting ligands (peptides, proteins, peptide ligands, etc.) for enhanced efficiency. During the synthesis procedure, the shape and size of the nanoparticles can be controlled to achieve optimal delivery efficiency into tumors. In addition, the surface of the nanoparticles can also be modified by tumor-targeting ligands for targeted tissue binding. [123] Similarly, platinum nanoparticles combined with other metals were employed to multifunctional imaging and photothermal therapy in the detection and ablation of breast cancer therapy *in vivo*.

Consequently, requirements for the PTT materials are dependent on their specific purposes and applications. Also, some general PTT material's properties need to identify as followed. i) optimal optical properties in the range of 800 nm-1000 nm; ii) non-toxic or harmful to the cells or tissues; iii) surface modifiable for the targeting therapy; v) optimal size for loading or targeting for the further research. PTT materials with the above properties are a considerable candidate for photothermal cancer therapy in the future.

In conclusion, exosomes derived from the stem cells are a very good candidate for tissue regeneration, including cardiac and kidney repairing, and cancer therapy, including chemotherapy and photothermal therapy due to its good biocompatibility, low immune reaction, stability, and permeability.

Based on tissue regeneration related backgrounds, a **hypothesis** is described that **exosomes derived from the stem cells could induce the osteogenesis of hMSCs *in vitro* and promote bone tissue regeneration *in vivo* by implantation of an exosome-Ti scaffold.** This hypothesis is based on the following observation. First, MSCs-derived exosomes could induce osteogenic differentiation of stem cells depending on altered osteogenic exosomal microRNA profiles *in vivo,* in which the exosomes were derived from the MSCs at different differentiated stage. [124] Second, Titanium foam mimics the bone structure to induce bone formation successfully by their permeabilities and porosity properties.[125] Moreover, a 3D printed titanium scaffold is confirmed to have good biocompatibility and osteointegration capability and it also has a similar induction performance of the polyester ether ketone material..[126] To test this hypothesis, four specific aims were carried out: i) Identification and quantification of osteogenic exosomes derive from pre-differentiated stem cells. ii) Evaluation of the osteogenic differentiation of hMSCs *in vitro* in the absence of osteogenic supplements. iii) Evaluation of *in vivo* bone tissue regeneration by exosome-coated titanium scaffold in the absence of seeded stem cells. iv) Mechanism exploration of osteogenic exosomes in osteogenesis of the hMSCs *in vitro* and bone tissue regeneration *in vivo*. All the proposed objectives for this work have been achieved and are described in Chapter 2.

Breast cancer therapy is always challenging in malignant tumor therapeutics. Based on previous studies described in Chapter 1, section 1.5, a **hypothesis** is described that **tumor-homing exosomes loaded with ultra-small PtNPs could kill breast cancer cells *in vitro* and inhibit the**

tumor growth *in vivo* when exposed to NIR laser. This hypothesis is based on the following studies. First, Exosomes derived from bovine milk can carry chemotherapeutic chemicals, including paclitaxel and doxorubicin to cancer cells for cells' apoptosis. [127] Another study reported that 12 nm FePtNPs in a cubic shape could induce the necrosis of cancer cells, which is similar to the effect of Au nanorods (40 nm) after NIR irradiation.[128] Here, three specific aims were carried out to test his hypothesis. i) Identification of exosome-internalizing peptides from a Ph.D.-12 phage library by biopanning. ii) Evaluation of photothermal properties for all developed Exo-PtNPs nano complex in aqueous solutions. iii) Evaluation of breast cancer cells (MCF-7)-killing and tumor inhibition efficiency of Exo-PtNPs *in vitro* and *in vivo* with NIR laser irradiation. The first two objectives for this work have been achieved and described in Chapter 3. Animal study for this work has just finished the pre-test stage, and it showed promises for PPT therapy by Exo-PtNPs nano complexes.

Chapter 2: Human mesenchymal stem cell-derived exosomes enhance cell-free bone regeneration by altering the exosomal miRNAs profiles

2.1 Introduction

Bone defects can be caused by various clinical diseases such as bone infections, bone tumor, skeletal abnormalities, congenital malformation, fractures, avascular necrosis, atrophic non-unions, osteoporosis, and bone trauma.[129] They are traditionally treated with autografts, allografts, and xenografts.[77] However, these therapies have their own limitations. For the autografts, they are limited to donor sources and mismatched with the defect sites. For the allografts and xenografts, they have the risks of disease transmission and immune rejection.[130] Meanwhile, the implantation of the stem cells, such as the human mesenchymal stem cells (hMSCs)[131] and human adipose-derived stem cells,[131] are considered an alternative strategy. However, implantation of stem cells faces significant challenges, including immune rejection,[132] teratoma formation,[133] and undirected cell differentiation.[134, 135] When seeded with the stem cells before implantation, the 3D scaffolds may cause immune rejection,[136] induce teratoma formation,[137] and lead to undirected cell differentiation.[138] Therefore, bone regeneration without the use of externally seeded stem cells, termed cell-free regeneration, is a promising approach to solving these cell-derived problems. Indeed, implantation of cell-free scaffolds for cell-free bone tissue regeneration[139] has developed as a promising strategy to avoid these problems. [139 140 141]

To achieve cell-free tissue regeneration, the cell-free 3D scaffolds should bear biochemical and physical cues that can induce osteogenesis.[142] One of the possible biochemical cues is the exosomes secreted by donor cells, which are nanoparticles (30-200 nm) with lipid-bilayers encapsulating signaling cargoes such as miRNAs.[26] Stem cell-derived exosomes are less immunogenic than stem cells themselves because exosomes contain a low amount of membrane

proteins (e.g., major histocompatibility complex, MHC).[143] The exosomes can keep their biological activities for a long time.[144] Small soluble molecules in the exosomes, including miRNAs, growth factors, cytokines, and transcription factors, are protected by the lipid bilayer and can be released to target tissues.[145] Since the exosomes contain a range of genetic information,[27] like miRNAs, they can direct immune modulation and cell-to-cell communication.[28] Finally, when released from the cells, exosomes can have interactions with the recipient cells by adhering to their surface and communicate with them by the lipid-ligand interactions, endocytosis, or fusion with the cell membrane.[30]

Since MSCs will secret exosomes into the culture medium, MSC-conditioned medium will contain exosomes. This might explain the reported findings that MSC-conditioned medium could be used to promote tissue regeneration. For example, MSC-conditioned medium could decrease the infarct size to treat myocardial ischemia.[33] Such medium enhanced the migration and proliferation of kidney-derived epithelial cells and increased the survival of the tubular cells *in vivo*.[34] Intravenous injection of MSC-derived exosomes promoted neurovascular remodeling.[146] These findings indicate that the biochemical cues encapsulated in the exosomes might also induce the osteogenesis *in vitro* and *in vivo*. Therefore, a hypothesis is described that exosomes derived from the stem cells could induce the osteogenesis of hMSCs *in vitro* and promote the bone tissue regeneration *in vivo* by an exosome-Ti scaffold post-implantation.

In this work, osteogenic exosomes secreted from hMSCs were identified and used to decorate 3D printed titanium alloy scaffolds (Ti-scaffolds) to achieve cell-free bone regeneration (**Scheme 2.1**). Specifically, the exosomes derived from the hMSCs pre-differentiated in osteogenic differentiation medium for 0, 4, 10, 15 and 20 days (termed EXO-D0, EXO-D4, EXO-D10, EXO-D15, and EXO-D20, respectively) were employed to identify the exosomes that could induce the

osteogenic differentiation of hMSCs into osteoblasts *in vitro*. Then cell-free 3D printed Ti-scaffolds with the osteogenic exosomes were filled to achieve cell-free bone regeneration. Ti-scaffolds were used to support the exosomes because Ti is biocompatible, does not elicit immune reaction with the tissue,[147 148] and supports the attachment of bone cells and the mineralized bone matrix without any interposition.[147] In addition, Ti-scaffolds have desired properties, including the uniform structure, strength, lower stiffness, higher porosity, corrosion resistance, and higher coefficient friction.[149]

Real-time PCR, immunofluorescence staining, Alizarin Red Staining, and alkaline phosphatase (ALP) activity were used to confirm the osteogenesis of the hMSCs under the induction of hMSC-derived exosomes. The cell-free 3D Ti-scaffolds were also applied to induce bone tissue regeneration for 4 weeks and 12 weeks *in vivo*. It was found that the exosomes (EXO-D10 and EXO-D15) carried the differentiation-inducing miRNAs (like Hsa-miR-146a-5p, Hsa-miR-503-5p, Hsa-miR-483-3p, Hsa-miR-129-5p and Hsa-miR-32-5p, Hsa-miR-133a-3p and Hsa-miR-204-5p) and thus could promote the osteogenic differentiation of the hMSCs *in vitro* and enable the cell-free Ti-scaffolds to achieve bone tissue regeneration *in vivo* by activating of PI3K/Akt and MAPK signaling pathway. Thus, the exosomes from the osteogenically pre-differentiated hMSCs are inducers for the cell-free bone tissue regeneration.

2.2 Materials and experiments

2.2.1 Cell culture, exosome isolation, identification and quantification

The hMSCs were obtained from the Lonza group Ltd (Lonza, Morristown, NJ, USA). Cells after fewer than 5 passages were maintained in a humidified atmosphere containing 5% CO_2 at 37 ^oC in the Mesenchymal stem cell growth medium Bulletkit (Lonza, Morristown, NJ, USA). hMSCs

were pre-differentiated for 4 days, 10 days, 15 days, and 20 days, respectively, by the hMSC Osteogenic BulletKit (Lonza, Morristown, NJ, USA), and exosomes were isolated and termed EXO-D0, EXO-D4, EXO-D10, EXO-D15, and EXO-D20, respectively. After pre-differentiation, the osteogenic hMSCs were cultured in the hMSCs Basal Medium (Lonza, Morristown, NJ, USA) in the presence of the osteogenic exosomes. Exosomes were isolated by the ExoQuick-TC kit (System Bioscience, Palo Alto, CA, USA) and were resuspended into the 1X PBS. The isolated exosomes were also quantified by the EXOCET Exosome Quantitation kit (System Bioscience, Palo Alto, CA, USA). The exosomes were also identified and qualified by the Atomic force microscopy (AFM), Transmission electron microscopy (TEM), and NanosightNS300 (Piscataway, NJ, US), (Zeiss Neon 40 EsB, NY, USA), respectively. The isolated exosomes were quantified by the EXOCET Exosome Quantitation kit (System Bioscience, Palo Alto, CA, USA). For the EXOCET exosome quantification kit, it is based on the activity on Acetyl-CoA Acetylcholinesterase (AChE),[150 151] which is a kind of enzyme enriched in the most kind of the exosomes. The included calibration standard was able to calculate the standard curve (FS1). It is an easy and quick colorimetric assay. The procedure for the colorimetric assay as following: 20 μL exosome was lysate by the 80 μL lysis buffer, and incubated at 37 ^{0}C to liberate exosome proteins. Those proteins were prepared with the Buffer A and B, which are provided by the SBI company for the colorimetric assay at 405 nm using a spectrophotometric plate reader.

2.2.2 The osteogenesis of the hMSCs induced by the osteogenic exosomes

The hMSCs, is in 60% confluency were cultured in the hMSCs Basal Medium (Lonza, Morristown, NJ, USA) in the presence of the osteogenic exosomes (EXO-D4, EXO-D10, EXO-D15, and EXO-D20) for another 20 days. During this time, 100 μL of the 1.0 x 10^{8} osteogenic exosomes were added into the exosome-free medium to the hMSCs, which is seeded into the 24-

well plates for the induction of the osteogenesis of the hMSCs. The above medium was changed every two days.

2.2.3 Immunofluorescence staining

The hMSCs induced by EXO-D0, EXO-D4, EXO-D10, EXO-D15, and EXO-D20, respectively for 20 days were fixed by the 4% PFA at room temperature for 30 min. After the cell membrane was permeabilized by the 0.3 % Triton X-100 for 8 min, osteopontin (OPN) and collagen 1 (COL-1) were immunostained using the corresponding antibody. After the cells were blocked by the 5% BSA, OPN and COL-1 were further labeled with the secondary antibody conjugated with the tetramethylrhodamine-5-isothiocyanate (TRITC) (Abcam, Cambridge, MA, USA). FITC-labeled phalloidin (green) and DAPI (4',6-diamidino-2-phenylindole) (blue) were used to stain the actin filament and nuclei, respectively. The cells were then imaged by immunofluorescence microscopy. The quantity of the immunofluorescence staining was calculated by the Image J. And the relative fluorescence intensity (RFU)= Integrated density- (Area of selected cell * Mean fluorescence of background readings).

2.2.4 Real-Time PCR

The real-time PCR was used to analyze the osteo-specific genes (Alkaline Phosphatase (*ALP*), Runt related transcription factor 2 (*Runx2*), *OPN*) and osteo-non-specific genes (*COL-1*). The Glyceraldehyde 3-phosphate dehydrogenase (*GAPDH*) was used as a reference gene. Cells were collected on the ice, and real-time PCR was performed by Ambion Power SYBR Green cells-to-Ct Kit (Invitrogen, US). The template cDNA was amplified by genetic primers of *ALP*, *Runx2*, *OPN*, *COL-1* and *GAPDH*. The primer sequences are listed as follows. *ALP*: Forward primer: 5'-CAACCCTGGGGAGGAGAC-3', Reverse primer: 5'-GCATTGGTGTTGTACGTCTTG-3';[152] *Runx2*: Forward primer: 5'-CCAGATGGGACTGTGGTTACC-3', Reverse primer: 5'-

ACTTGGTGCAGAGTTCAGGG-3';[153] *OPN*: Forward primer: 5'-GACGGCCGAGGTGATAGCTT-3', Reverse primer: 5'-CATGGCTGGTCTTCCCGTTGC-3';[154] *COL-1*: Forward primer: 5'-GACGGCCGAGGTGATAGCTT-3', Reverse primer: 5'-CATGGCTGGTCTTCCCGTTGC-3'. [154] *GAPDH:* Forward primer 5'-CATGTTCGTCATGGGGTGAACCA-3', Reverse primer: 5'-AGTGATGGCATGGACTGTGGTCAT-3'.[155] The real-time PCR was performed under the following procedure: initially denatured at 95 °C for 5 min, followed by 45 cycles of PCR (95 °C for 30 s, 58 °C for 30 s and 72 °C for 45 s).

2.2.5 Alkaline phosphatase (ALP) activity and Alizarin red staining

Cells were tested for the ALP activity and calcium nodule staining (Alizarin red staining) after 20 days of incubation with the osteogenic exosomes (EXO-D0, EXO-D4, EXO-D10, EXO-D15, and EXO-D20), respectively. ALP activity was evaluated by the ρ-Nitrophenyl phosphate (pNPP) assay. Briefly, pNPP (Invitrogen, Waltham, MA, USA) was used as a substrate for the ALP activity analysis where the ALP was hydrolyzed to form a soluble yellow solution at 37 °C. The staining reaction was terminated by adding 3 M NaOH and the absorbance was read at 405 nm. For the alizarin red staining, cells were firstly fixed by the 4% PFA at 4 °C for 15 min and stained with 0.2% alizarin red for 15 min. The staining images were captured by the optical microscope.

2.2.6 Colocalization of the exosomes and clathrin or caveolin-1 membrane protein

The hMSCs were incubated with the osteogenic exosomes labeled with the Exo-Green (System Bioscience, Palo Alto, CA, USA) for 4 hours. Meanwhile, the 2mM RGD-peptide blocked hMSCs and exosomes-Green were also incubated together for 4 hrs. Cells were rinsed and fixed by 4% PFA for 30 min. They were subsequently permeabilized using 0.3 % Triton X-100 for 8 min, followed by blocking with the 5% BSA for 1 h. After blocking, the clathrin (Abcam) and caveolin-

1(Abcam) antibody were applied to the fixed cell at 4 ^{o}C overnight, respectively. The secondary antibody conjugated with the TRITC was used for labeling the clathrin and caveolin-1 for 1 h. The images were captured using confocal microscopy (Leica SP8 Upright CLS/multiphoton/FLIM microscope, Rockland, MA, USA).

2.2.7 Exosome next-generation sequencing (EXONGS)

The exosomes were isolated from the different culture mediums (hMSCs pre-differentiated for 4, 10, 15, and 20 days, respectively) by following the commercial protocol by the System Bioscience. Then the next generation sequencing (System Bioscience, Palo Alto, CA, USA) was applied to track the miRNA expression. The raw fastq data quality was checked by the FASTQC, meanwhile, the adaptor was removed to trim quality bases by the Trimmomatic. The leading and trailing ambiguous or low-quality bases, which are below Phred quality scores of 3, were also removed after adapter clipping. The miRNA read counting was detected by the Chimirra and the miRNA expressions were normalized by the trimmed mean of M-values (TMM). The edgeR program was further used to identify the differentially expressed genes. The fold change of the gene expression of more than 1.5 was defined as the differentially expressed. The miRNA target gene prediction was detected by the IPA and the clusterProfile R was also performed to do the GO and pathway enrichment analysis.

2.2.8 Construction of the osteogenic 3D Ti-scaffold

The Ti-scaffolds (8 mm in length, and 3 mm in diameter), 3D-printed from Ti6Al4V powder, were firstly autoclaved and then cooled to the room temperature. The poly-L-lysine was coated on the 3D Ti-scaffolds by incubating the scaffolds in a solution of poly-L-lysine overnight before exosome coating. The exosomes (EXO-D0, EXO-D4, EXO-D10, and EXO-D15) were seeded

onto the Ti-scaffold overnight at 4 ^{0}C. The osteogenic exosomes attached on the surface were confirmed by the SEM (Zeiss Neon 40 ESB, NY, USA).

2.2.9 The exosome loading and releasing behaviors of the 3D Ti-scaffold

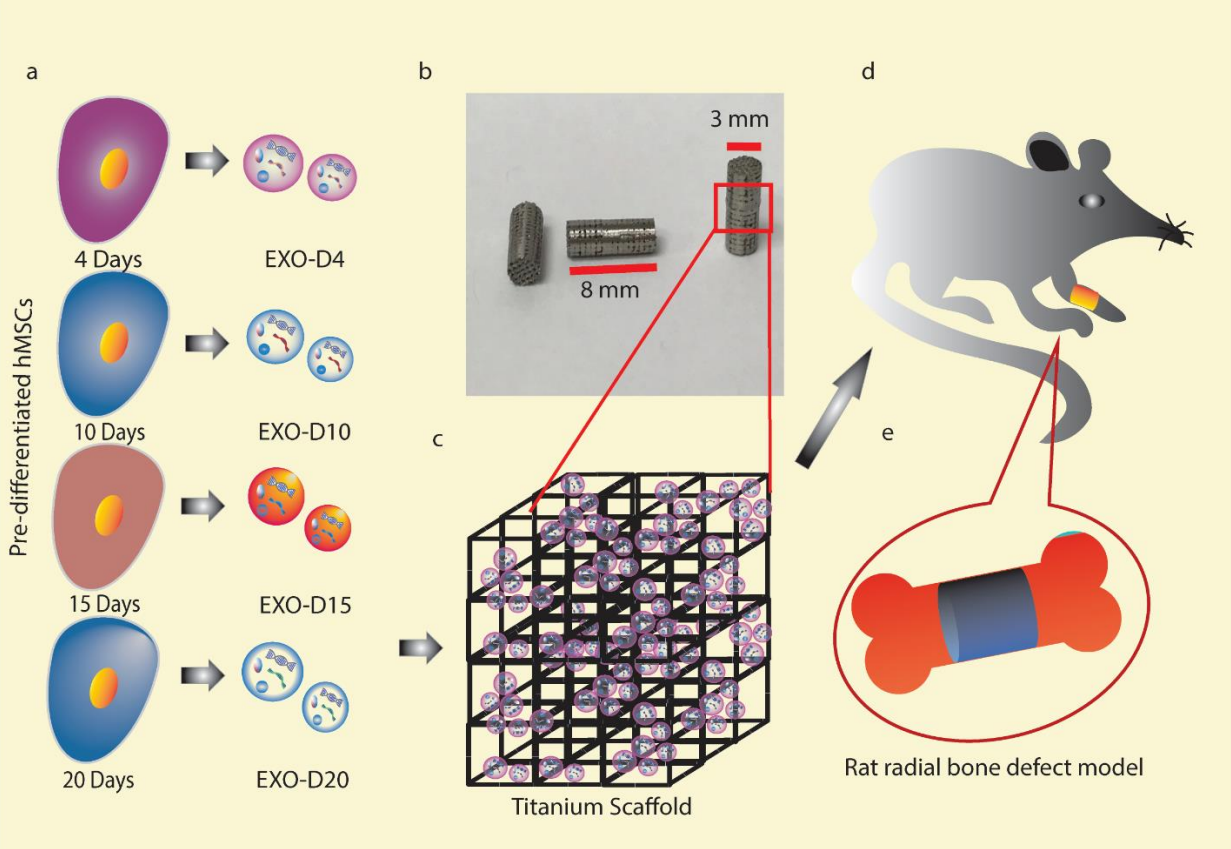
The 3.99 x10^{9} exosomes were incubated with the poly-L-lysine coated 3D Ti-scaffolds for 12 hrs and 24 hrs, respectively, at 4 ^{0}C. The loading efficiency %= the # of the exosomes loaded to the 3D Ti-scaffolds (# of initial exosomes-# of rest of exosomes)/ the # of initial exosomes * 100%. The exosomes releasing from the 3D Ti-scaffolds performed at the basal medium, pH=7.4, 37 ^{0}C at 1, 2, 3, 5, 7, 12, 24, and 48 hrs. The exosome releasing efficiency %= # of exosomes in the supernatant/ # of exosomes loaded into the 3D Ti-scaffolds * 100%.

2.2.10 *In vivo* evaluation of the osteogenic 3D Ti-scaffold

The male 5-6 weeks old Sprague Dawley (SD) rats (Harlan, ~125 g) were randomly separated into 7 groups (n=5), including healthy group, negative group, EXO-D0, EXO-D4, EXO-D10, EXO-D15, and hMSCs cell-seeded group. The SD rats were anesthetized with the isoflurane, and a segmental defect about 8 mm was created. The exosome seeded 3D Ti-scaffold and its positive/negative control was loaded into the defect zone. The blank control was also created without loading any implantation. The animals were sacrificed to evaluate the bone tissue regeneration using the hematoxylin and eosin (H&E), Masson's Trichrome, Toluidine blue, and Van Gieson staining. The osteogenic 3D-Ti scaffolds were collected from the rats 4 and 12 weeks post-implantation, respectively, put into 10% fresh formalin solution and immersed for 1 day. The fixed 3D-Ti scaffolds were encapsulated by a paraffin block. After that, the implanted scaffolds were sectioned into 4-μm-thick slices and placed onto the glass slides. After deparaffinated, these slices were stained with H&E, Masson's Trichrome, Toluidine blue, and Van Gieson, and then imaged.

2.2.11 Statistical analysis

The data were presented as the mean ± standard deviation. They were analyzed by the one-way ANOVA with Tukey's post-hoc test using SPSS21 (IBM, USA) with $p<0.05$ showing the significant difference.



Scheme 2.1. Cell-free bone tissue regeneration by the stem cell-derived exosomes. a. Exosomes were isolated from the pre-differentiated hMSCs induced by the osteogenic medium for 4, 10, 15, 20 days, respectively. Osteogenic differentiation was tested to identify the exosomes that could induce the osteogenic differentiation of hMSCs. b, Representative structure, and morphology of Ti-scaffolds (8 mm in length and 3 mm in diameter). c-e. Osteogenic exosomes were seeded into the Ti-scaffolds, which were then implanted into the rat radial bone defect model (d and e) for 4 and 12 weeks, respectively.

2.3 results and discussion

2.3.1 The identification and quantification of the exosomes derived from the hMSCs

The exosomes secreted by the pre-differentiated hMSCs were found to be indeed nearly spherical nanoparticles around 143.0 ± 9.3 nm by the NanosightNS300 (Figure 2.1c), consistent with the observations by AFM and TEM (Figure 2.1a-b). Their concentrations were determined to be as high as ~ 4.0 x10^9 particles/ μL (Figure 2.1d) for EXO-D0, EXO-D4, EXO-D10, EXO-D15, and EXO-D20. The exosomal protein marker CD63 was also detected by the western blot (Figure 2.1e).

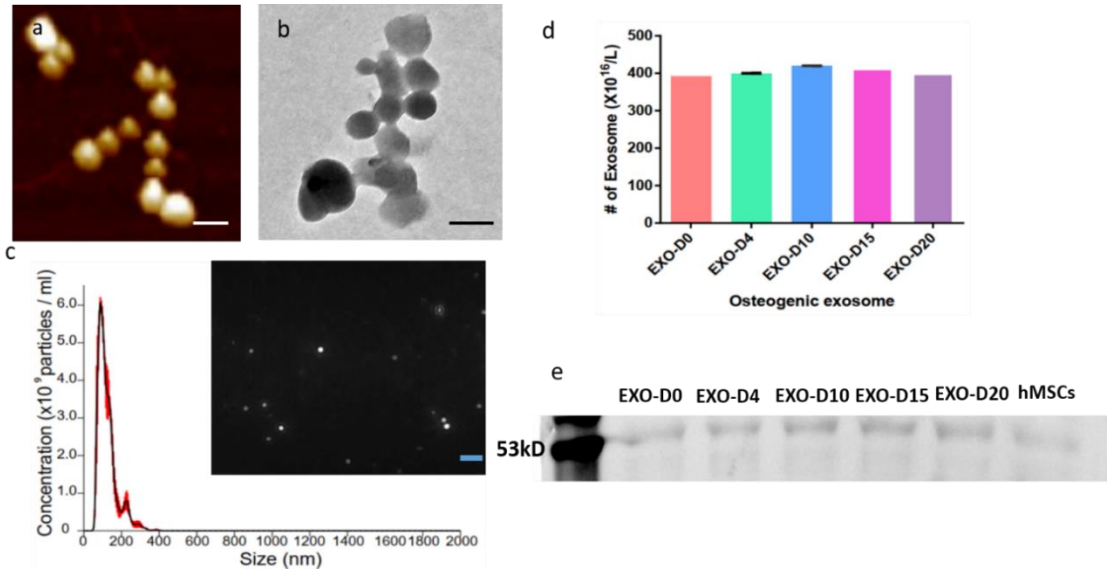


Figure 2.1 The characterization of the stem cell-derived exosomes. (a-b) AFM (a) and TEM (b) showing the size and morphology of the exosomes derived from hMSCs. Scale bar: 200 nm. (c) The size and concentration of the hMSCs-derived exosomes by the NanosightNS300. The inset is an image showing the snapshot of video tracking. Scale bar:800 nm. (d) The concentration of exosomes (derived from the pre-differentiated hMSCs on Day 0, Day 4, Day 10, Day 15, and Day 20, respectively) determined by the ExoQuick-TC kit**.** (e) The Western blot analysis of the exosome derived from the pre-differentiated hMSCs and hMSCs. 20 μg of the exosome proteins were loaded into the lane. All of the exosome's specific anti-CD63 primary antibody was used.

2.3.2 The exosomes derived from the pre-differentiated stem cells induce the osteogenic differentiation of hMSCs *in vitro*

To evaluate the osteogenic performance of the exosomes, the osteogenic exosomes were used as an inducer to activate the osteogenesis of the hMSCs. The hMSCs were incubated with the EXO-D0, EXO-D4, EXO-D10, EXO-D15, EXO-D20 for 20 days. Immunofluorescence microscopy (Figure 2.2A, a-e) shows that the type 1 collagen (COL-1) expression of the cells treated with different osteogenic exosomes is almost the same because COL-1 is not an osteo-specific differentiation marker, which is similar with the osteogenic medium induced hMSCSs (Figure 2.2 B, a-e). Meanwhile, the immunofluorescence intensity of the Col-1expression of the hMSCs induced by the osteogenic exosomes and medium were also quantified. The Col-1 immunofluorescence intensity of the cells induced by the osteogenic medium for about 15 dan 25 days is much higher than other groups (Figure 2.3a). While, the Col-1 immunofluorescence intensity of the cells treated by the EXO-D15 also shown the highest signal comparing to the other groups (Figure 2.3a), but there is no significant difference between the osteogenic exosome treatment and osteogenic medium treated. However, the osteopontin (OPN) expression in Figure 2.2A, h-j is much higher than that in Figure 2.2A, f-g, indicating that the EXO-D10, EXO-D15, and EXO-D20 have the higher differentiation-inducing ability for the osteogenesis of the hMSCs, which is also consisted with the osteogenic medium induced cells (Figure 2.2B, h-j). For the quantity of the immunofluorescence staining, it was also found that OPN expression of the cells induced by osteogenic medium for about 4 days and 10 days show the higher signal (Figure 2.3b). And the OPN expression of the cells treated by the EXO-D10, EXO-D15 also show the high signal than the other groups (Figure 2.3b), but no significant difference between the osteogenic exosome treatment and osteogenic medium treated. To further confirm the exosome's osteogenic

differentiation ability, the real-time PCR analysis of the osteo-specific markers (Runx2, ALP, and OPN) was performed. Figure 2.3c shows that OPN gene expression of the cells treated with the EXO-D10 is the highest, and OPN gene expression in the EXO-D15 group is a little bit lower than that in the EXO-D10 group but still higher than the other groups. For the ALP gene expression, the cells incubated with the EXO-D10 have the highest expression among those groups. For the COL-1 gene expression, the EXO-D15 treated cells are much higher than the other groups but still lower. Runx2 gene expression of the EXO-D10 treated cells is higher than the other groups but still lower. These results demonstrate that the EXO-D10 and EXO-D15 can induce the osteogenic differentiation of the hMSCs more efficiently than the other exosome samples. Matrix mineralization is a crucial step towards the formation of calcified extracellular matrix associated with the true bone, so Alizarin Red was used to determine the presence of the calcium deposition by the osteogenic lineage. The red deposition in Figure 2.2A m and n is more obvious than that in Figure 2.2A k, l, and o, further indicating that EXO-D10 and EXO-D15 can induce the osteogenic differentiation of the hMSCs more efficiently than the other exosomes. Meanwhile, the ALP activity was also tested to confirm the osteogenesis of hMSCs. In Figure 2.3d, EXO-D10 and EXO-D15 show a higher ALP activity than the others, consistent with the results of real-time PCR and immunofluorescence assay. Therefore, EXO-D10 and EXO-D15 showed the best ability to induce the osteogenic differentiation of hMSCs due to the significant enhancement in OPN gene and protein expression, calcium deposition, and ALP activity in comparison with the other exosomes.

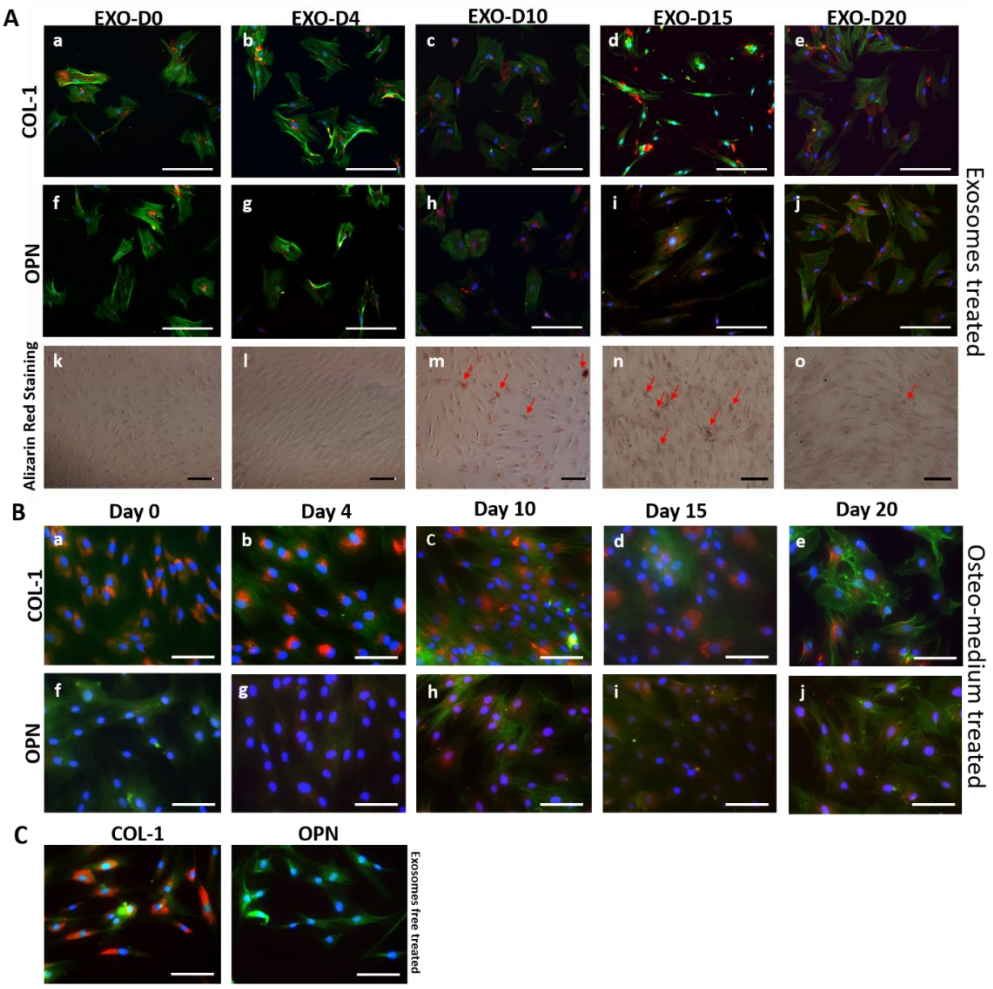


Figure 2.2. Osteogenic differentiation of hMSCs by the osteogenic exosomes. A. (a-j) Immunofluorescence staining of the osteogenic markers (a-e, COL-1; f-j, OPN) in the hMSCs showing the osteogenic differentiation on Day 20 induced by hMSCs-derived osteogenic exosomes (EXO-D0, EXO-D4, EXO-D10, EXO-D15, and EXO-D20) and the osteogenic medium (B). The red color of the cells (h, i, j in A) treated with the EXO-D10, EXO-D15, and EXO-D20 is much deeper than that of the cells in f and g. Similarly, the red color of the cells (h, i, j in B) treated with the osteogenic medium is more deeper than the other control cell in f and g. Blue (DAPI), nuclei; green (FITC), F-actin; red (TRITC), OPN and COL-1. (k-o) Bright-field images

of the Alizarin Red S staining for the osteogenesis of hMSCs induced by the osteogenic exosomes. The red deposit is the calcium nodule and indicated by the arrow. Scale bar: 100 μm.

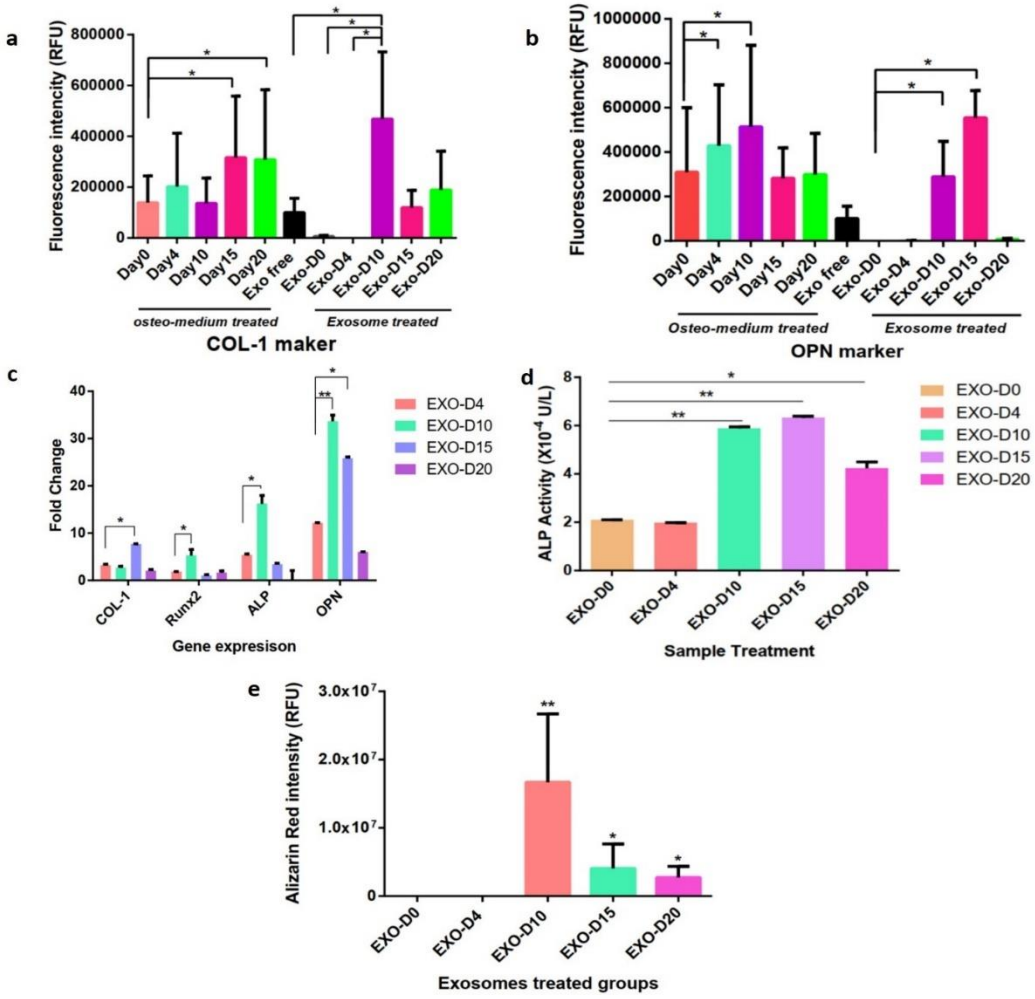


Figure 2.3. The quantitation of the Immunofluorescence staining, Gene expression, and ALP activity. The Relative Fluorescence intensity (RFU) of the Col-1 (a) and OPN (b) marker of the immunofluorescence staining. (c) Real-Time PCR analysis of the osteogenic markers (COL-1, Runx2, ALP, and OPN) showing the osteogenesis of hMSCs induced by the osteogenic exosomes at the gene level. For each gene expression, it was compared by the EXO-D4 treated group. (d) ALP activity of osteogenesis of hMSCs induced by the osteogenic exosomes. For each ALP activity, it was compared by the EXO-DO treated group. (e) The Alizarin Red intensity after all

kinds of exosomes induction. Each exosome treated group was compared with the EXO-D0 treated group. * $p<0.05$; ** $p< 0.0$, N=3.

2.3.3 The cell-free 3D Ti-scaffolds with the exosomes derived from the stem cells induced the bone tissue regeneration *in vivo*

To demonstrate that the osteogenic exosomes (EXO-D10 and EXO-D15) identified by *in vitro* differentiation assay could enable the cell-free 3D-printed Ti-scaffolds to induce bone regeneration *in vivo*, the cell-free but exosome-seeded scaffolds were implanted (Figure 2.3) into the rat radial bone defect model to evaluate bone regeneration after 4 and 12 weeks. SEM confirms the porous structures of the cell-free 3D-printed scaffolds with and without exosomes (Figure 2.3). The exosomes (EXO-D15) are attached to the surface of the scaffold. All kinds of exosomes are attached to the scaffolds (data is not shown). The loading and releasing patterns of the exosomes to the Ti-scaffold were also evaluated. After 12 hours of incubation, the exosome loading efficiency is higher than the 24 hours incubation and is calculated as 79.48% (Figure 2.4b). The exosomes released from the scaffold continuously and the releasing efficiency can reach up to 50% after 2 hours (Figure 2.4c). It is shown that the exosomes could successfully be loaded into the scaffold and release into the around environment continuously. As a control group, hMSCs-seeded scaffolds were also prepared (Figure 2.5) to demonstrate that exosome-coated cell-free scaffolds can perform as well as hMSC-seeded exosome-free ones in osteogenesis. The newly formed bone tissue and blood vessels were examined by H&E staining, Masson trichrome staining, Toluidine blue staining, and Van Gieson staining (Figure 2.5 and 2.6). The H&E staining assays indicate that the Ti-scaffolds seeded with the osteogenic exosomes (EXO-D10 & EXO-D15) induce the new bone formation, which is evidenced by the presence of new bone cells and Haversian canals like structures (red arrows in Figure 2.5 and 2.6), as well as the formation of the blood vessels (blue

arrow in Figure 2.7 h) inside or around the scaffold channels. The collagen production was also confirmed by the three-color staining (Massion Trichrome Staining, Figure 2.5 b and d). The light green color (collagen protein) was further enhanced in the EXO-D15 decorated Ti-scaffolds (Figure 2.5 d) compared to the other EXO-coated group after 12 weeks of implantation, suggesting that more collagen was produced in the former than in the latter. Meanwhile, osteoblasts (in blue) were also obviously observed both in the hMSCs-seeded and EXO-D10, EXO-D15 groups by the Toluidine blue staining, and Van Gieson staining in Figure 2.6, and the Haversian canals like structures can be found in Figure 2.6 c and d. It suggested that the EXO-D10 and EXO-D15 seeded scaffolds could induce bone tissue regeneration as the hMSCs seeded scaffolds. Overall, the bone formation in the cell-free scaffolds seeded with the osteogenic exosomes is comparable to that in the hMSCs seeded group 4 and 12 weeks post-implantation. For the 12 weeks of implantation, the bone tissue regeneration was further enhanced for the EXO-D15 coated Ti-scaffolds compared to the EXO-D10 coated Ti-scaffolds. In addition, the reduced bone formation was detected in the exosome-free Ti-scaffolds (Data is not shown) compared to the exosome-coated Ti-scaffolds.

Hence, the combination of the 3D Ti-scaffolds and the osteogenic exosomes could enhance the bone tissue regeneration without externally seeding hMSCs in the scaffolds due to the osteogenesis-induction capability of exosomes.

It is known that the implantation of biomaterials would cause inflammatory responses *in vivo*. Given this, it is likely that the implantation of the scaffolds could influence the body healing by itself at the early stage of the implantation. It is reported that the migration of the inflammatory cells (microphage and giant cells) to the biomaterial's surface may activate the inflammatory response through the production of a wide range of the inflammation involved cytokines in the first two or four weeks.[156] In our study, the H&E staining results for 4 weeks post-implantation

show that only a few neutrophils are dispersed in the tissue/scaffold connection area in the hMSCs seeded Ti-scaffold (Figure 2.7 a and b). However, no neutrophils were found in the exosome decorated Ti-scaffold groups (Figure 2.7 c, d, and g, h). This observation indicated that no inflammatory response was caused by the exosomes decorated scaffolds at the early stage of the implantation. Furthermore, it was found that there were no inflammatory cells in both the hMSCs coated and exosome-decorated Ti-scaffold groups 12 weeks post-implantation (Figure 2.7 e and f). These results further confirm that the inflammatory response would take place at the early stage of biomaterials implantation.

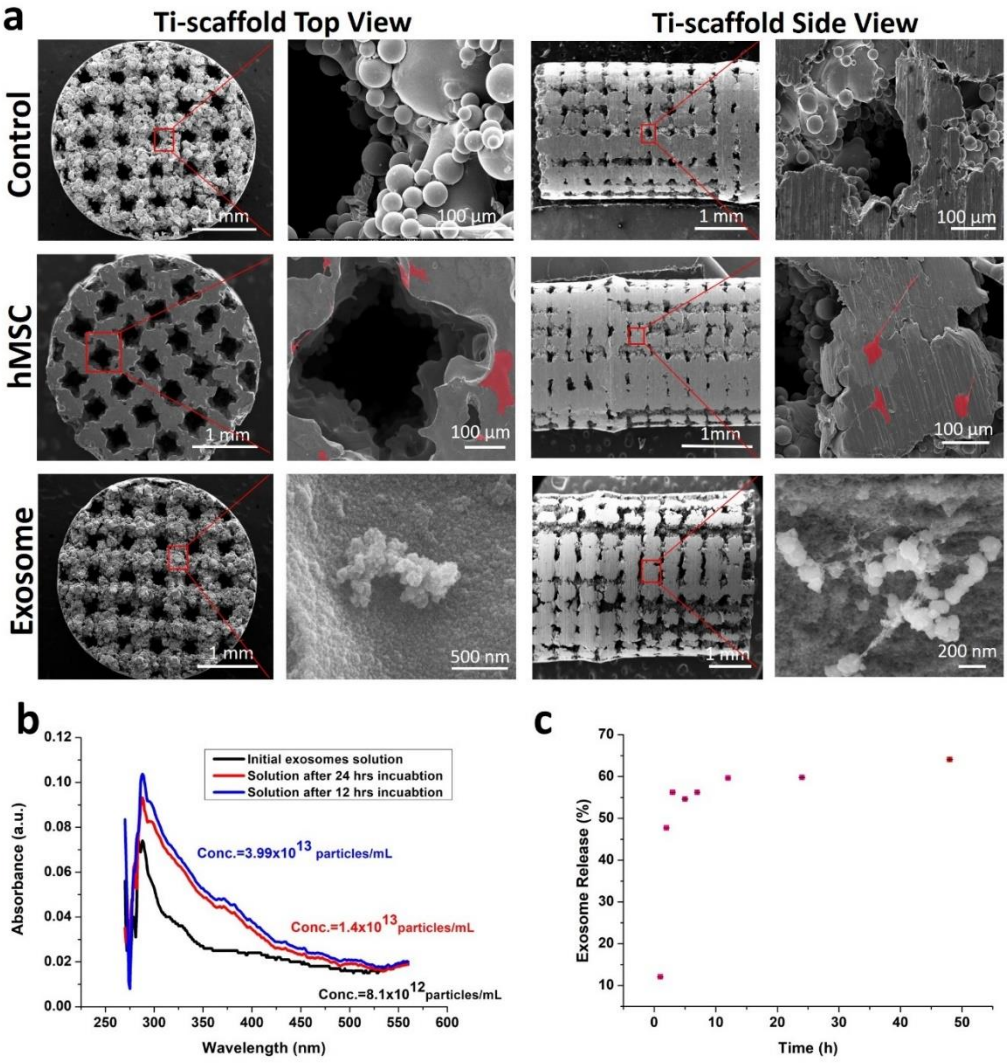


Figure 2.4. SEM images of the Ti-scaffolds, hMSCs-Ti-scaffolds, and exosome-Ti-scaffolds (a) and exosomes loading (b) and releasing pattern (c) of the exosomes from the exosome-3D-Ti-scaffold. (a) The SEM images of the Ti-scaffolds, hMSCs-Ti-scaffolds, and exosome (EXO-D15)-Ti-scaffolds. (b) UV-Vis absorption spectra of the initial exosomes solution and the supernatant after 12 or 24 hours loading into the Ti-scaffold. And the exosomes loading efficiency is calculated as 79.48%. (c) The exosomes releasing from the Ti-scaffold in the basal medium (pH=7.4). hMSCs are pseudo-colored into the red on the hMSCs-Ti-scaffolds. The Conc. of the exosome is calculated as the number of exosome particles per mL.

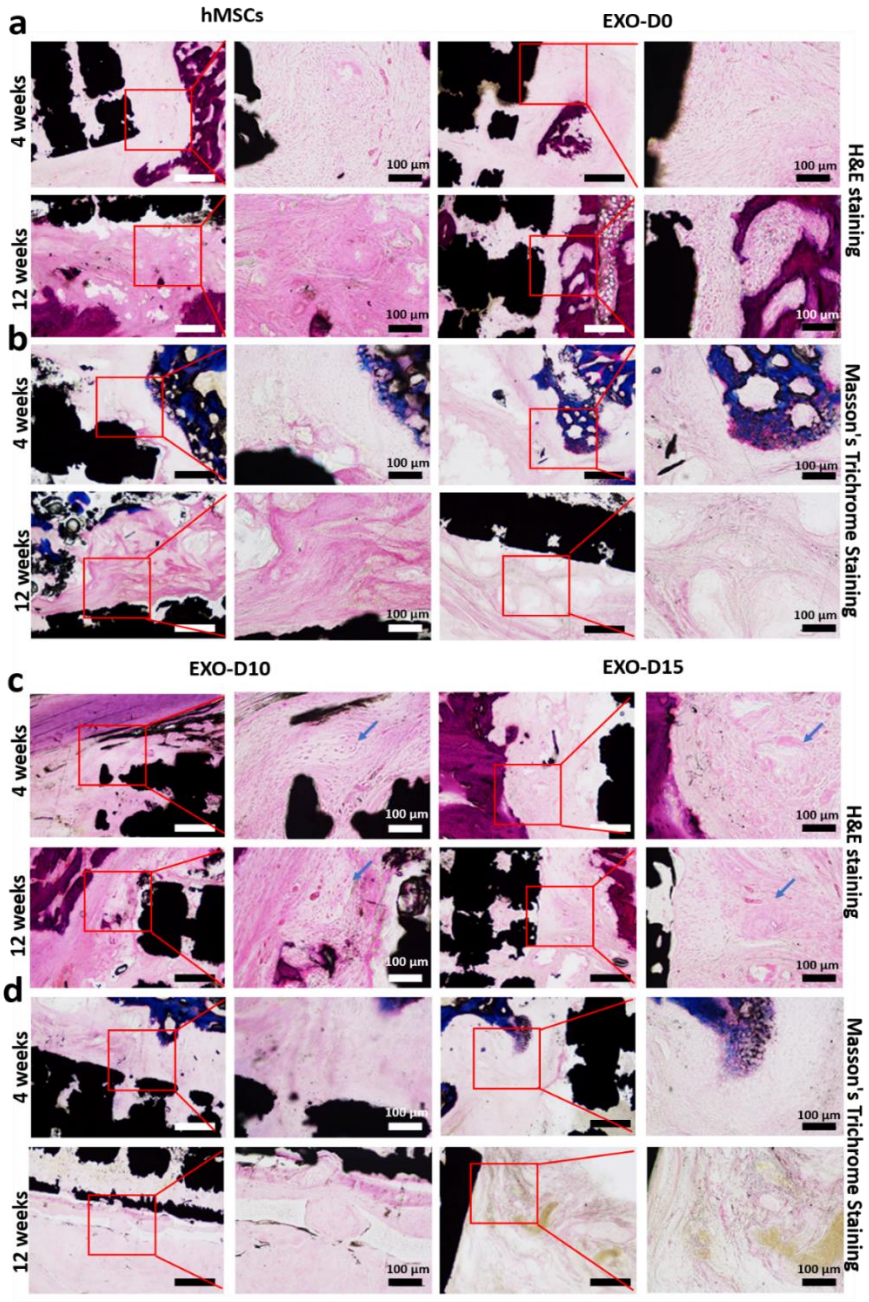


Figure 2.5. H&E staining and Masson's trichrome staining confirmed the new bone formation *in vivo* after 4 and 12 weeks. (a,c) H&E staining; (b,d) Masson's trichrome staining; low magnification scale bar: 250 μm. The arrows indicated the newly formed bone. The black areas reflect the section of the Ti-scaffolds. N=5. The area framed by red square highlights the presence of bone cells.

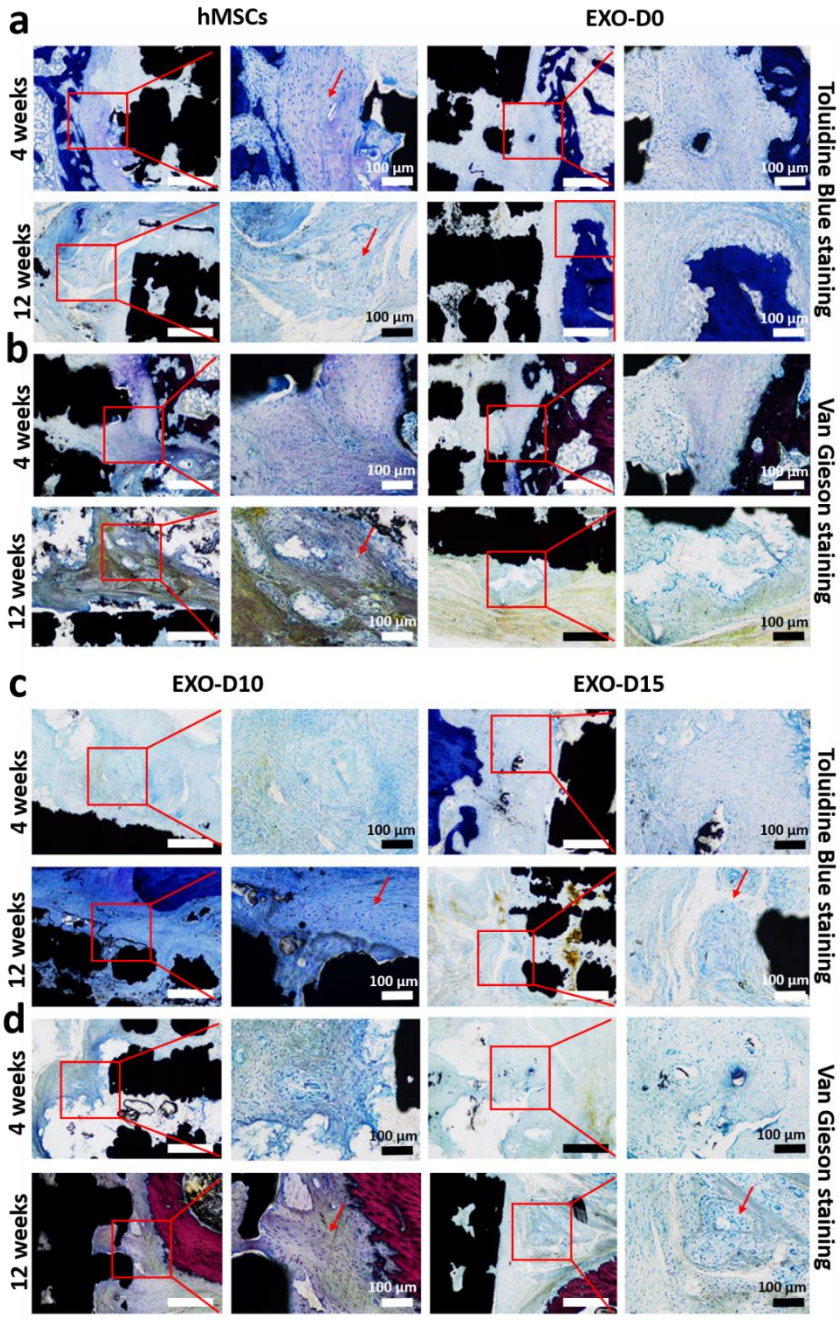


Figure 2.6. Toluidine Blue staining and Van Gienson staining confirmed the new bone formation *in vivo* after 4 and 12 weeks. (a, c) Toluidine Blue staining; (b, d) Van Gienson staining; low magnification scale bar: 250 μm. The arrows indicated the new bone formation. The black areas are the sections of the Ti-scaffolds. Light pink: the collagen fiber; light blue: the osteoblast cells. N=5.

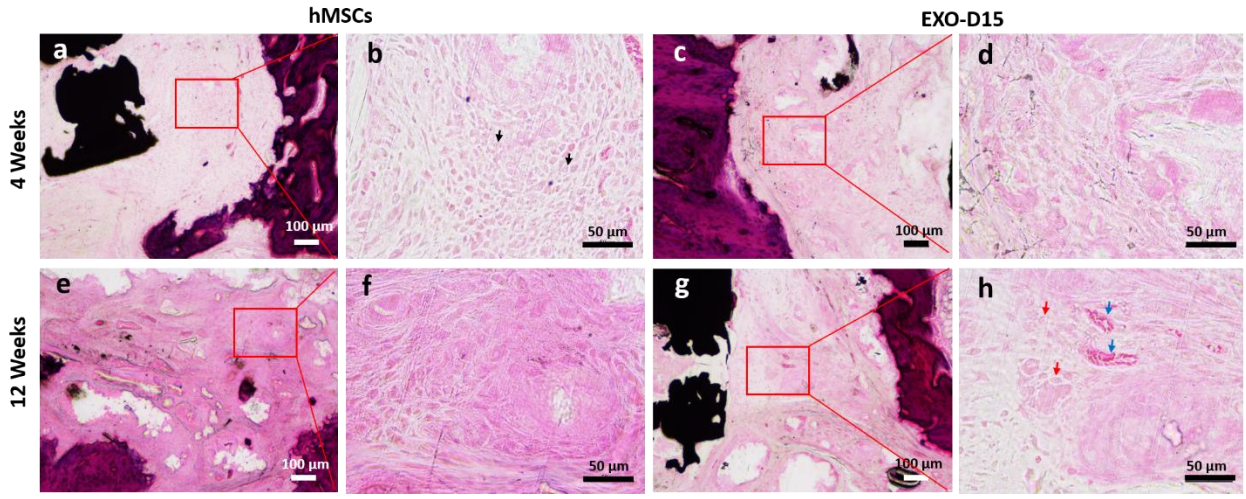


Figure 2.7. Histological analysis of the hMSCs decorated Ti-scaffolds (a, b, e and f) and EXO-D15 decorated Ti-scaffolds (c, d, g and h). The black arrows show that the neutrophils were dispersed in the boundary between the tissue and Ti-scaffold 4 weeks post-implantation but were not present 12 weeks post-implantation, suggesting that some immune reaction after 4 weeks of implantation (a and b) and no obvious immune response after 12 weeks of implantation (e and f) in the hMSCs decorated Ti-scaffolds. No obvious inflammatory response was found in the EXO-D15 decorated Ti-scaffolds after both 4 (c and d) and 12 weeks (g and h) of implantation, suggesting the absence of immune reaction in EXO-D15 decorated Ti-scaffolds. Red arrows: osteoblasts. Blue arrows: blood vessels.

2.4 Mechanism for osteogenesis of hMSCs induced by osteogenic exosomes

To understand why the two osteogenic exosomes, EXO-D10 and EXO-D15, can induce the osteogenic differentiation of the hMSCs *in vitro*, the exosome endocytosis and next-generation sequencing (EXONGS) was performed. Firstly, the Exo-green labeled osteogenic exosomes were incubated with the hMSCs followed by incubation with the Clathrin and Caveolin-1 antibody. Ideally, the exosomes, as well as Clathrin or Caveolin-1 protein, should be colocalized because the exosomes are endocytosed by a pathway involved with Clathrin or Caveolin-1.[157] To confirm

if the integrin on the cell membrane and/or exosome membrane are involved in. The cell membrane and exosome membrane are blocked with the 2mM RGD peptide. The high concentration of the RGD peptide could saturate all the integrin receptors on both membranes. And from Figure 7a, it showed that after the RGD peptide blocking, the colocalization of the exosome and anti-caveolin-1 and clathrin are more obvious than the no blocked one. It is further shown that the exosomes are colocalized with the Caveolin-1 and Clathrin mostly on the cell membrane and minorly inside of the cells. However, there are more exosomes colocalized with the Caveolin-1 (Figure 2.8a). Therefore, it is most likely that the exosomes go into the cells predominantly by the Caveolin-1 involved signaling pathway.

To evaluate whether the miRNAs in the exosomes are involved in the osteogenesis *in vitro*, the exosome next-generation sequencing (NGS) was performed to track the difference in miRNAs in the exosomes among different exosomes samples. Millions of RNAs were detected by the NGS from the commercial service (System Bioscience). The changes in miRNAs expression were shown in Figure 2.8 e-h. Compared to the miRNAs expression in EXO-D0 exosomes, the expression of 160, 166, 193, and 136 miRNAs were upregulated and that of 130, 139, 150, 191 miRNAs was downregulated in the EXO-D4, EXO-D10, EXO-D15, and EXO-D20 exosomes, respectively. More importantly, osteogenic miRNAs, such as Hsa-miR-146a-5p,[158, 159] Hsa-miR-503-5p,[160] Hsa-miR-483-3p,[161, 162] and Hsa-miR-129-5p,[163] were upregulated in the EXO-D10 and EXO-D15 (Figure 2.8 i). Namely, these miRNAs in EXO-D10 and EXO-D15 have a higher abundance than in the other exosomes, which is the possible reason for the enhanced bone tissue regeneration by EXO-D10 and EXO-D15 *in vitro* and *in vivo* compared to other exosome groups. Meanwhile, like Hsa-miR-32-5p,[164] Hsa-miR-133a-3p,[165] and Hsa-miR-204-5p,[166] were downregulated in the EXO-D10 and EXO-D15 (Figure 2.8j) obviously. MiRNAs might interact

with the growth factors or receptors, like BMPR2/MAP2K, BMP1, and RUNX2 (according to NGS data analysis, not shown). In conclusion, the overexpression of pro-osteogenic miRNAs, such as Hsa-miR-146a-5p, Hsa-miR-503-5p, Hsa-miR-483-3p, and Hsa-miR-129-5p and the inhibition of anti-osteogenic miRNAs, such as Hsa-miR-32-5p, Hsa-miR-133a-3p and Hsa-miR-204-5p, were taken together to induce the osteogenic differentiation of the hMSCs in vitro and in vivo. According to the analysis of the NGS sequencing results, the PI3K/Akt signaling pathway[167] and MAPK signaling pathway[168 169] (Scheme 2.2) might play a leading role in the osteogenesis of the hMSCs,[170] especially for the osteogenic exosomes of EXO-D10 and EXO-D15. MiRNAs might interact with the growth factors or receptors, like TARF6, FGF2, BMPR, BMP1, and RUNX2 (according to NGS data analysis, not shown) to activate the PI3K/Akt and MAPK signaling pathway for the osteogenesis of the hMSCs. Therefore, NGS data explains why two groups of the exosomes, EXO-D10, and EXO-D15, can induce the osteogenic differentiation of the hMSCs *in vitro* and bone tissue regeneration *in vivo*. Namely, the exosomes, especially EXO-D10 and EXO-D15, carry the osteogenic miRNAs to induce the osteogenesis of the hMSCs *in vitro* and bone tissue regeneration *in vivo* (Scheme 2).

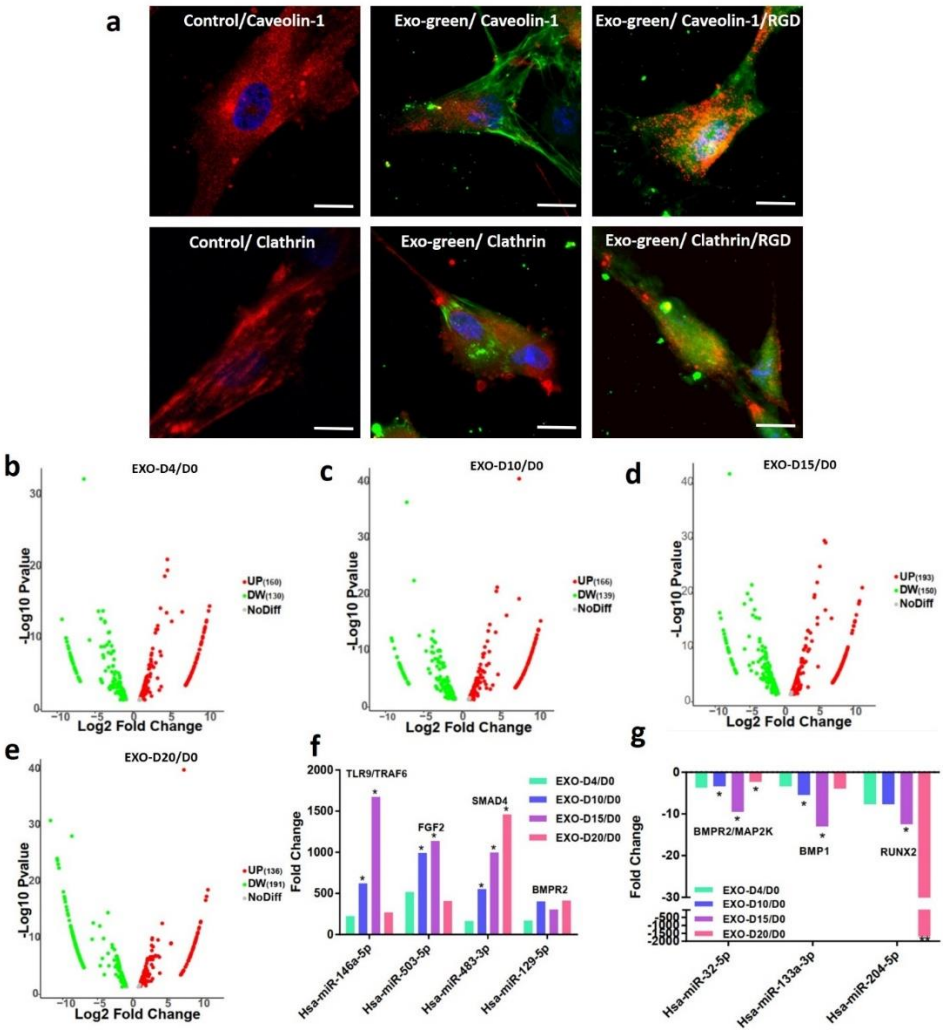
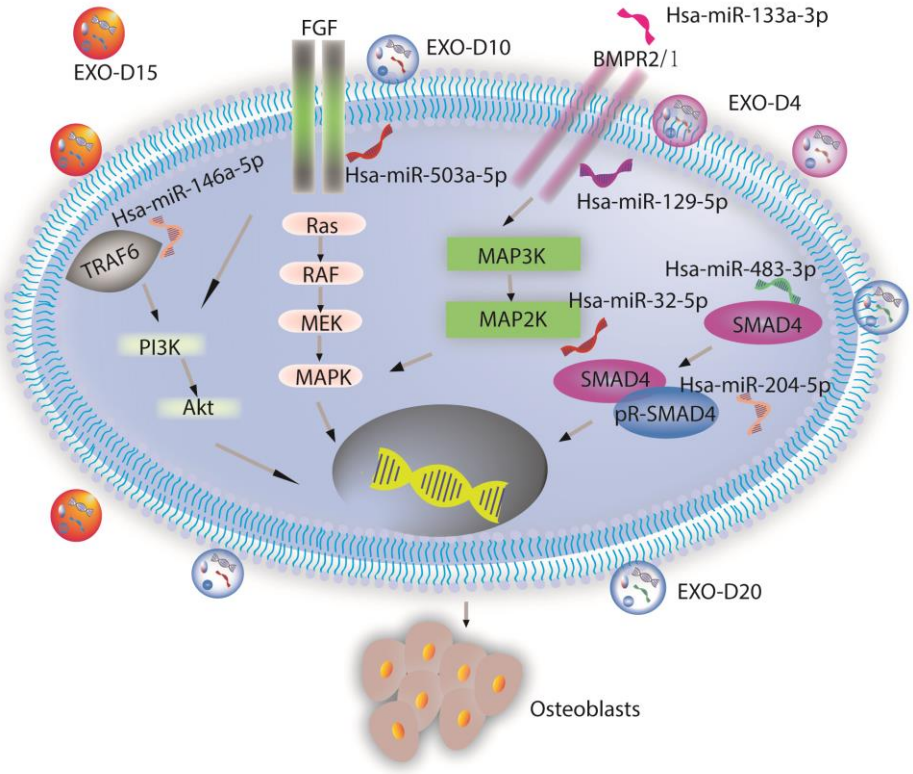


Figure 2.8. The mechanism for the osteogenesis of hMSCs induced by the osteogenic exosomes. (a) Colocalization of the exosomes and clathrin/caveolin-1 protein. Anti-caveolin-1 protein is colocalized with the exosomes labeled with the green fluorescence of the hMSCs and the RGD-peptide blocked hMSCs as well, but anti-clathrin protein is not as obvious as the anti-caveolin-1. The images are captured by the confocal microscopy. (b-e) Volcano analysis for the miRNA expression of different osteogenic exosomes. (f) upregulation and (g) downregulation of the miRNAs expression (fold change) involved in the osteogenesis of the hMSCs. FGF: Fibroblast growth factor; BMPR2: Bone Morphogenetic Protein Receptor 2; TRAF6: TNF receptor-associated factor; SMAD4: Mothers against decapentaplegic homolog 4; MAP2K: Mitogen-

activated protein kinase; BMP1: Bone morphogenetic protein 1; RUNX2: Runt-related transcription factor 2. The significant differences are calculated by comparing the EXO-D4/D0 in each group. Scale bar: 10 μm. * $p<0.05$, N=3; ** $p< 0.01$, N=3.



Scheme 2.2. The possible signaling pathways for the exosome-induced osteogenic differentiation of hMSCs *in vitro* and *in vivo*. It is likely that the osteogenic exosomes induce the osteogenesis of the hMSCs by the PI3K/Akt and MAPK signaling pathways. FGF: Fibroblast growth factor; BMPR2: Bone Morphogenetic Protein Receptor 2; TRAF6: TNF receptor-associated factor; SMAD4: Mothers against decapentaplegic homolog 4; PI3K: The phosphoinositide 3-kinase; Akt: serine/threonine-specific protein kinase; MAPK: microtubule-associated protein kinase.

2.4 Discussion

Small soluble molecules associated with exosomes, which are secreted from the stem cells at the different stages of differentiation, might have different positive effects on the cell differentiation *in vitro* and tissue regeneration in *vivo*. Meanwhile, the exosomes can be easily endocytosed into the host cells by the Caveolin-1 involved signaling pathway (Figure 2.8d). Current researchers isolated the exosomes from pre-differentiated stem cells and allowed them to be incubated with the stem cells in basal medium to figure out whether the osteogenic exosomes isolated from different stages could induce the osteogenesis of hMSCs. It was found that EXO-D10 and EXO-D15 carried osteogenic miRNAs, like Hsa-miR-146a-5p, Hsa-miR-503-5p, Hsa-miR-483-3p, Hsa-miR-129-5p (Figure 2.8i), and Hsa-miR-32-5p, Hsa-miR-133a-3p and Hsa-miR-204-5p (Figure 2.8j) enabling them to induce the osteogenic differentiation of hMSCs by activating the PI3K/Akt signaling pathway[167] and MAPK signaling pathway[168] (Figure 2.7). Those signaling pathways play important roles in the osteogenesis of the hMSCs and could help to confirm the osteogenic ability of the exosomes. Interestingly, another batch of miRNAs profiles, like miR31,[171] miR211,[172] and miR-21[173] [174] were reported to be negative inducers of osteogenesis and downregulated during the osteogenic differentiation of the MSCs, even though our NGS data did not include those miRNAs profiles. In conclusion, the overexpression of pro-osteogenic miRNAs, such as Hsa-miR-146a-5p, Hsa-miR-503-5p,Hsa-miR-483-3p, and Hsa-miR-129-5p and the inhibition of anti-osteogenic miRNAs, such as Hsa-miR-32-5p, Hsa-miR-133a-3p and Hsa-miR-204-5p, were combined together to induce the osteogenic differentiation of the hMSCs *in vitro* and *in vivo*. In the previous study, the hMSCs derived exosomes could also induce the osteogenic differentiation of the hMSCs from the late stage differentiation hMSCs derived exosomes and osteogenic miRNAs profiles, like the miR-31-3p/5p and miR-10b-5p, were also included. [174] The

exosomes from the pre-differentiated hMSCs, especially for 21 days pre-differentiated, could promote the osteogenic differentiation of the hMSCs obviously with the strong ALP activity, accumulation of the mineralization in ECM. In a word, the microRNAs profiles in the exosomes derived from the pre-osteo-differentiated stem cells can change the communicated hMSCs, especially for the osteogenic differentiation. Furthermore, the osteogenesis of the stem cells was also confirmed by the RT-PCR, immunofluorescence staining, Alizarin Red S Staining, and ALP activity.

The exosomes derived from the stem cells can be easily attached to the poly-L-lysine coated 3D Ti-scaffold (Figure 2.4). After implantation, the exosomes could release the small molecules, like the miRNAs, to the microenvironments and recruit the cells, then communicate with the surrounding cells by the lipid-ligand receptor interactions, endocytic uptake, or fusion of vesicles and cell membrane.[29] Compared with the exosome-free Ti-scaffold implants, the exosome-coated Ti-scaffolds showed enhanced bone regeneration, as evidenced by obvious collagen formation and matrix mineralization (Figure 2.5 and 2.6). These results show that the identified osteogenic exosomes can be used to decorate scaffolds to achieve cell-free bone regeneration.

2.5 Conclusion

In conclusion, exosomes secreted by hMSCs differentiated in the osteogenic medium at different times were isolated. Then, the exosomes were added into the basal medium to test whether the exosomes could induce the osteogenic differentiation of hMSCs. It was found that exosomes secreted by the hMSCs osteogenically pre-differentiated for 10 and 15 days could most efficiently induce the osteogenic differentiation of hMSCs in basal medium. Finally, it showed that the resultant osteogenic exosomes could be used to decorate the 3D-printed Ti-scaffolds to achieve cell-free bone regeneration within 12 weeks. The exosome-coated cell-free Ti-scaffolds could

induce bone regeneration as efficiently as the hMSC-seeded exosome-free Ti-scaffolds because of the formation of the Haversian canal structure (Figure 2.5 a and c), which is an earlier stage of newly formed bone structure. This structure was also consistent with Maggiano et al. 's detection.[175] Utilizing the RNA-sequencing technique, it was verified that the exosomes could induce the osteogenic differentiation because they contained upregulated osteogenic miRNAs and thus triggered at least two osteogenic differentiation pathways (PI3K/Akt and MAPK). Hence, this study shows that osteogenic exosomes can be identified from pre-differentiated stem cells and thus used to replace stem cells in tissue regeneration.

According to current studies, stem cell-derived exosomes are widely employed in the regenerative medical area, including skin wound healing, cardiac, liver, kidney, and nerve repairing, but has limited application to bone defect regeneration.[176] In one previous study, MSCs-derived exosomes could induce osteogenic differentiation of stem cells depending on altered osteogenic exosomal microRNA profiles *in vivo*, but there was no related *in vivo* study.[124] So far, the traditional bone defect treatment such as autograft, allograft, xenografts as described in Chapter 1.4.2, could cause immune rejection and disease transmission after implantation.[77] Therefore, bone tissue engineering is considered a promising method where a 3D scaffold including the biochemical and physical cues is introduced into the defective bone to induce bone tissue regeneration. In particular, the metallic 3D scaffold, such as porous Ti [124], Mg [177] scaffold, is the most popular candidate for the loading-bearing bone tissue regeneration compared to ceramics, or polymers owing to their high mechanical strength, resistance, and printing possibilities. Moreover, 3D printed titanium scaffold was verified to have good biocompatibility and osteointegration capability and it also possessed a similar induction performance of the polyester ether ketone material. [124] It is known that the human adipose stem

cells- derived exosomes were used to coat PLGA scaffold to promote the bone regeneration in calvarial defect model.[178] And macrophage-derived exosomes can also be integrated with titanium oxide nanotubes for bone tissue regeneration *in vitro.* [179] In summary, previous studies showed that, i) stem cells-derived exosomes could be used for osteogenesis of MSCs *in vitro*, but no further *in vivo* applications, especially for the loading-bearing bone tissue regeneration was estimated. ii) 3D metal scaffold seeded with cells could be implanted into the defective bone site for tissue regeneration, but could also cause critical immune responses especially at the early stage after implantation.

In this work, a novel strategy for bone tissue regeneration was developed to treat bone disease. Firstly, the stem cell-derived exosomes are used as a bone formation inducer for decorating the 3D-printed Ti-scaffolds. Such cell-free bone tissue regeneration based on the exosomes is a new way to cure bone tissue disease. The cell-free strategy will not only avoid the immune rejection resulting from the implantation of the foreign cells into the body but also will decrease the expense of treating bone defects (data is not shown). In addition, exosomes derived from the stem cells are successfully used to induce osteogenic differentiation. Achieving such directed differentiation is very important in bone regenerative medicine. Since exosomes can now be isolated using the commercial kits, the use of exosomes is a new and facile approach to directing stem cell differentiation in cell-free tissue regeneration.

Based on this work, for the loading-bearing bone tissue regeneration, an implanted scaffold needs to fulfill the following requirement: i) materials are biocompatible; ii) scaffold is biodegradable. The degradation rates are adjustable, and non-toxic or harmful after implantation. iii) scaffolds own good mechanical strength to support the bone with highly resistant and loading properties. iv) optimal porosity for cell migration and proliferation; v) high surface/volume for cell attachment.

In this work, osteogenic exosome has been confirmed as a good inducer for osteogenesis *in vitro* and tissue regeneration *in vivo*. However, the 3D implanted titanium scaffold is not biodegradable or the degradation rate is pretty low after implantation. So, an ideal 3D scaffold with all the above good properties is expected to be developed for the loading-bearing bone tissue regeneration in the future.

2.6 Author contribution statement

This study was designed and directed by Dr. Chuanbin Mao and Dr. Mingying Yang as the principal investigators. Mengmeng Zhai planned and performed all of the experiments in this study. Wen Yang, Jing Guo, and Kegan Sunderland helped with animal surgery in this work. This manuscript was written by Mengmeng Zhai and edited by Dr. Chuanbin Mao and Dr. Mingying Yang.

Chapter 3: Discovery of exosome-internalizing peptides for targeted breast cancer therapy

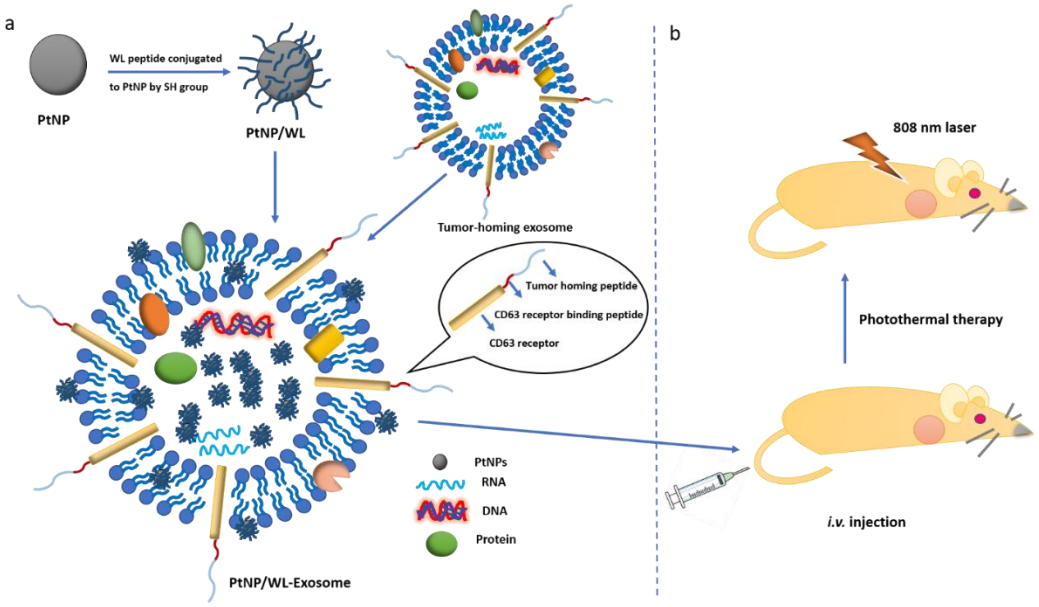
3.1 Instruction

Cancer has been the most common cause of death in the US in recent years.[180] Photothermal therapy (PTT) is a promising method for cancer treatment due to selectively killing cancer cells and its limited side effects on the patients compared to the surgery, chemotherapy, and radiotherapy.[181] [182, 183] For the PTT, a PTT material is applied to absorb near-infrared light (NIR) and generate the heat to efficiently kill cancer cells. NIR light (800-1000nm) has much greater body transparency without causing damages to normal tissues. [181] Recently, lots of PTT materials, including noble metal nanoparticles,[184] gold(Au) and silver(Ag), magnetite iron oxide nanoparticles,[185-187] organic nanomaterials,[188, 189] and selenides[190] have been discussed for the photothermal therapy. Although applications of the inorganic nanoparticles have high efficiency for cancer therapy, clinical usage of those is limited due to the biotoxicity of the cells, tissues, and organs in the human body.[191] The organic nanoparticles have good biocompatibility, however, the biodegradability and accumulation toxicity are still challenging in the clinical. [189, 192-194] Therefore, a novel safe and highly effective PTT material will be needed for cancer therapy in the future. The platinum nanoparticles are considered as a type of suitable PTT nanoparticles, which has a good NIR absorbance and generates heat. The platinum has an ultra-small size, which is around 10 nm, and it is also good for the biodegradability and less of accumulation toxicity due to the easy kidney clearance.

The stem cell-derived exosomes originate from the cells and are a good vector for the PPT agent delivery. It has seemed that all cells can produce and take up the exosomes. The cell-derived exosomes can also be applied to every therapeutic area due to its obvious advantages. Compared

to liposome delivery, the exosomes can avoid the immune clearance owing to the abundance of CD47 on the exosomes.[195] Furthermore, the tumor-targeting peptide can enhance passive cellular uptake. Therefore, a hypothesis is described that tumor-homing exosomes loaded with ultra-small PtNPs can kill breast cancer cell *in vitro* and inhibit the tumor growth *in vivo* with the NIR laser irradiation.

In this study, a novel nano complex was developed, of which the platinum nanoparticles loaded into the tumor-targeting exosomes, then the novel complex was applied to the breast cancer photothermal therapy with the irradiation of the 808 nm NIR laser *in vitro* and *in vivo*, respectively.



Scheme 3.1. The overall idea of photothermal therapy. a. Strategy for preparing the platinum nanoparticles exosomes carried systems: PtNPs were first modified by the exosome internalizing peptide by forming the PtNP/WL nano complex. Then above nano complex was loaded into the tumor-homing exosomes by forming the PtNP/WL-Exosome (EAPW). b. A sketch of the photothermal therapy *in vivo*. Mice were irradiated after 24 hours of injection of EAPW, with a pulsed 808 nm laser to trigger the release of PtNPs.

3.2 Methods and materials

3.2.1 MCF-7 cell culture

The human MCF-7 breast cancer cells (ATCC, Manassas, VA, USA) were cultured in Dulbecco's Modified Eagle's medium (DMEM) (ATCC) with 10% fetal bovine serum (ATCC) with the humidified atmosphere containing 5% CO_2 at 37 ^{0}C.

3.2.2 Cell culture and exosome isolation

The human mesenchymal stem cells were obtained from the Lonza group Ltd (Lonza, USA). Cells less than 5 passengers were maintained in a humidified atmosphere containing 5% CO2 at 37 ^{0}C in the Mesenchymal stem cell growth medium Bulletkit (PT-3001, Lonza). hMSCs were pre-differentiated for 15 days by the hMSC Osteogenic BulletKit (PT-3002, Lonza). Exosomes were isolated by the ExoQuick-TC kit (EXOTC50A-1, System Bioscience) and were resuspended into 1x PBS.

3.2.3 Selection of the exosome-internalizing peptides from a Ph.D.-12 phage library

The Ph.D.-12 Phage Display Peptide Library from New England Biolabs was used in this work. In this library, random dodecapeptides were fused to a minor coat protein, pIII, which include five identical copies at one tip of the filamentous M13 phage. The displayed peptide (12-residues) is expressed at the N-terminus of pIII and is followed by a short linker (Gly-Gly-Gly-Ser) before the wild-type pIII sequence. First, the phage library was depleted with a culture dish for 1 hour at 37 ℃ to remove the phages specifically binding to the culture dish. Then the resultant phage library was incubated with stem cell-derived exosomes for another 1 hour. The unbound and nonspecifically bound phages were removed after ten washes with 0.1% Tween-20 containing washing buffer. The

exosome surface-binding phages were collected using a pH 2.2 elution buffer. During the incubation, some phages may become internalized into the exosomes. To isolate these exosome-internalizing phages, the exosomes were lysed with a lysis buffer after the surface-binding phage were eluted. The eluted and internalized phages were then amplified, purified, and used as an input library for the next round of biopanning, respectively (Scheme 3. 2). The peptide sequences were determined by DNA sequencing.

3.2.4 Phage capture ELISA

The actual exosome affinity to the selected peptides was confirmed by using phage capture ELISA. In this test, the selected phages (10^{12}) were first coated on the 96-well plate overnight. The uncoated phages were removed from the petri dish on the next day. The stem cell-derived exosomes were then incubated with coating phage for another hour. The unbound exosomes were removed by repeatedly washing. Following this, exosomes bound to phages were detected by anti-CD63 (Abcam) conjugated with horseradish peroxidase (HRP) enzyme. After that, 450 nm absorbance was detected by a plate reader.

3.2.5 Phage affinity and specificity to exosome by the atomic force microscopy (AFM)

The stem cells derived exosomes (10^{12}) were incubated with the WL displayed phages and wild type phages for about one hour at 4 ^{0}C, respectively. The exosome/phage nano complex was isolated by the ExoQuick-TC kit (EXOTC50A-1, System Bioscience). Then the exosome/phage nano complex was dropped on the mica sheet by spin-coating methods. The morphology of the exosome/phage nano complex was captured by AFM.

3.2.6 Platinum nanoparticles synthesis

K_2PtCl_4 of 6 mM was reduced by 10 mg/ml $NaBH_4$ and 40 mM sodium citrate in a 60 ^{0}C oil bath under vigorous stirring for a few hours (at least 4 hours). The generation of the Pt nanoparticles was observed by the formation of a light-dark solution.

3.2.7 Construction of the Exo-PtNPs nano complex

The stem cell-derived exosomes were incubated with the CRHSQMTVTSRL[196]-G-AREGTRFSLIGGYR[197] (ARS pep) at 4 ^{0}C, overnight. It was reported that the CRHSQMTVTSRL peptide can specifically bind to the CD63 protein fragment containing the second extracellular loop (LEL), which is enriched in the exosomes derived from all kinds of cell sources, such as melanoma cells, lymphoblastoid cell lines, and hMSCs. [198-202] Current researchers also reported a tumor-targeting peptide, AREGTRFSLIGGYR, which can specifically target breast cancer tumors *in vivo*.[203] The conjugated peptide (ARS) can specifically help to target breast cancer tumors. After incubation, the ARS-peptide modified exosomes (EXO_{ARS}) were purified by the ExoQuick-TC kit. Besides, the Pt nanoparticles were incubated with the WL peptide (exosome internalized peptide) for another 2 hours at room temperature. The WL-peptide-modified Pt nanoparticles (PtW) were further incubated with the EXO_{ARS} overnight at 4 ^{0}C to form the tumor-homing Exo-Pt nano complex (EAPW), which is loaded with PtW (exosome internalized peptide (WL) modified Platinum nanoparticles).

3.2.8 Characterization of PtNPs and Exo-PtNPs nano complex by Transmission electron microscopy (TEM)

The EAPW nano complex and exosomes were diluted into 1X PBS with a density of 10^9 particles/ ml and fixed by an equal volume of 4% PFA, respectively. Then, the Exo-PtNPs nano complex

(EXO, EPT, EPW, and EAPW) was absorbed and stained onto a carbon-coated formvar film attached to a metal specimen grid by the published protocol. [196] TEM was utilized to identify the morphology of these nano complexes. PtNPs were also loaded onto a carbon-coated formvar film attached to a metal specimen grid with a density of 10^9 particles/ ml and identified by TEM.

3.2.9 Photothermal properties of the PtNPs and Exo-PtNPs nano complex by an infrared camera

The PtNPs, Exo-PtNPs (EPT), Exo-PtNPs/WL(EPW), Exo/ARS-PtNPs/WGV(EAPW) solution were prepared according to the above methods, respectively. Next, each 100 ul solution was irradiated by the NIR 808nm laser for 10 minutes at a power density of 8.6 W/cm^2 at a time. The thermal images of the above solutions were captured by an infrared camera (ICI 7320, Infrared Cameras, Inc, Beaumont, TX, USA) to track the temperature changes of the nano complex solution with irradiation of the NIR light (808 nm).

3.2.10 Photothermal killing of the MCF-7 cell using the Exo-PtNPs nano complex

The MCF-7 cells were seeded in a 96-well plate with a density of 10^5 ahead of the experiment day. Then 0.1 mL of PtNPs, EPT, EPW, and EAPW were dissolved into the DMEM cell culture medium without serum. After 4 hours of incubation, the above medium was removed, and cells were washed by the 1X PBS twice. Then 0.1 mL fresh medium was refilled into the 96-well plate. MCF-7 cells treated with above Exo-Pt nano complexes were irradiated by NIR 808 nm laser at a power density of 8.6 W/cm^2 for about 10 min.

3.2.11 Cell viability of the MCF-7 breast cancer cells

After four hours' incubation of the EXO, PtNPs, EPT, EPW, and EAPW nano complex, the MCF-7 cells were then washed by 1X PBS twice and nutritional by fresh medium. The Alamar Blue

regents (Invitrogen, US) were applied to cells for another four hours' incubation for cell viability detection. Besides, MCF-7 cell viability after the laser irradiation was performed to verify the Exo-Pt nano complexes cancer-killing efficiency. After that, 570 nm and 600 nm absorbance was detected by a plate reader for cells' cytotoxicity detection. Moreover, a live/dead cell staining was also applied to visualize cell death. Calcein AM and ethidium homodimer-1(1:4) were added to the MCF-7 cells after irradiation by 808 nm NIR light with all EXO-Pt treatment to verify live/dead cells.

3.2.12 *In vivo* study of the photothermal therapy

The nude mice (Female, Athymic nude-Foxn1^{nu}, 3-5 weeks) bearing about a five mm diameter tumor in the infra-axillary region were randomly separated into six groups. The six groups were injected intravenously by the saline, PtNPs, EXO, EPT, EPW, and EAPW for about 24 hours of blood circulation. 1 mg/kg of the above nano complex was injected in mice by the tail veil. After that, the tumor sites were irradiated by the 808 nm NIR for about five minutes with a power density of 8.6 W/cm^2. The laser size is about 10 mm. The temperature tracking of the tumor was recorded by an infrared camera (ICI 7320, Infrared Cameras, Inc, Beaumont, TX, USA). Tumor dimensions were measured every two days and lasted for 15 days' photothermal therapy. Then mice were sacrificed, and tumors were collected for further research applications. Tumor size was also calculated with the equation: Volume= length X Width^2/2.

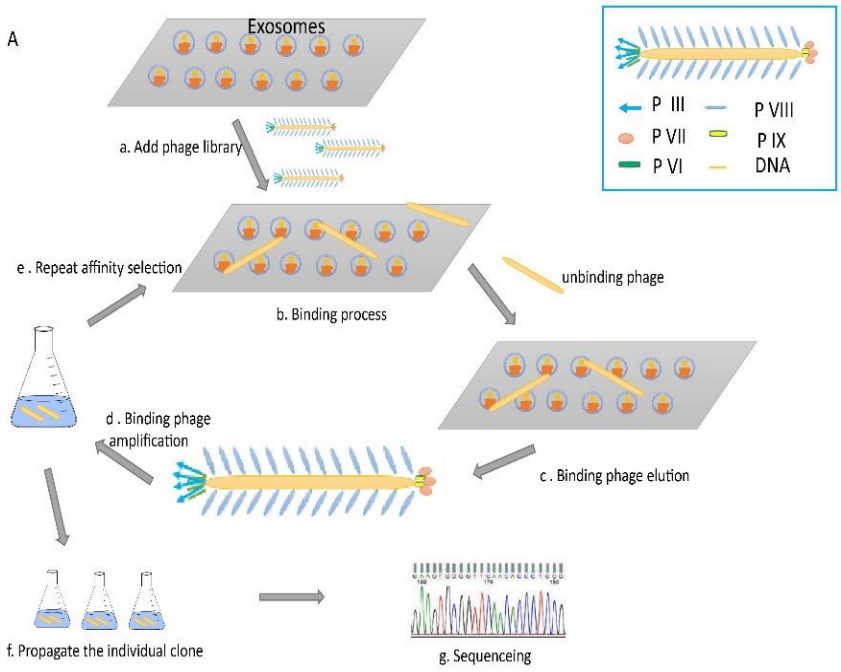
3.2.13 Organ biodistribution of the Exo-PtNPs nano complex

The Exo-PtNPs nano complex was injected into the tumor-bearing mice by tail veil for 24 hours of blood circulation. Next, tumors and other organs, including heart, liver, spleen, lung, and kidney, were collected after the heart perfusion then dried by a freeze-drying system. Finally, tumors and

organs were milled and digested by the aqua regia, then diluted by 2.5% HNO_3. The above supernatants were collected by centrifugation and further diluted by 2.5% HNO_3 to detect the concentration of Pt by ICP-MS.

3.2.14 Statistical analysis

The data were presented as the mean ± standard deviation. They were analyzed by the one-way ANOVA with Tukey's post-hoc test using SPSS21 (IBM, USA) with $p<0.05$ showing the significant difference.



Scheme 3.2. Exosome-internalized peptide selection. A major coat (pIII) displayed phage library, composed of billions of phage clones. The phage clones display a unique peptide fused to each of the 5 copies of pIII. The phage library was depleted first to remove the peptides that can bind to the Petri dish and control cells. The depleted phage clones interacted with the hMSCs derived exosomes. The non-binding phages were washed away from the exosome surface by washing buffer. The exosome binding phages were eluted by the elution buffer. The eluate phages were amplified by infecting the ER2738 E.Coli. The output phages from the former round were used as the input library for the next round of selection. Four rounds of biopanning were completed until some phage clones were dominant, which was distinguished by the DNA sequence analysis. Consequently, the dominant phage clones were considered as the exosome-binding phages.

3.3 Results

3.3.1 Identification of exosome-internalizing peptides from a Ph.D-12 phage library by biopanning

The stem cell-derived exosomes from the cell culture medium were collected by ExoQuick-TC kit. The stem cell-derived exosomes are around 200 nm by AFM (Figure 3.1-A) and TEM (Figure 3.2-A). The *in vitro* phage biopanning was performed for about 4 rounds for affinity testing against the stem cell-derived exosomes. At the end of the biopanning, 240 colonies were picked out and sent for sequencing. Among those sequences, the ones with the top 4 highest frequencies are WL, IR, SY, and HP (data is not shown here). The phage affinity and specificity to the exosomes were confirmed by AFM (Figure 3.1 C-D) and phage capture ELISA (Figure 3.1-G), respectively. The as-selected phage can bind (Figure 3.1C) and penetrate or fold (Figure 3.1 D) to the exosomes, in versa, the wild type phage can neither bind nor penetrate the exosome (Figure 3.1 F). In particular, phages containing WL and IR sequences showed higher absorbance (Figure 3.1 G) than the wild type phages, indicating a higher affinity of the selected phages to exosomes. This confirms that the phages selected by biopanning against exosomes are indeed specifically targeting the exosomes. In conclusion, as-selected phages can be internalized into the exosomes specifically.

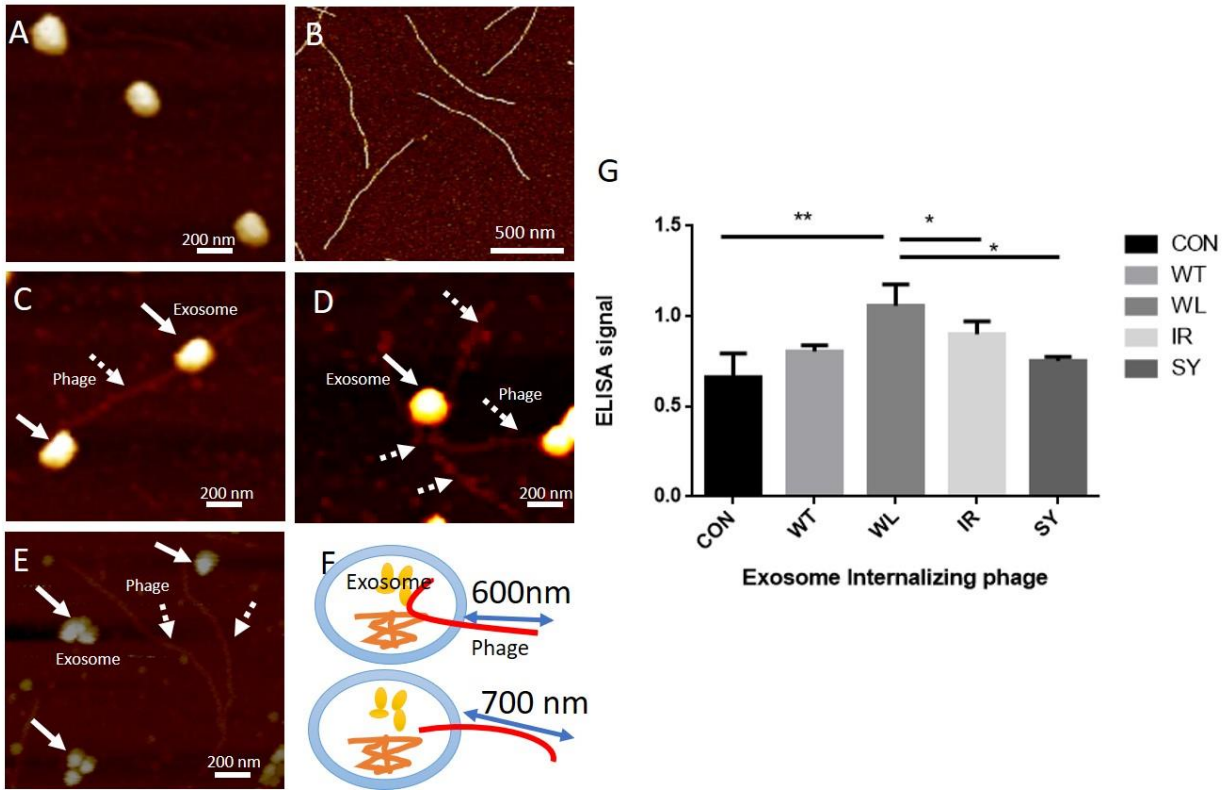


Figure 3.1. Identification of exosome-internalizing phage. Peptides from a Ph.D.-12 phage library by biopanning. A-F images show the internalization of the tips of Filamentous M13 phage nanofibers due to the display of an exosome-internalizing peptide at the tip. (A)Exosomes; (B) M13 phage nanofibers with the exosome-internalizing peptide (WL) displayed at the tip. (C-D) typical morphology of the phage-exosome complex, showing the internalization of the phage tips in the exosomes. (E) Wild type phages do not bind or penetrate exosomes. (F) Cartoon showing the internalization of phage tips resulted in the segments of phage protruding from exosomes. (C-D) being shorter than the original phages (B). It should be noted that due to the significant difference in the height between the phage (~7 nm) and exosomes (~100-200 nm), phages and exosomes cannot be visualized simultaneously under AFM although they are still visible. G shows the binding of control wild type phages and affinity phage to exosomes evaluated by ELISA. The X-axis indicates the affinity selected peptide sequence displayed on the tips of the phages. The Y-

axis shows the absorbance of the ELISA signal. CON: Control group, no phage treatment; WT: Wild Type phage; WL, IR, and SY represent the 12-mer foreign exosome targeting peptides (the sequence is not shown here) displayed engineered phages, respectively. N=5, *P<0.05, **P<0.01

3.3.2 Prepare the platinum nanoparticles loaded into tumor-homing exosome and characterize the photothermal properties of Exo-PtNPs nano complex

The PtNPs around 10-15 nm (Figure 3.2 B) were synthesized by our protocol as described in the method part. The 1mg/ml exosome internalized peptide (WL) was incubated with PtNPs at room temperature about 2 hours to form WL-PtNPs (PtW) complex. Meanwhile, stem cell-derived exosomes (Figure 3.2 A) was modified by tumor-targeting peptide (ARS) to form the EXO_{CRS} nano complex and the modification efficiency was about 40% by flow cytometry. The WL-PtNPs (PtW) complex was further loaded inside the EXO_{CRS} nano complex at 4 ^{0}C overnight with gentle shaking to form the EAPW nano complex (Figure 3.2 C and D). The PtNPs loading efficiency into the exosomes was time-dependent and also detected by ICP-MS (Figure 3.2 G and H). The result also showed that after 36 hours of incubation among those Exo-PtNPs nano complex, the PtNPs loading efficiency into EAPW could reach up to 88.98% compared to after 24 hours incubation (50.17%). Moreover, UV-Vis absorbance spectrum of the Exo-PtNPs nano complex (Figure 3.2 F) demonstrated that a considerable absorbance existed in all the Exo-nano complexes among the NIR range (800 nm - 1000 nm). It showed that above Exo-nano complexes were able to convert NIR light to heat and can be further applied to the photothermal therapy. Next, the photothermal properties of the EXO, PtNPs, EPT, EPW, and EAPW solution were evaluated by using an infrared camera by applying the NIR light (Figure 3.2 E). It indicated that EAPW nano complex has the highest photothermal properties compared to the other Exo-PtNPs nano complex, in which the temperature can reach up to 42 ^{0}C by the irradiation of 808 nm NIR laser at a power density of 8.6

W/cm^2 after 250s irradiation. That could be considered as a reasonable time for the photothermal therapy *in vivo.* To confirm the toxic of the nano complex to cells, the cell viability of MCF-7 cells was also performed after 4 hours' incubation with Exo-PtNPs nano complex treatment with and without laser irradiation (Figure 3.3). Figure 3.3 B demonstrated that the various Exo-PtNPs, especially for EAPW, didn't impact the cell viability of the MCF-7 cells compared to the pure PtNPs after 4 hours' incubation without laser irradiation. After that, 808 nm NIR laser was further applied to the MCF-7 cells for 10 min with a power density of 8.6 W/cm^2 after all the Exo-PtNPs' nano complex treatment. From Figure 3.3 C, it showed that EPT, EPW, and EAPW nano complex could kill the MCF-7 cells after 10 min laser irradiation compared to PtNPs, EXO nano complex. To further confirm the cell viability of the MCF-7 cells, the live/dead cell staining was also performed (Figure 3.3A) after laser irradiation. The images showed that EPT, EPW, and EAPW treated cells were killed more efficiently than the other nano complex treated group after NIR laser irradiation. In conclusion, the novel EAPW, EPT and EPW nano complex can be considered as good photothermal material to convert the light to heat for breast cancer therapy and might be applied to *in vivo* study in the future.

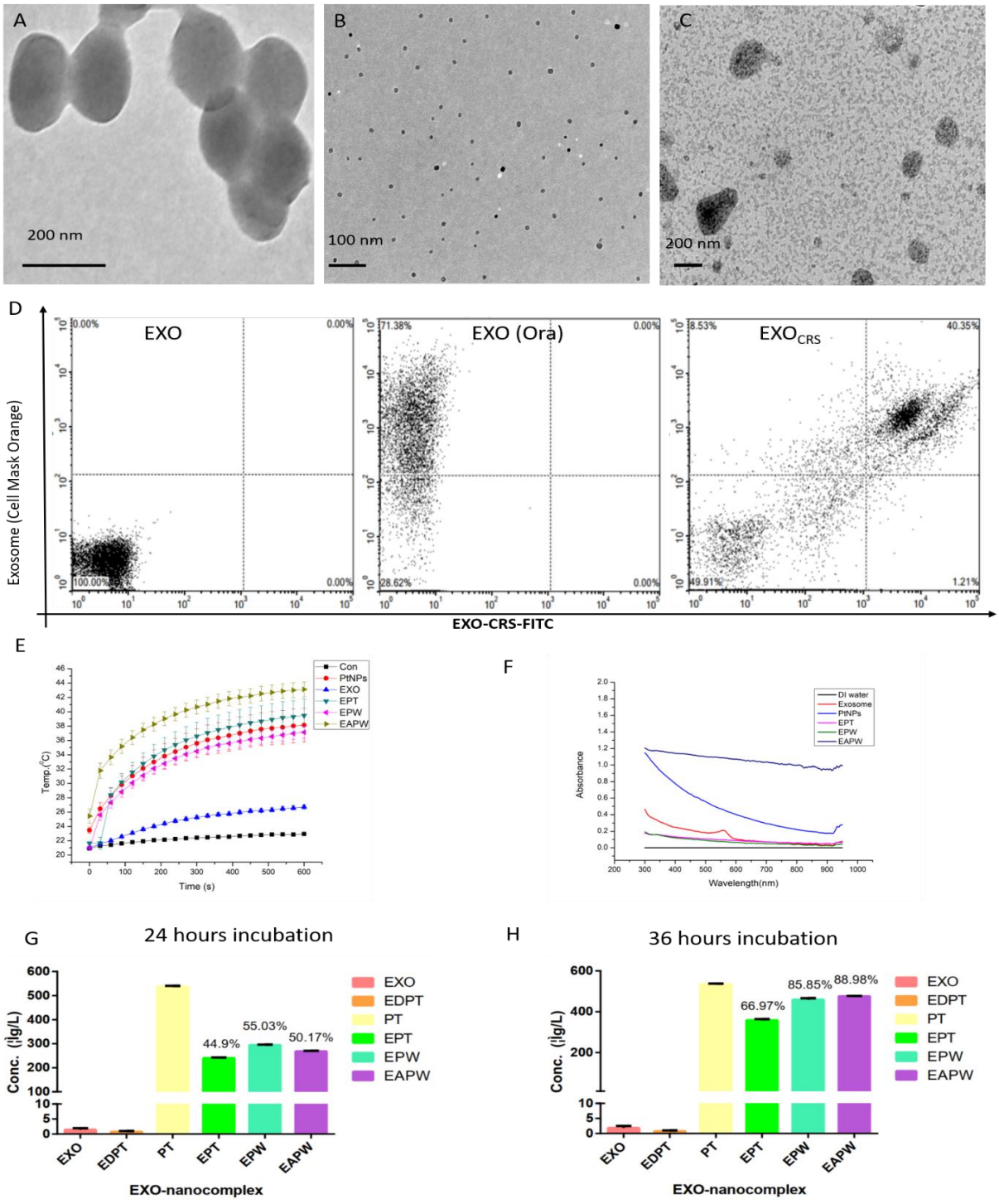


Figure 3.2. Characterizations of the Exo-PtNPs nano complex. TEM image of exosome (A), PtNPs (B), and EAPW nano complex (C). (D) Flow cytometry for measuring the modification efficiency of a tumor-targeting peptide (ARS) on exosomes. FITC-labeled ARS (1mg/ml) and

Exo-Red staining labeled exosome membrane were used. (E) The temperature tracking of EXO, EPT, EPW, and EAPW aqueous solution irradiated by the 808 nm NIR laser at a power density of 8.6 W/cm^2 for 10 min; (F) The UV-Vis absorbance spectrum of Exo-PtNPs nano complex in aqueous solution from 300nm -900nm; (G) and (H) PtNPs loading efficiency to tumor-targeting exosomes after 24 and 36 hours' incubation. EXO: Exosomes; EDPT: The platinum particles precipitated by the EXO-Quick kit; PT: Platinum nanoparticles; EPT: Exosomes loaded with the PtNPs; EPW: Exosomes loaded with the exosome-internalized peptide modified PtNPs; EAPW: Tumor homing exosomes loaded with the exosome-internalized peptide modified PtNPs.

3.3.3 *In vivo* study Photothermal therapy (PTT) using the EAPW

The PTT was performed on a nude mouse model bearing MCF-7 breast cancer tumor in the infra-axillary region. Firstly, the *in vivo* organ biodistribution of saline, EXO, EPT, EPW, and EAPW nanoparticles was performed after 24 hours' blood circulation. From Figure 3.4 C, Pt concentration in the liver and spleen are much higher than the other organs, such as heart, lung, and tumor. However, Pt concentration in the tumor was still a little bit higher than the other organs, including the heart and lung. It showed that EAPW can specifically penetrate and cumulated at the tumor site with a high concentration of Pt detected by ICP-MS, even though the significant difference is not obvious. Next, the NIR laser was applied on the tumor site with a power density of 8.6 W/cm^2 for 5 min. Besides, temperature changes of tumor sites were tracked by an infrared camera with NIR irradiation after 24 hours injection of EAPW. From the thermographs and temperature curve (Figure 3.5 A and B), it indicated that a higher skin temperature of 40 ^{0}C was captured after 4 min NIR irradiation compared to the saline and PtNPs group. Tumor's temperature was likely a little bit higher than 40 ^{o}C. The skin temperature could be improved by increasing the injection dosage of EAPW in the future. Moreover, tumors were irradiated with NIR laser every 2 days for 15 days

PTT therapy and tumor size was also recorded. After two weeks of PTT therapy, the tumor size of EAPW treated group obviously decreased from 60 mm^3 to 40 mm^3 compared to saline groups (Figure 3.5D). The tumor weights of EAPW treated groups were also lighter than the other groups (Saline and PtNPs) after 15 days' PTT therapy (Figure 3.5E). All these results showed that EAPW-mediated PTT could efficiently inhibit tumor growth *in vivo*. In addition, the body weight did not lose during the EAPW injection period (Figure 3.5 C). It further indicated that the EAPW didn't have any systemic toxicity during the therapeutic period. In conclusion, the novel developed EAPW nano complex could specifically penetrate and accumulated into the tumor site without the toxicity for the body system. Also, EAPW could efficiently kill breast cancer cells and inhibit tumor growth *in vitro* and *in vivo* under NIR exposure.

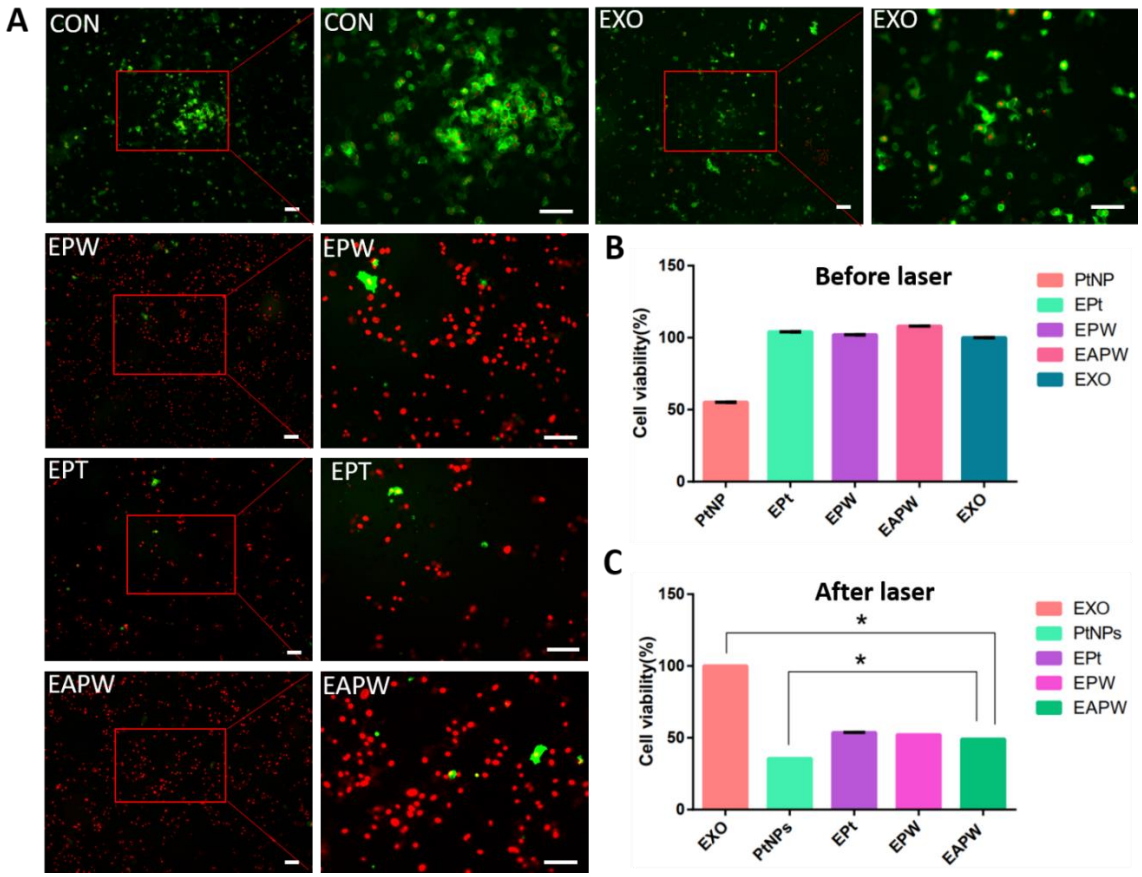


Figure 3.3. Cell viability of MCF-7 breast cancer cells before and after NIR laser irradiation. (A) Live/ dead cell staining of MCF-7 cells, which were irradiated by 808 nm NIR laser at a power density of 8.6 W/cm^2 for 10 min followed by 4 hours' incubation with various Exo-PtNPs nano complex (EXO, EPT, EPW, and EAPW). Cell viability of MCF-7 cells after 4 hours' incubation with various Exo-PtNPs nano complex (EXO, EPT, EPW, and EAPW) before (B) and after (C) laser irradiation. EXO: Exosomes; PtNPs: Platinum nanoparticles; EPt: Exosomes loaded with the PtNPs; EPW: Exosomes loaded with the exosome-internalized peptide modified PtNPs; EAPW: Tumor homing exosomes loaded with the exosome-internalized peptide modified PtNPs. Scale bar: 100 µm. * $P<0.05$, N=3.

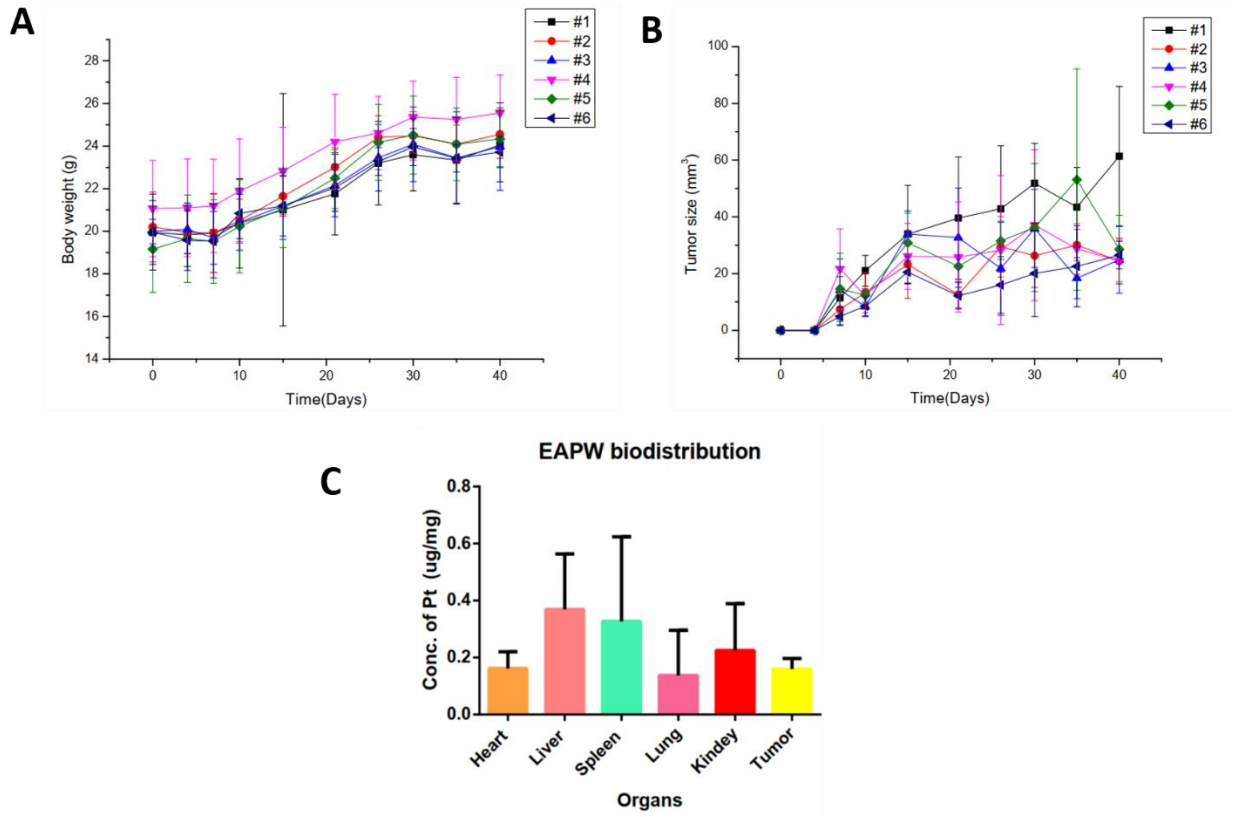


Figure 3.4. MCF-7 breast cancer mice model constructions and organ biodistribution of EAPW. Tracking of bodyweights (A) and tumor sizes (B) of MCF-7 breast cancer tumor-bearing mice before PTT. Organ biodistribution (C) of EAPW after 24 hours of blood circulation. EAPW:Tumor homing exosomes loaded with the exosome-internalized peptide modified PtNPs.

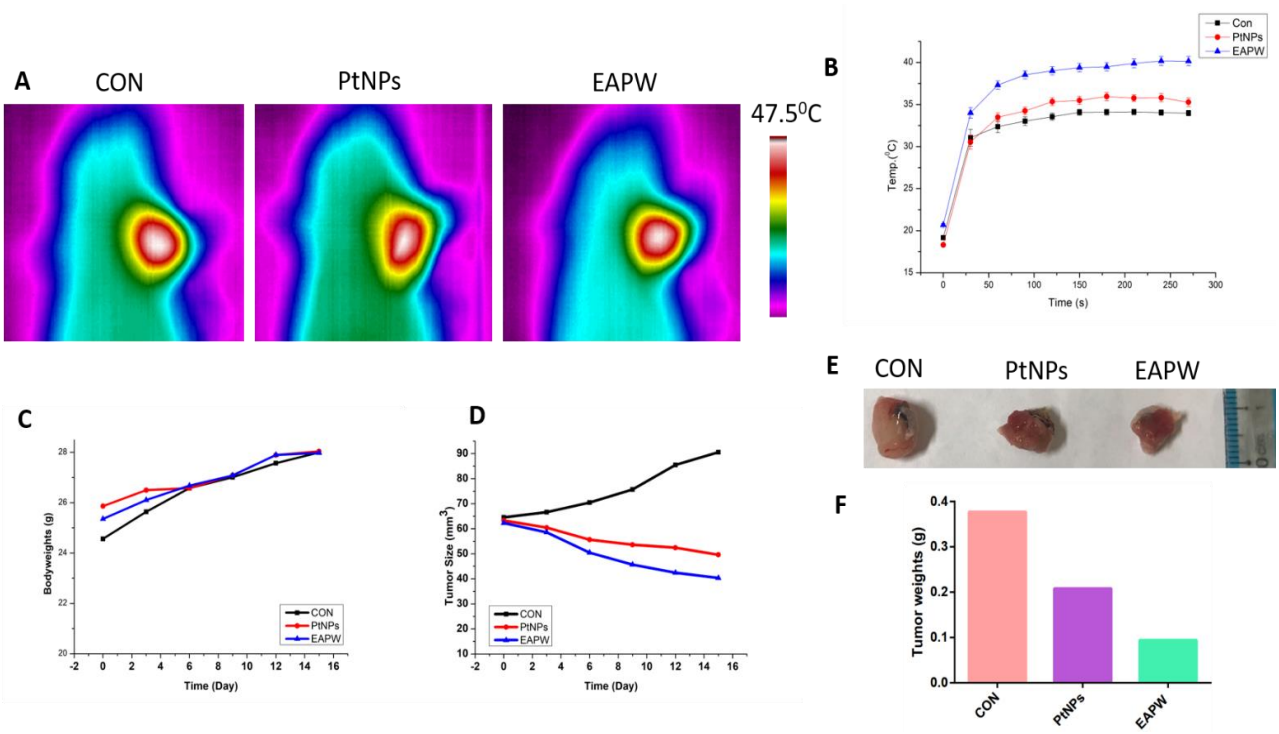


Figure 3.5. *in vivo* PTT by using EAPW. The thermograph (A) and temperature curve (B) of tumor sites by the infrared camera after 24 hours' blood circulation of the Saline, PtNPs, and EAPW during NIR irradiation. Mice bodyweights (C) and tumor sizes (D) changes of CON, PtNPs, and EAPW treated groups during PTT therapeutics periods. Excised tumors (E) and excised tumor weights (F) from CON, PtNPs, and EAPW treated groups after 15 days' PTT therapy. CON: Saline treated group; PtNPs: Platinum nanoparticles; EAPW: Tumor homing exosomes loaded with the exosome-internalized peptide modified PtNPs.

3.4 Discussion and Conclusion

Exosomes are considered a promising therapeutic vector for various pathologies, such as cancer therapy. These about 200 nm' vesicles (Figure 3.1 A) were secreted from different cell types and can communicate with recipient cells to deliver the therapeutic molecules by endocytosis.[204] In particular, the MSC derived exosomes exhibit some properties, including low immune response,

decreasing inflammation, etc.[205] In this work, a novel tumor-homing exosome nano complex (EAPW) (Figure 3.2 C) were developed to deliver platinum nanoparticles for photothermal breast cancer therapy. PtNPs were delivered to breast cancer tumors with the protection of exosomes, which can cross biological barriers, such as blood-brain barrier and deliver cargos, including therapeutic drugs and genes to recipient cells.[206] These exosomes were also modified with a breast cancer tumor-homing peptide (ARS) by CD63 antibody conjugation, which method was developed by Gao et al.[196] The ARS-peptide was selected by *in vivo* biopanning method and identified the high targeting affinity by *in vivo* fluorescence imaging.[207] The Exosomes' modified efficiency by ARS peptides was detected by about 40% by flow cytometry (Figure 3.2 D). It reported that 12 nm FePtNPs in a cubic shape could induce the necrosis of cancer cells, which is similar to the effect of Au nanorods (40 nm) after NIR exposure. [128] Therefore, PtNP as a kind of ultra-small PTT material can be applied to generate heat to kill cancer cells under NIR exposure as same as Au. Moreover, the ultra-small PtNPS could be loaded easily by either passive or active methods. Interestingly, the PtNPs loading efficiency into EAPW (Figure 3.2 H) can reach up to approximately 90% after 36 hours of incubation among all exosomes, including EPT, EPW, and EAPW in our study. In addition, PtNPs in ultra-small size could be easily cleaned by the kidney after releasing from exosomes so it isn't harmful to the cells, tissues, and organs in the animals.[208] For *in vitro* study, there was no cell cytotoxicity caused among EPT, EPW, and EAPW nano complex before NIR exposure (Figure 3.3 B). Vice versa, cell viability was dramatically decreased to lower than 50% after NIR exposure (Figure 3.3 A and C). It indicated that these nano complexes cannot impact cell life without any NIR irradiation, but can efficiently kill the cancer cells when exposed to NIR. It is likely that these nano complexes would not influence the normal cells, such as MCF-10 (normal breast cells) although this test was not performed. Furthermore, there is no

significant difference in cell viability and live/dead staining after the treatment of EPT, EPW, and EAPW nano complex (Figure 3.3 A and C). It further confirmed that ARS-peptide might specifically bind to the tumor *in vivo,* not breast cancer cells *in vitro* due to the high selected affinity to tumors. [207] Moreover, the tumor-targeting exosomes nanovesicles might find and retain into the tumor sites by a ligand-receptor interaction (ARS-peptide binding to the ligand on the tumor) after blood circulation and extravasation, then target to the tumor and release the platinum nanoparticles in a tumor.[209] *In vivo* study was also performed by tail vein injection of EXO, PtNPs, and EAPW nano complex on tumor-bearing mice. After 15 days of PTT therapy, the tumor volume of EAPW treated mice is obviously smaller than Saline treated mice (Figure 3.5 E and F). The tumor site's temperature could reach up to 40 ^{0}C (Figure 3.5 B) during NIR laser irradiation with the injection of 1mg/kg EAPW compared to 42 ^{0}C detected by Zhou et al. [121] Normally, the temperature of the tumor site is likely a little bit higher than the skin. However, it is still unknown whether inside organ temperature can reach up to 42^{0}C or higher to induce necrosis of tumors with a dose of 1mg/kg EAPW by *i.v.* injection. Next, a high dosage of EAPW would be applied to a tumor-bearing mouse with a range of 1mg/kg ~ 2 mg/kg for efficient PTT therapy by increasing temperature to 42 ^{0}C. Besides, the ARS-peptide did not show obvious tumor-targeted affinity to breast cancer tumor by organ biodistribution of EAPW (Figure 3.4 C) in tumor-bearing mice after 24 hours' injection. It is likely caused by the experimental operation or 24 hour's blood circulation periods of EAPW are longer so that EAPW has already been cleaned by the kidney. Therefore, the ARS- peptide tumor affinity needs to be further confirmed in the future.

In conclusion, a novel nano complex was developed, which can carry the targeting PtNPs homing to the breast cancer tumor. As a novel photothermal "drug", the enhanced cancer-killing efficacy has been improved by *in vitro* and *in vivo* study. The tumor-targeting exosomes can specifically

bind to the tumor and release the PtNPs with a high concentration of Pt by the detection of ICP-MS. This effective loading method can progressively improve the cancer-killing efficiency *in vitro* and tumor inhibition *in vivo*, respectively. The tumor attenuation was further detected by the application of the 808nm NIR laser. Finally, this novel method has provided a promising method for photothermal cancer therapy by the effective loading "drug" in the future.

Currently, traditional breast cancer therapies, including chemotherapy, radiotherapy, surgery, hormonal therapy, and targeted therapy could cause serious side effects, such as vomiting, hair loss, pain, and hot flashes on patients and impact the patient's normal life. Here, PTT, as a photo-based therapy, can convert NIR light (808 nm) to heat (42 ^{0}C) to kill cancer cells without any damage on skin and organs. The ultra-small noble metal nanoparticles, such as PtNP, AuNP, gold nanorods, and gold nanoshells, are considered as good PTT materials because of their good absorption, which is about four-five higher compared to other conventional molecular PTT materials.[210] However, theses nanoparticles might be cleared by the immune system before targeting to the tumor *in vivo*. Therefore, a vector is necessary to protect these metal nanoparticles to avoid the clearance by immune systems and deliver it to the tumor site. Exosomes are good original vectors that can protect and deliver the therapeutic nanoparticles to the tumor sites by good biocompatibility as well. In a previous study, it was shown that 12 nm FePtNPs in a cubic shape could induce the necrosis of cancer cells, which is similar to gold nanorods (40 nm)' effect with NIR exposure.[128] Zhou et al. found that the platinum-copper alloy nanoparticles can not only help track the tumor by guiding of photoacoustic imaging but also can efficiently inhibit tumor growth by photothermal therapy *in vivo*.[121] Another study also established that hollow gold nanoparticle loaded within exosomes could be applied to melanoma cancer(B16-F10) photothermal therapy. [211] Based on these former studies, i) ultra-small inorganic metal

nanoparticles, such as AuNP, PtNP can be applied to cancer photothermal therapy. However, immune clearance cannot be avoided before targeting and retaining to a tumor. ii) PTT materials (AuNPs) loaded within exosomes had been developed for the photoacoustic imaging and photothermal therapy, but lack of specific tumor-targeting is an issue.

In this study, a novel Exo-PtNPs nano complex has been developed by PtNPs loaded within tumor-homing peptide modified exosomes. This nano complex possesses the following advantageous properties: i) avoid the immune system clearance by exosome's protection when going through the blood circulation; ii) target and retain (EPR effect) to the tumor by the tumor-homing peptide and receptor interaction; iii) PtNPs are no-toxic and harmful after releasing from the exosomes; iv) have absorbance in the NIR range (800-1000 nm); v) no accumulation of PtNPs in ultra-small size and easily cleaned by kidney after releasing from exosomes. Besides, PtNPs synthesis developed and generated by our protocol is easy and less expensive. This study did not find any critical side effects on cells or animal studies. However, the fabrication procedure of the nano complex is complicated and requires two purification steps after peptide modification. It is challenging and necessary to improve the fabrication procedure of Exo-Pt nano complex for a high percentage yield in the future. Moreover, PtNP is also a good material for photoacoustic imaging. Actually, a double functional Exo-PtNPs nano complex was developed for photothermal therapy and photoacoustic imaging in this work, even though the photoacoustic efficiency has not been verified yet. It is vital for us to target the tumor and track the tumor metastasis by the photoacoustic imaging technique in the future. Furthermore, therapeutic chemicals, such as Doxorubicin, could also be packaged into the Exo-PtNPs nano complex to form a triple functional nano complex, which can be applied to the photoacoustic imaging and chemo-photothermal therapy (CPT) in cancer diagnosis and therapy in the future.

3.5 Author contribution statement

This study was designed and directed by Dr. Chuanbin Mao as the principal investigator. Mengmeng Zhai planned and performed all of the experiments and analyzed all data in this study. Dr. Penghe Qiu designed and generated the PtNPs synthesis. Liwei Zhang also helped with animal surgery. This chapter of thesis was written by Mengmeng Zhai and edited by Dr. Penghe Qiu.

Reference:

1. Bjørge, I.; Kim, S.; Mano, J.; Kalionis, B.; Chrzanowski, W. J. B. s., Extracellular vesicles, exosomes and shedding vesicles in regenerative medicine–a new paradigm for tissue repair. **2018,** *6* (1), 60-78.

2. Johnsen, K. B.; Gudbergsson, J. M.; Skov, M. N.; Pilgaard, L.; Moos, T.; Duroux, M. J. B. e. B. A.-R. o. C., A comprehensive overview of exosomes as drug delivery vehicles—endogenous nanocarriers for targeted cancer therapy. **2014,** *1846* (1), 75-87.

3. Xie, Y.; Dang, W.; Zhang, S.; Yue, W.; Yang, L.; Zhai, X.; Yan, Q.; Lu, J. J. M. c., The role of exosomal noncoding RNAs in cancer. **2019,** *18* (1), 37.

4. Goodarzi, P.; Larijani, B.; Alavi-Moghadam, S.; Tayanloo-Beik, A.; Mohamadi-Jahani, F.; Ranjbaran, N.; Payab, M.; Falahzadeh, K.; Mousavi, M.; Arjmand, B., Mesenchymal stem cells-derived exosomes for wound regeneration. In *Cell Biology and Translational Medicine, Volume 4*, Springer: 2018; pp 119-131.

5. Sarikaya, M.; Tamerler, C.; Schwartz, D. T.; Baneyx, F. J. A. R. M. R., Materials assembly and formation using engineered polypeptides. **2004,** *34*, 373-408.

6. Krag, D. N.; Shukla, G. S.; Shen, G.-P.; Pero, S.; Ashikaga, T.; Fuller, S.; Weaver, D. L.; Burdette-Radoux, S.; Thomas, C. J. C. r., Selection of tumor-binding ligands in cancer patients with phage display libraries. **2006,** *66* (15), 7724-7733.

7. Chopin, M.-C.; Rouault, A.; Ehrlich, S. D.; Gautier, M. J. J. o. b., Filamentous phage active on the gram-positive bacterium Propionibacterium freudenreichii. **2002,** *184* (7), 2030-2033.

8. Smith, G. P. J. S., Filamentous fusion phage: novel expression vectors that display cloned antigens on the virion surface. **1985,** *228* (4705), 1315-1317.

9. Huang, W.; Petrosino, J.; Palzkill, T. J. A. a.; chemotherapy, Display of functional β-lactamase inhibitory protein on the surface of M13 bacteriophage. **1998,** *42* (11), 2893-2897.

10. Lee, Y. J.; Yi, H.; Kim, W.-J.; Kang, K.; Yun, D. S.; Strano, M. S.; Ceder, G.; Belcher, A. M. J. S., Fabricating genetically engineered high-power lithium-ion batteries using multiple virus genes. **2009,** *324* (5930), 1051-1055.

11. Nam, K. T.; Peelle, B. R.; Lee, S.-W.; Belcher, A. M. J. N. l., Genetically driven assembly of nanorings based on the M13 virus. **2004,** *4* (1), 23-27.

12. Cao, B.; Yang, M.; Mao, C. J. A. o. c. r., Phage as a genetically modifiable supramacromolecule in chemistry, materials and medicine. **2016,** *49* (6), 1111-1120.

13. Li, Y.; Whyburn, G. P.; Huang, Y. J. J. o. t. A. C. S., Specific peptide regulated synthesis of ultrasmall platinum nanocrystals. **2009,** *131* (44), 15998-15999.

14. Whaley, S. R.; English, D.; Hu, E. L.; Barbara, P. F.; Belcher, A. M. J. N., Selection of peptides with semiconductor binding specificity for directed nanocrystal assembly. **2000,** *405* (6787), 665-668.

15. Dang, X.; Yi, H.; Ham, M.-H.; Qi, J.; Yun, D. S.; Ladewski, R.; Strano, M. S.; Hammond, P. T.; Belcher, A. M. J. N. N., Virus-templated self-assembled single-walled carbon nanotubes for highly efficient electron collection in photovoltaic devices. **2011,** *6* (6), 377.

16. Sanghvi, A. B.; Miller, K. P.-H.; Belcher, A. M.; Schmidt, C. E. J. N. m., Biomaterials functionalization using a novel peptide that selectively binds to a conducting polymer. **2005,** *4* (6), 496-502.

17. Ozer, I.; Chilkoti, A. J. B. c., Site-specific and stoichiometric stealth polymer conjugates of therapeutic peptides and proteins. **2017,** *28* (3), 713-723.

18. Hamley, I. W.; Castelletto, V. J. B. c., Self-assembly of peptide bioconjugates: selected recent research highlights. **2017,** *28* (3), 731-739.

19. Boyd, B. J.; Bergström, C. A.; Vinarov, Z.; Kuentz, M.; Brouwers, J.; Augustijns, P.; Brandl, M.; Bernkop-Schnürch, A.; Shrestha, N.; Préat, V. J. E. J. o. P. S., Successful oral delivery of poorly water-soluble drugs both depends on the intraluminal behavior of drugs and of appropriate advanced drug delivery systems. **2019,** *137*, 104967.

20. Banas, A.; Teratani, T.; Yamamoto, Y.; Tokuhara, M.; Takeshita, F.; Quinn, G.; Okochi, H.; Ochiya, T. J. H., Adipose tissue-derived mesenchymal stem cells as a source of human hepatocytes. **2007,** *46* (1), 219-228.

21. Lai, R. C.; Arslan, F.; Tan, S. S.; Tan, B.; Choo, A.; Lee, M. M.; Chen, T. S.; Teh, B. J.; Eng, J. K. L.; Sidik, H. J. J. o. m.; cardiology, c., Derivation and characterization of human fetal MSCs: an alternative cell source for large-scale production of cardioprotective microparticles. **2010,** *48* (6), 1215-1224.

22. Sato, T.; Iso, Y.; Uyama, T.; Kawachi, K.; Wakabayashi, K.; Omori, Y.; Soda, T.; Shoji, M.; Koba, S.; Yokoyama, S.-I. J. L. i., Coronary vein infusion of multipotent stromal cells from bone marrow preserves cardiac function in swine ischemic cardiomyopathy via enhanced neovascularization. **2011,** *91* (4), 553-564.

23. Yu, B.; Zhang, X.; Li, X. J. I. j. o. m. s., Exosomes derived from mesenchymal stem cells. **2014,** *15* (3), 4142-4157.

24. Pap, E.; Pallinger, E.; Pasztoi, M.; Falus, A., Highlights of a new type of intercellular communication: microvesicle-based information transfer. *Inflammation Research* **2009,** *58* (1), 1-8.

25. Théry, C.; Zitvogel, L.; Amigorena, S., Exosomes: composition, biogenesis and function. *Nature Reviews Immunology* **2002,** *2* (8), 569-579.

26. Müller, G.; Schneider, M.; Biemer-Daub, G.; Wied, S., Microvesicles released from rat adipocytes and harboring glycosylphosphatidylinositol-anchored proteins transfer RNA stimulating lipid synthesis. *Cellular signalling* **2011,** *23* (7), 1207-1223.

27. Ludwig, A.-K.; Giebel, B., Exosomes: small vesicles participating in intercellular communication. *The international journal of biochemistry & cell biology* **2012,** *44* (1), 11-15.

28. Eldh, M.; Ekström, K.; Valadi, H.; Sjöstrand, M.; Olsson, B.; Jernås, M.; Lötvall, J., Exosomes communicate protective messages during oxidative stress; possible role of exosomal shuttle RNA. *PloS one* **2010,** *5* (12), e15353.

29. Bang, C.; Thum, T., Exosomes: New players in cell–cell communication. *The international journal of biochemistry & cell biology* **2012,** *44* (11), 2060-2064.

30. Pêche, H.; Heslan, M.; Usal, C.; Amigorena, S.; Cuturi, M. C., Presentation of donor major histocompatibility complex antigens by bone marrow dendritic cell-derived exosomes modulates allograft rejection1. *Transplantation* **2003,** *76* (10), 1503-1510.

31. Timmers, L.; Lim, S. K.; Arslan, F.; Armstrong, J. S.; Hoefer, I. E.; Doevendans, P. A.; Piek, J. J.; El Oakley, R. M.; Choo, A.; Lee, C. N., Reduction of myocardial infarct size by human mesenchymal stem cell conditioned medium. *Stem cell research* **2008,** *1* (2), 129-137.

32. Colombo, M.; Raposo, G.; Théry, C., Biogenesis, secretion, and intercellular interactions of exosomes and other extracellular vesicles. *Annual review of cell and developmental biology* **2014,** *30*, 255-289.

33. Bi, B.; Schmitt, R.; Israilova, M.; Nishio, H.; Cantley, L. G., Stromal cells protect against acute tubular injury via an endocrine effect. *Journal of the American Society of Nephrology* **2007,** *18* (9), 2486-2496.

34. Xin, H.; Li, Y.; Cui, Y.; Yang, J. J.; Zhang, Z. G.; Chopp, M., Systemic administration of exosomes released from mesenchymal stromal cells promote functional recovery and neurovascular plasticity after stroke in rats. *Journal of Cerebral Blood Flow & Metabolism* **2013,** *33* (11), 1711-1715.

35. Wang, Z.; Ding, L.; Zheng, X.-L.; Wang, H.-X.; Yan, H.-M. J. Z. s. y. x. y. x. z. z., DC-derived exosomes induce osteogenic differentiation of mesenchymal stem cells. **2014,** *22* (3), 600-604.

36. Lamparski, H. G. M.-D., A.: Yao J. Y.; Patel ,S.; , Production and characterization of clinical grade exosomes derived from dendritic cells. *J Immunological Methods* **2002**.

37. Raposo, G.; Stoorvogel, W., Extracellular vesicles: exosomes, microvesicles, and friends. *J Cell Biol* **2013,** *200* (4), 373-83.

38. Ronne, W. Y. Y. R., C. L.; Kok, H. T.; Sai, K. L.;, Exosome: A Novel and Safer Therapeutic Refinement of Mesenchymal Stem Cell. *Intech* **2013**.

39. Vlassov, A. V.; Magdaleno, S.; Setterquist, R.; Conrad, R., Exosomes: current knowledge of their composition, biological functions, and diagnostic and therapeutic potentials. *Biochim Biophys Acta* **2012,** *1820* (7), 940-8.

40. Valadi, H.; Ekstrom, K.; Bossios, A.; Sjostrand, M.; Lee, J. J.; Lotvall, J. O., Exosome-mediated transfer of mRNAs and microRNAs is a novel mechanism of genetic exchange between cells. *Nature cell biology* **2007,** *9* (6), 654-9.

41. Haney, M. J.; Klyachko, N. L.; Zhao, Y.; Gupta, R.; Plotnikova, E. G.; He, Z.; Patel, T.; Piroyan, A.; Sokolsky, M.; Kabanov, A. V. J. J. o. C. R., Exosomes as drug delivery vehicles for Parkinson's disease therapy. **2015,** *207*, 18-30.

42. Pascucci, L.; Coccè, V.; Bonomi, A.; Ami, D.; Ceccarelli, P.; Ciusani, E.; Viganò, L.; Locatelli, A.; Sisto, F.; Doglia, S. M. J. J. o. C. R., Paclitaxel is incorporated by mesenchymal stromal cells and released in exosomes that inhibit in vitro tumor growth: a new approach for drug delivery. **2014,** *192*, 262-270.

43. Kim, M. S.; Haney, M. J.; Zhao, Y.; Mahajan, V.; Deygen, I.; Klyachko, N. L.; Inskoe, E.; Piroyan, A.; Sokolsky, M.; Okolie, O. J. N. N., Biology; Medicine, Development of exosome-encapsulated paclitaxel to overcome MDR in cancer cells. **2016,** *12* (3), 655-664.

44. Fuhrmann, G.; Serio, A.; Mazo, M.; Nair, R.; Stevens, M. M. J. J. o. C. R., Active loading into extracellular vesicles significantly improves the cellular uptake and photodynamic effect of porphyrins. **2015,** *205*, 35-44.

45. Sato, Y. T.; Umezaki, K.; Sawada, S.; Mukai, S.-a.; Sasaki, Y.; Harada, N.; Shiku, H.; Akiyoshi, K. J. S. r., Engineering hybrid exosomes by membrane fusion with liposomes. **2016,** *6*, 21933.

46. Johnsen, K. B.; Gudbergsson, J. M.; Skov, M. N.; Christiansen, G.; Gurevich, L.; Moos, T.; Duroux, M. J. C., Evaluation of electroporation-induced adverse effects on adipose-derived stem cell exosomes. **2016,** *68* (5), 2125-2138.

47. Podolak, I.; Galanty, A.; Sobolewska, D. J. P. R., Saponins as cytotoxic agents: a review. **2010,** *9* (3), 425-474.

48. Smyth, T.; Petrova, K.; Payton, N. M.; Persaud, I.; Redzic, J. S.; Graner, M. W.; Smith-Jones, P.; Anchordoquy, T. J. J. B. c., Surface functionalization of exosomes using click chemistry. **2014,** *25* (10), 1777-1784.

49. Higginbotham, J. N.; Zhang, Q.; Jeppesen, D. K.; Scott, A. M.; Manning, H. C.; Ochieng, J.; Franklin, J. L.; Coffey, R. J. J. J. o. e. v., Identification and characterization of EGF receptor in individual exosomes by fluorescence-activated vesicle sorting. **2016,** *5* (1), 29254.

50. Luan, X.; Sansanaphongpricha, K.; Myers, I.; Chen, H.; Yuan, H.; Sun, D. J. A. P. S., Engineering exosomes as refined biological nanoplatforms for drug delivery. **2017,** *38* (6), 754-763.

51. Munagala, R.; Aqil, F.; Jeyabalan, J.; Gupta, R. C. J. C. l., Bovine milk-derived exosomes for drug delivery. **2016,** *371* (1), 48-61.

52. Yano, J.; Hirabayashi, K.; Nakagawa, S.-i.; Yamaguchi, T.; Nogawa, M.; Kashimori, I.; Naito, H.; Kitagawa, H.; Ishiyama, K.; Ohgi, T. J. C. C. R., Antitumor activity of small interfering RNA/cationic liposome complex in mouse models of cancer. **2004,** *10* (22), 7721-7726.

53. Sioud, M.; Sørensen, D. R. J. B.; communications, b. r., Cationic liposome-mediated delivery of siRNAs in adult mice. **2003,** *312* (4), 1220-1225.

54. Patil, M. L.; Zhang, M.; Taratula, O.; Garbuzenko, O. B.; He, H.; Minko, T. J. B., Internally cationic polyamidoamine PAMAM-OH dendrimers for siRNA delivery: effect of the degree of quaternization and cancer targeting. **2009,** *10* (2), 258-266.

55. Thomas, M.; Lu, J. J.; Ge, Q.; Zhang, C.; Chen, J.; Klibanov, A. M. J. P. o. t. N. A. o. S., Full deacylation of polyethylenimine dramatically boosts its gene delivery efficiency and specificity to mouse lung. **2005,** *102* (16), 5679-5684.

56. Kesharwani, P.; Gajbhiye, V.; Jain, N. K. J. B., A review of nanocarriers for the delivery of small interfering RNA. **2012,** *33* (29), 7138-7150.

57. Alvarez-Erviti, L.; Seow, Y.; Yin, H.; Betts, C.; Lakhal, S.; Wood, M. J. J. N. b., Delivery of siRNA to the mouse brain by systemic injection of targeted exosomes. **2011,** *29* (4), 341-345.

58. Lai, C. P.; Mardini, O.; Ericsson, M.; Prabhakar, S.; Maguire, C. A.; Chen, J. W.; Tannous, B. A.; Breakefield, X. O. J. A. n., Dynamic biodistribution of extracellular vesicles in vivo using a multimodal imaging reporter. **2014,** *8* (1), 483-494.

59. Betzer, O.; Perets, N.; Angel, A.; Motiei, M.; Sadan, T.; Yadid, G.; Offen, D.; Popovtzer, R., In vivo neuroimaging of exosomes using gold nanoparticles. *ACS nano* **2017,** *11* (11), 10883-10893.

60. Egan, P. F. J. M., Integrated design approaches for 3D printed tissue scaffolds: Review and outlook. **2019,** *12* (15), 2355.

61. Arabnejad, S.; Johnston, R. B.; Pura, J. A.; Singh, B.; Tanzer, M.; Pasini, D. J. A. b., High-strength porous biomaterials for bone replacement: A strategy to assess the interplay between cell morphology, mechanical properties, bone ingrowth and manufacturing constraints. **2016,** *30*, 345-356.

62. Kačarević, Ž. P.; Rider, P. M.; Alkildani, S.; Retnasingh, S.; Smeets, R.; Jung, O.; Ivanišević, Z.; Barbeck, M. J. M., An introduction to 3D bioprinting: possibilities, challenges and future aspects. **2018,** *11* (11), 2199.

63. Egan, P. F.; Gonella, V. C.; Engensperger, M.; Ferguson, S. J.; Shea, K. J. P. o., Computationally designed lattices with tuned properties for tissue engineering using 3D printing. **2017,** *12* (8), e0182902.

64. Lacroix, D.; Planell, J. A.; Prendergast, P. J. J. P. T. o. t. R. S. A. M., Physical; Sciences, E., Computer-aided design and finite-element modelling of biomaterial scaffolds for bone tissue engineering. **2009,** *367* (1895), 1993-2009.

65. Egan, P.; Sinko, R.; LeDuc, P. R.; Keten, S. J. N. c., The role of mechanics in biological and bio-inspired systems. **2015,** *6*, 7418.

66. Egan, P.; Cagan, J.; Schunn, C.; Chiu, F.; Moore, J.; LeDuc, P. J. J. o. M. D., The D3 methodology: bridging science and design for bio-based product development. **2016,** *138* (8).

67. Kang, H.; Hollister, S. J.; La Marca, F.; Park, P.; Lin, C.-Y. J. J. o. b. e., Porous biodegradable lumbar interbody fusion cage design and fabrication using integrated global-local topology optimization with laser sintering. **2013,** *135* (10).

68. Hollister, S. J.; Flanagan, C. L.; Zopf, D. A.; Morrison, R. J.; Nasser, H.; Patel, J. J.; Ebramzadeh, E.; Sangiorgio, S. N.; Wheeler, M. B.; Green, G. E. J. A. o. b. e., Design control for clinical translation of 3D printed modular scaffolds. **2015,** *43* (3), 774-786.

69. Egan, P. F.; Bauer, I.; Shea, K.; Ferguson, S. J. J. J. o. M. D., Mechanics of three-dimensional printed lattices for biomedical devices. **2019,** *141* (3).

70. Guyot, Y.; Papantoniou, I.; Luyten, F.; Geris, L. J. B.; mechanobiology, m. i., Coupling curvature-dependent and shear stress-stimulated neotissue growth in dynamic bioreactor cultures: a 3D computational model of a complete scaffold. **2016,** *15* (1), 169-180.

71. Chen, T.-H.; Ghayor, C.; Siegenthaler, B.; Schuler, F.; Rüegg, J.; De Wild, M.; Weber, F. E. J. T. E. P. A., Lattice microarchitecture for bone tissue engineering from calcium phosphate compared to titanium. **2018,** *24* (19-20), 1554-1561.

72. Habib, F. N.; Nikzad, M.; Masood, S. H.; Saifullah, A. B. M. J. D. P.; Manufacturing, A., Design and development of scaffolds for tissue engineering using three-dimensional printing for bio-based applications. **2016,** *3* (2), 119-127.

73. Feng, B.; Jinkang, Z.; Zhen, W.; Jianxi, L.; Jiang, C.; Jian, L.; Guolin, M.; Xin, D. J. B. M., The effect of pore size on tissue ingrowth and neovascularization in porous bioceramics of controlled architecture in vivo. **2011,** *6* (1), 015007.

74. Nikolova, M. P.; Chavali, M. S., Recent advances in biomaterials for 3D scaffolds: A review. *Bioactive materials* **2019,** *4*, 271-292.

75. Jimi, E. H., S.; Osawa, K.; Tearashita, M.; Kitamura, C.;, Bone regeneration: current concepts and future directions. *International Journal of Dentistry* **2011**.

76. Stevens, M. M., Biomaterials for bone tissue engineering. *Materials today* **2008,** *11* (5), 18-25.

77. Holdsworth, D. W.; Thornton, M. M., Micro-CT in small animal and specimen imaging. *Trends in Biotechnology* **2002,** *20* (8), S34-S39.

78. Ker, E. D.; Nain, A. S.; Weiss, L. E.; Wang, J.; Suhan, J.; Amon, C. H.; Campbell, P. G. J. B., Bioprinting of growth factors onto aligned sub-micron fibrous scaffolds for simultaneous control of cell differentiation and alignment. **2011,** *32* (32), 8097-8107.

79. Li, P.; Jiang, W.; Yan, J.; Hu, K.; Han, Z.; Wang, B.; Zhao, Y.; Cui, G.; Wang, Z.; Mao, K. J. J. o. B. M. R. P. A., A novel 3D printed cage with microporous structure and in vivo fusion function. **2019,** *107* (7), 1386-1392.

80. Bobe, K.; Willbold, E.; Morgenthal, I.; Andersen, O.; Studnitzky, T.; Nellesen, J.; Tillmann, W.; Vogt, C.; Vano, K.; Witte, F. J. A. b., In vitro and in vivo evaluation of

biodegradable, open-porous scaffolds made of sintered magnesium W4 short fibres. **2013,** *9* (10), 8611-8623.

81. Komlev, V. S.; Popov, V. K.; Mironov, A. V.; Fedotov, A. Y.; Teterina, A. Y.; Smirnov, I. V.; Bozo, I. Y.; Rybko, V. A.; Deev, R. V. J. F. i. b.; biotechnology, 3D printing of octacalcium phosphate bone substitutes. **2015,** *3*, 81.

82. Pietak, A. M.; Reid, J. W.; Stott, M. J.; Sayer, M. J. B., Silicon substitution in the calcium phosphate bioceramics. **2007,** *28* (28), 4023-4032.

83. Pertici, V.; Amendola, J.; Laurin, J.; Gigmes, D.; Madaschi, L.; Carelli, S.; Marqueste, T.; Gorio, A.; Decherchi, P., The use of poly (N-[2-hydroxypropyl]-methacrylamide) hydrogel to repair a T10 spinal cord hemisection in rat: a behavioural, electrophysiological and anatomical examination. **2013**.

84. Valdes-Sánchez, T.; Rodriguez-Jimenez, F. J.; García-Cruz, D. M.; Escobar-Ivirico, J. L.; Alastrue-Agudo, A.; Erceg, S.; Monleón, M.; Moreno-Manzano, V. J. J. o. t. e.; medicine, r., Methacrylate-endcapped caprolactone and FM19G11 provide a proper niche for spinal cord-derived neural cells. **2015,** *9* (6), 734-739.

85. Xie, M.; Wang, L.; Ge, J.; Guo, B.; Ma, P. X. J. A. a. m.; interfaces, Strong electroactive biodegradable shape memory polymer networks based on star-shaped polylactide and aniline trimer for bone tissue engineering. **2015,** *7* (12), 6772-6781.

86. Wang, W.; Yeung, K. W. J. B. M., Bone grafts and biomaterials substitutes for bone defect repair: A review. **2017,** *2* (4), 224-247.

87. Li, W.; Yang, J.; Luo, L.; Jiang, M.; Qin, B.; Yin, H.; Zhu, C.; Yuan, X.; Zhang, J.; Luo, Z., Targeting photodynamic and photothermal therapy to the endoplasmic reticulum enhances immunogenic cancer cell death. *Nature communications* **2019,** *10* (1), 1-16.

88. Weissleder, R. J. N. b., A clearer vision for in vivo imaging. **2001,** *19* (4), 316-317.

89. Braun, C. L.; Smirnov, S. N. J. J. o. C. E., Why is water blue? **1993,** *70* (8), 612.

90. GRAHAM, E. G.; MACNEILL, C. M.; LEVI-POLYACHENKO, N. H. J. N. L., Review of metal, carbon and polymer nanoparticles for infrared photothermal therapy. **2013,** *3* (03), 1330002.

91. Gu, Q.; Zhao, H.; Xu, B.; Jiang, X.; Lv, J. J. N.; Letters, N., Photothermal modeling of plasmonic nanostructures: a review. **2017,** *9* (5), 599-608.

92. Sun, Y.; Wiley, B.; Li, Z.-Y.; Xia, Y. J. J. o. t. A. C. S., Synthesis and optical properties of nanorattles and multiple-walled nanoshells/nanotubes made of metal alloys. **2004,** *126* (30), 9399-9406.

93. Skrabalak, S. E.; Chen, J.; Au, L.; Lu, X.; Li, X.; Xia, Y. J. A. M., Gold nanocages for biomedical applications. **2007,** *19* (20), 3177-3184.

94. Chen, J.; Wang, D.; Xi, J.; Au, L.; Siekkinen, A.; Warsen, A.; Li, Z.-Y.; Zhang, H.; Xia, Y.; Li, X. J. N. l., Immuno gold nanocages with tailored optical properties for targeted photothermal destruction of cancer cells. **2007,** *7* (5), 1318-1322.

95. Cheng, F.-Y.; Chen, C.-T.; Yeh, C.-S. J. N., Comparative efficiencies of photothermal destruction of malignant cells using antibody-coated silica@ Au nanoshells, hollow Au/Ag nanospheres and Au nanorods. **2009,** *20* (42), 425104.

96. Yang, P.; Xu, Q. Z.; Jin, S. Y.; Lu, Y.; Zhao, Y.; Yu, S. H. J. C. A. E. J., Synthesis of multifunctional Ag@ Au@ phenol formaldehyde resin particles loaded with folic acids for photothermal therapy. **2012,** *18* (30), 9294-9299.

97. Huang, X.; Kang, B.; Qian, W.; Mackey, M. A.; Chen, P. C.; Oyelere, A. K.; El-Sayed, I. H.; El-Sayed, M. A. J. J. o. b. o., Comparative study of photothermolysis of cancer cells

with nuclear-targeted or cytoplasm-targeted gold nanospheres: continuous wave or pulsed lasers. **2010,** *15* (5), 058002.

98. Shen, J.; Wang, S.; Zhang, Y. J.; Kappil, M.; Wu, H. C.; Kibriya, M. G.; Wang, Q.; Jasmine, F.; Ahsan, H.; Lee, P. H. J. H., Genome-wide DNA methylation profiles in hepatocellular carcinoma. **2012,** *55* (6), 1799-1808.

99. Kuo, W.-S.; Chang, Y.-T.; Cho, K.-C.; Chiu, K.-C.; Lien, C.-H.; Yeh, C.-S.; Chen, S.-J. J. B., Gold nanomaterials conjugated with indocyanine green for dual-modality photodynamic and photothermal therapy. **2012,** *33* (11), 3270-3278.

100. Kumar, P. S.; Pastoriza-Santos, I.; Rodriguez-Gonzalez, B.; De Abajo, F. J. G.; Liz-Marzán, L. M. J. N., High-yield synthesis and optical response of gold nanostars. **2007,** *19* (1), 015606.

101. Wu, X.; Ming, T.; Wang, X.; Wang, P.; Wang, J.; Chen, J. J. A. n., High-photoluminescence-yield gold nanocubes: for cell imaging and photothermal therapy. **2010,** *4* (1), 113-120.

102. Kirui, D. K.; Rey, D. A.; Batt, C. A. J. N., Gold hybrid nanoparticles for targeted phototherapy and cancer imaging. **2010,** *21* (10), 105105.

103. Zhao, Z.; Huang, Y.; Shi, S.; Tang, S.; Li, D.; Chen, X. J. N., Cancer therapy improvement with mesoporous silica nanoparticles combining photodynamic and photothermal therapy. **2014,** *25* (28), 285701.

104. Chen, C.-L.; Kuo, L.-R.; Lee, S.-Y.; Hwu, Y.-K.; Chou, S.-W.; Chen, C.-C.; Chang, F.-H.; Lin, K.-H.; Tsai, D.-H.; Chen, Y.-Y. J. B., Photothermal cancer therapy via femtosecond-laser-excited FePt nanoparticles. **2013,** *34* (4), 1128-1134.

105. Luther, J. M.; Jain, P. K.; Ewers, T.; Alivisatos, A. P. J. N. m., Localized surface plasmon resonances arising from free carriers in doped quantum dots. **2011,** *10* (5), 361-366.

106. Yang, K.; Zhang, S.; Zhang, G.; Sun, X.; Lee, S.-T.; Liu, Z. J. N. l., Graphene in mice: ultrahigh in vivo tumor uptake and efficient photothermal therapy. **2010,** *10* (9), 3318-3323.

107. Xie, J.; Ahmad, M. N.; Bai, H.; Li, H.; Yang, W. J. S. C. C., Concentration and temperature controlled oxidation and cutting of single-walled carbon nanotubes by ammonium persulfate. **2010,** *53* (9), 2026-2032.

108. Wang, J.; Qiu, J. J. C. R. F., A review of organic nanomaterials in photothermal cancer therapy. **2016,** *2* (1), 67-84.

109. Yuan, A.; Wu, J.; Tang, X.; Zhao, L.; Xu, F.; Hu, Y. J. J. o. p. s., Application of near-infrared dyes for tumor imaging, photothermal, and photodynamic therapies. **2013,** *102* (1), 6-28.

110. Zhou, Y.; Pei, W.; Zhang, X.; Chen, W.; Wu, J.; Yao, C.; Huang, L.; Zhang, H.; Huang, W.; Loo, J. S. C. J. B., A cyanine-modified upconversion nanoprobe for NIR-excited imaging of endogenous hydrogen peroxide signaling in vivo. **2015,** *54*, 34-43.

111. Zhao, C.; Rehman, F. U.; Yang, Y.; Li, X.; Zhang, D.; Jiang, H.; Selke, M.; Wang, X.; Liu, C. J. S. r., Bio-imaging and photodynamic therapy with tetra sulphonatophenyl porphyrin (TSPP)-TiO 2 nanowhiskers: new approaches in rheumatoid arthritis theranostics. **2015,** *5*, 11518.

112. MacDonald, T. D.; Liu, T. W.; Zheng, G. J. A. C. I. E., An MRI-sensitive, non-photobleachable porphysome photothermal agent. **2014,** *53* (27), 6956-6959.

113. Yang, J.; Choi, J.; Bang, D.; Kim, E.; Lim, E. K.; Park, H.; Suh, J. S.; Lee, K.; Yoo, K. H.; Kim, E. K. J. A. C. I. E., Convertible organic nanoparticles for near-infrared photothermal ablation of cancer cells. **2011,** *50* (2), 441-444.

114. Mishra, A.; Behera, R. K.; Behera, P. K.; Mishra, B. K.; Behera, G. B. J. C. r., Cyanines during the 1990s: a review. **2000,** *100* (6), 1973-2012.

115. Volkova, K. D.; Kovalska, V. B.; Tatarets, A. L.; Patsenker, L. D.; Kryvorotenko, D. V.; Yarmoluk, S. M. J. D.; Pigments, Spectroscopic study of squaraines as protein-sensitive fluorescent dyes. **2007,** *72* (3), 285-292.

116. de la Torre, G.; Claessens, C. G.; Torres, T. J. C. c., Phthalocyanines: old dyes, new materials. Putting color in nanotechnology. **2007,** (20), 2000-2015.

117. Killoran, J.; McDonnell, S. O.; Gallagher, J. F.; O'Shea, D. F. J. N. J. o. C., A substituted BF 2-chelated tetraarylazadipyrromethene as an intrinsic dual chemosensor in the 650–850 nm spectral range. **2008,** *32* (3), 483-489.

118. Oldenburg, S.; Averitt, R.; Westcott, S.; Halas, N. J. C. P. L., Nanoengineering of optical resonances. **1998,** *288* (2-4), 243-247.

119. Sun, Y.; Mayers, B. T.; Xia, Y. J. N. L., Template-engaged replacement reaction: a one-step approach to the large-scale synthesis of metal nanostructures with hollow interiors. **2002,** *2* (5), 481-485.

120. Zhou, Z.; Wang, Y.; Yan, Y.; Zhang, Q.; Cheng, Y., Dendrimer-templated ultrasmall and multifunctional photothermal agents for efficient tumor ablation. *ACS nano* **2016,** *10* (4), 4863-4872.

121. Zhou, Z.; Hu, K.; Ma, R.; Yan, Y.; Ni, B.; Zhang, Y.; Wen, L.; Zhang, Q.; Cheng, Y., Dendritic platinum–copper alloy nanoparticles as theranostic agents for multimodal imaging and combined chemophotothermal therapy. *Advanced Functional Materials* **2016,** *26* (33), 5971-5978.

122. Zhou, F.; Da, X.; Ou, Z.; Wu, B.; Resasco, D. E.; Chen, W. R. J. J. o. b. o., Cancer photothermal therapy in the near-infrared region by using single-walled carbon nanotubes. **2009,** *14* (2), 021009.

123. Doughty, A. C.; Hoover, A. R.; Layton, E.; Murray, C. K.; Howard, E. W.; Chen, W. R. J. M., Nanomaterial applications in photothermal therapy for cancer. **2019,** *12* (5), 779.

124. Wang, X.; Omar, O.; Vazirisani, F.; Thomsen, P.; Ekström, K., Mesenchymal stem cell-derived exosomes have altered microRNA profiles and induce osteogenic differentiation depending on the stage of differentiation. *PLoS One* **2018,** *13* (2).

125. Ker, E. D.; Nain, A. S.; Weiss, L. E.; Wang, J.; Suhan, J.; Amon, C. H.; Campbell, P. G., Bioprinting of growth factors onto aligned sub-micron fibrous scaffolds for simultaneous control of cell differentiation and alignment. *Biomaterials* **2011,** *32* (32), 8097-8107.

126. Li, P.; Jiang, W.; Yan, J.; Hu, K.; Han, Z.; Wang, B.; Zhao, Y.; Cui, G.; Wang, Z.; Mao, K., A novel 3D printed cage with microporous structure and in vivo fusion function. *Journal of Biomedical Materials Research Part A* **2019,** *107* (7), 1386-1392.

127. Luan, X.; Sansanaphongpricha, K.; Myers, I.; Chen, H.; Yuan, H.; Sun, D., Engineering exosomes as refined biological nanoplatforms for drug delivery. *Acta Pharmacologica Sinica* **2017,** *38* (6), 754-763.

128. Wang, C.; Cai, X.; Zhang, J.; Wang, X.; Wang, Y.; Ge, H.; Yan, W.; Huang, Q.; Xiao, J.; Zhang, Q., Trifolium-like platinum nanoparticle-mediated photothermal therapy inhibits tumor growth and osteolysis in a bone metastasis model. *Small* **2015,** *11* (17), 2080-2086.

129. Dimitriou, R.; Jones, E.; McGonagle, D.; Giannoudis, P. V., Bone regeneration: current concepts and future directions. *BMC medicine* **2011,** *9* (1), 66.

130. Yoo, S. Y.; Merzlyak, A.; Lee, S.-W., Synthetic phage for tissue regeneration. *Mediators of inflammation* **2014,** *2014*.

131. Chocholata, P.; Kulda, V.; Babuska, V. J. M., Fabrication of scaffolds for bone-tissue regeneration. **2019,** *12* (4), 568.

132. Shi, Y.; Hu, G.; Su, J.; Li, W.; Chen, Q.; Shou, P.; Xu, C.; Chen, X.; Huang, Y.; Zhu, Z. J. C. r., Mesenchymal stem cells: a new strategy for immunosuppression and tissue repair. **2010,** *20* (5), 510.

133. Zhao, T.; Zhang, Z.-N.; Rong, Z.; Xu, Y. J. N., Immunogenicity of induced pluripotent stem cells. **2011,** *474* (7350), 212.

134. Taran, R.; Mamidi, M. K.; Singh, G.; Dutta, S.; Parhar, I. S.; John, J. P.; Bhonde, R.; Pal, R.; Das, A. K. J. J. o. b., In vitro and in vivo neurogenic potential of mesenchymal stem cells isolated from different sources. **2014,** *39* (1), 157-169.

135. Pittenger, M. F.; Mackay, A. M.; Beck, S. C.; Jaiswal, R. K.; Douglas, R.; Mosca, J. D.; Moorman, M. A.; Simonetti, D. W.; Craig, S.; Marshak, D. R. J. s., Multilineage potential of adult human mesenchymal stem cells. **1999,** *284* (5411), 143-147.

136. Shi, Y.; Hu, G.; Su, J.; Li, W.; Chen, Q.; Shou, P.; Xu, C.; Chen, X.; Huang, Y.; Zhu, Z., Mesenchymal stem cells: a new strategy for immunosuppression and tissue repair. *Cell research* **2010,** *20* (5), 510-518.

137. Zhao, T.; Zhang, Z.-N.; Rong, Z.; Xu, Y., Immunogenicity of induced pluripotent stem cells. *Nature* **2011,** *474* (7350), 212-215.

138. Taran, R.; Mamidi, M. K.; Singh, G.; Dutta, S.; Parhar, I. S.; John, J. P.; Bhonde, R.; Pal, R.; Das, A. K., In vitro and in vivo neurogenic potential of mesenchymal stem cells isolated from different sources. *Journal of biosciences* **2014,** *39* (1), 157-169.

139. Konala, V. B. R.; Mamidi, M. K.; Bhonde, R.; Das, A. K.; Pochampally, R.; Pal, R., The current landscape of the mesenchymal stromal cell secretome: a new paradigm for cell-free regeneration. *Cytotherapy* **2016,** *18* (1), 13-24.

140. Vishnubhatla, I.; Corteling, R.; Stevanato, L.; Hicks, C.; Sinden, J., The development of stem cell-derived exosomes as a cell-free regenerative medicine. *Journal of Circulating Biomarkers* **2014,** *3*, 2.

141. Deville, S.; Saiz, E.; Tomsia, A. P., Freeze casting of hydroxyapatite scaffolds for bone tissue engineering. *Biomaterials* **2006,** *27* (32), 5480-5489.

142. Tamaddon, M.; Samizadeh, S.; Wang, L.; Blunn, G.; Liu, C., Intrinsic osteoinductivity of porous titanium scaffold for bone tissue engineering. *International journal of biomaterials* **2017,** *2017*.

143. Yeo, R. W. Y.; Lai, R. C.; Tan, K. H.; Lim, S. K., Exosome: a novel and safer therapeutic refinement of mesenchymal stem cell. *Exosomes and Microvesicles* **2013,** *1*, 7.

144. Vlassov, A. V.; Magdaleno, S.; Setterquist, R.; Conrad, R., Exosomes: current knowledge of their composition, biological functions, and diagnostic and therapeutic potentials. *Biochimica et Biophysica Acta (BBA)-General Subjects* **2012,** *1820* (7), 940-948.

145. Valadi, H.; Ekström, K.; Bossios, A.; Sjöstrand, M.; Lee, J. J.; Lötvall, J. O., Exosome-mediated transfer of mRNAs and microRNAs is a novel mechanism of genetic exchange between cells. *Nature cell biology* **2007,** *9* (6), 654.

146. Baglio, S. R.; Pegtel, D. M.; Baldini, N., Mesenchymal stem cell secreted vesicles provide novel opportunities in (stem) cell-free therapy. *Frontiers in physiology* **2012,** *3*.

147. Pohler, O. E., Unalloyed titanium for implants in bone surgery. *Injury* **2000,** *31*, D7-D13.

148. Jansen, J.; Von Recum, A.; Van Der Waerden, J.; De Groot, K., Soft tissue response to different types of sintered metal fibre-web materials. *Biomaterials* **1992,** *13* (13), 959-968.

149. Chang, Y.-S.; Oka, M.; Kobayashi, M.; Gu, H.-O.; Li, Z.-L.; Nakamura, T.; Ikada, Y., Significance of interstitial bone ingrowth under load-bearing conditions: a comparison between solid and porous implant materials. *Biomaterials* **1996,** *17* (11), 1141-1148.

150. Savina, A.; Vidal, M.; Colombo, M. I. J. J. o. c. s., The exosome pathway in K562 cells is regulated by Rab11. **2002,** *115* (12), 2505-2515.

151. Gupta, S.; Knowlton, A. A. J. A. J. o. P.-H.; Physiology, C., HSP60 trafficking in adult cardiac myocytes: role of the exosomal pathway. **2007,** *292* (6), H3052-H3056.

152. Fang, B.; Wan, Y.-Z.; Tang, T.-T.; Gao, C.; Dai, K.-R., Proliferation and osteoblastic differentiation of human bone marrow stromal cells on hydroxyapatite/bacterial cellulose nanocomposite scaffolds. *Tissue Engineering Part A* **2009,** *15* (5), 1091-1098.

153. Gilbert, L.; He, X.; Farmer, P.; Rubin, J.; Drissi, H.; Van Wijnen, A. J.; Lian, J. B.; Stein, G. S.; Nanes, M. S., Expression of the osteoblast differentiation factor RUNX2 (Cbfa1/AML3/Pebp2αA) is inhibited by tumor necrosis factor-α. *Journal of Biological Chemistry* **2002,** *277* (4), 2695-2701.

154. Wang, J.; Wang, L.; Li, X.; Mao, C., Virus activated artificial ECM induces the osteoblastic differentiation of mesenchymal stem cells without osteogenic supplements. *Scientific reports* **2013,** *3*.

155. Zhang, J.; Qian, X.; Ning, H.; Eickhoff, C. S.; Hoft, D. F.; Liu, J. J. T. J. o. I., Transcriptional suppression of IL-27 production by Mycobacterium tuberculosis-activated p38 MAPK via inhibition of AP-1 binding. **2011,** *186* (10), 5885-5895.

156. Anderson, J. M.; Rodriguez, A.; Chang, D. T. In *Foreign body reaction to biomaterials*, Seminars in immunology, Elsevier: 2008; pp 86-100.

157. Di Fiore, P. P.; De Camilli, P., Endocytosis and signaling: an inseparable partnership. *Cell* **2001,** *106* (1), 1-4.

158. Viti, F.; Landini, M.; Mezzelani, A.; Petecchia, L.; Milanesi, L.; Scaglione, S. J. P. o., Osteogenic differentiation of MSC through calcium signaling activation: Transcriptomics and functional analysis. **2016,** *11* (2), e0148173.

159. Fang, S.; Deng, Y.; Gu, P.; Fan, X. J. I. j. o. m. s., MicroRNAs regulate bone development and regeneration. **2015,** *16* (4), 8227-8253.

160. Sun, Y.; Xu, J.; Xu, L.; Zhang, J.; Chan, K.; Pan, X.; Li, G., MiR-503 promotes bone formation in distraction osteogenesis through suppressing Smurf1 expression. *Scientific reports* **2017,** *7* (1), 409.

161. Bertero, T.; Gastaldi, C.; Bourget-Ponzio, I.; Imbert, V.; Loubat, A.; Selva, E.; Busca, R.; Mari, B.; Hofman, P.; Barbry, P., miR-483-3p controls proliferation in wounded epithelial cells. *The FASEB Journal* **2011,** *25* (9), 3092-3105.

162. Xiao, Y.; Guo, Q.; Jiang, T. J.; Yuan, Y.; Yang, L.; Wang, G. W.; Xiao, W. F. J. M. m. r., miR-483-3p regulates osteogenic differentiation of bone marrow mesenchymal stem cells by targeting STAT1. **2019,** *20* (5), 4558-4566.

163. Xiao, W.; Gu, X.; Hu, B.; Liu, X.; Zi, Y.; Li, M. J. C.; Biology, M., Role of microRNA-129-5p in osteoblast differentiation from bone marrow mesenchymal stem cells. **2016,** *62* (3), 95-99.

164. Fu, X.; Liu, M.; Qu, S.; Ma, J.; Zhang, Y.; Shi, T.; Wen, H.; Yang, Y.; Wang, S.; Wang, J. J. J. o. E.; Research, C. C., Exosomal microRNA-32-5p induces multidrug resistance in hepatocellular carcinoma via the PI3K/Akt pathway. **2018,** *37* (1), 52.

165. Tang, Y.; Pan, J.; Huang, S.; Peng, X.; Zou, X.; Luo, Y.; Ren, D.; Zhang, X.; Li, R.; He, P. J. J. o. E.; Research, C. C., Downregulation of miR-133a-3p promotes prostate cancer bone metastasis via activating PI3K/AKT signaling. **2018,** *37* (1), 160.

166. Wang, Y.; Li, W.; Zang, X.; Chen, N.; Liu, T.; Tsonis, P. A.; Huang, Y. J. I. o.; science, v., MicroRNA-204-5p regulates epithelial-to-mesenchymal transition during human posterior capsule opacification by targeting SMAD4. **2013,** *54* (1), 323-332.

167. Zhang, S.; Chen, X.; Hu, Y.; Wu, J.; Cao, Q.; Chen, S.; Gao, Y., All-trans retinoic acid modulates Wnt3A-induced osteogenic differentiation of mesenchymal stem cells via activating the PI3K/AKT/GSK3β signalling pathway. *Molecular and cellular endocrinology* **2016,** *422*, 243-253.

168. Rodríguez-Carballo, E.; Gámez, B.; Ventura, F., p38 MAPK signaling in osteoblast differentiation. *Frontiers in cell and developmental biology* **2016,** *4*, 40.

169. Thouverey, C.; Caverzasio, J., Focus on the p38 MAPK signaling pathway in bone development and maintenance. *BoneKEy reports* **2015,** *4*.

170. Majidinia, M.; Sadeghpour, A.; Yousefi, B., The roles of signaling pathways in bone repair and regeneration. *Journal of cellular physiology* **2018,** *233* (4), 2937-2948.

171. Xie, Q.; Wang, Z.; Bi, X.; Zhou, H.; Wang, Y.; Gu, P.; Fan, X. J. B.; communications, b. r., Effects of miR-31 on the osteogenesis of human mesenchymal stem cells. **2014,** *446* (1), 98-104.

172. Bakhshandeh, B.; Hafizi, M.; Ghaemi, N.; Soleimani, M. J. B. l., Down-regulation of miRNA-221 triggers osteogenic differentiation in human stem cells. **2012,** *34* (8), 1579-1587.

173. Trohatou, O.; Zagoura, D.; Bitsika, V.; Pappa, K. I.; Antsaklis, A.; Anagnou, N. P.; Roubelakis, M. G. J. S. c. t. m., Sox2 suppression by miR-21 governs human mesenchymal stem cell properties. **2014,** *3* (1), 54-68.

174. Meng, Y. B.; Li, X.; Li, Z. Y.; Zhao, J.; Yuan, X. B.; Ren, Y.; Cui, Z. D.; Liu, Y. D.; Yang, X. J. J. J. o. O. R., microRNA-21 promotes osteogenic differentiation of mesenchymal stem cells by the PI3K/β-catenin pathway. **2015,** *33* (7), 957-964.

175. Maggiano, I. S.; Maggiano, C. M.; Clement, J. G.; Thomas, C. D. L.; Carter, Y.; Cooper, D. M., Three-dimensional reconstruction of Haversian systems in human cortical bone using synchrotron radiation-based micro-CT: morphology and quantification of branching and transverse connections across age. *Journal of anatomy* **2016,** *228* (5), 719-732.

176. Hong, P.; Yang, H.; Wu, Y.; Li, K.; Tang, Z., The functions and clinical application potential of exosomes derived from adipose mesenchymal stem cells: a comprehensive review. *Stem cell research & therapy* **2019,** *10* (1), 242.

177. Bobe, K.; Willbold, E.; Morgenthal, I.; Andersen, O.; Studnitzky, T.; Nellesen, J.; Tillmann, W.; Vogt, C.; Vano, K.; Witte, F., In vitro and in vivo evaluation of biodegradable, open-porous scaffolds made of sintered magnesium W4 short fibres. *Acta biomaterialia* **2013,** *9* (10), 8611-8623.

178. Li, W.; Liu, Y.; Zhang, P.; Tang, Y.; Zhou, M.; Jiang, W.; Zhang, X.; Wu, G.; Zhou, Y., Tissue-engineered bone immobilized with human adipose stem cells-derived exosomes promotes bone regeneration. *ACS applied materials & interfaces* **2018,** *10* (6), 5240-5254.

179. Wei, F.; Li, M.; Crawford, R.; Zhou, Y.; Xiao, Y., Exosome-integrated titanium oxide nanotubes for targeted bone regeneration. *Acta biomaterialia* **2019,** *86*, 480-492.

180. Heron, M. P., Deaths: leading causes for 2016. **2018**.

181. Gobin, A. M.; Lee, M. H.; Halas, N. J.; James, W. D.; Drezek, R. A.; West, J. L., Near-infrared resonant nanoshells for combined optical imaging and photothermal cancer therapy. *Nano letters* **2007,** *7* (7), 1929-1934.

182. Wang, Y.; Black, K. C.; Luehmann, H.; Li, W.; Zhang, Y.; Cai, X.; Wan, D.; Liu, S.-Y.; Li, M.; Kim, P., Comparison study of gold nanohexapods, nanorods, and nanocages for photothermal cancer treatment. *ACS nano* **2013,** *7* (3), 2068-2077.

183. Tang, S.; Chen, M.; Zheng, N., Multifunctional ultrasmall Pd nanosheets for enhanced near-infrared photothermal therapy and chemotherapy of cancer. *Nano Research* **2015,** *8* (1), 165-174.

184. Niemeyer, C. M., Nanoparticles, proteins, and nucleic acids: biotechnology meets materials science. *Angewandte Chemie International Edition* **2001,** *40* (22), 4128-4158.

185. Mahmoudi, M.; Sahraian, M. A.; Shokrgozar, M. A.; Laurent, S., Superparamagnetic iron oxide nanoparticles: promises for diagnosis and treatment of multiple sclerosis. *ACS chemical neuroscience* **2011,** *2* (3), 118-140.

186. Maier-Hauff, K.; Ulrich, F.; Nestler, D.; Niehoff, H.; Wust, P.; Thiesen, B.; Orawa, H.; Budach, V.; Jordan, A., Efficacy and safety of intratumoral thermotherapy using magnetic iron-oxide nanoparticles combined with external beam radiotherapy on patients with recurrent glioblastoma multiforme. *Journal of neuro-oncology* **2011,** *103* (2), 317-324.

187. Lee, J.-H.; Jang, J.-t.; Choi, J.-s.; Moon, S. H.; Noh, S.-h.; Kim, J.-w.; Kim, J.-G.; Kim, I.-S.; Park, K. I.; Cheon, J., Exchange-coupled magnetic nanoparticles for efficient heat induction. *Nature nanotechnology* **2011,** *6* (7), 418.

188. Wang, J.; Qiu, J., A review of organic nanomaterials in photothermal cancer therapy. *Cancer Res. Front* **2016,** *2* (1), 67-84.

189. Yang, K.; Xu, H.; Cheng, L.; Sun, C.; Wang, J.; Liu, Z., In vitro and in vivo near-infrared photothermal therapy of cancer using polypyrrole organic nanoparticles. *Advanced materials* **2012,** *24* (41), 5586-5592.

190. Hessel, C. M.; Pattani, V. P.; Rasch, M.; Panthani, M. G.; Koo, B.; Tunnell, J. W.; Korgel, B. A., Copper selenide nanocrystals for photothermal therapy. *Nano letters* **2011,** *11* (6), 2560-2566.

191. Seabra, A. B.; Paula, A. J.; de Lima, R.; Alves, O. L.; Duran, N., Nanotoxicity of graphene and graphene oxide. *Chemical research in toxicology* **2014,** *27* (2), 159-168.

192. Xu, L.; Cheng, L.; Wang, C.; Peng, R.; Liu, Z., Conjugated polymers for photothermal therapy of cancer. *Polymer Chemistry* **2014,** *5* (5), 1573-1580.

193. Yang, J.; Choi, J.; Bang, D.; Kim, E.; Lim, E. K.; Park, H.; Suh, J. S.; Lee, K.; Yoo, K. H.; Kim, E. K., Convertible organic nanoparticles for near-infrared photothermal ablation of cancer cells. *Angewandte Chemie International Edition* **2011,** *50* (2), 441-444.

194. Zha, Z.; Yue, X.; Ren, Q.; Dai, Z., Uniform polypyrrole nanoparticles with high photothermal conversion efficiency for photothermal ablation of cancer cells. *Advanced materials* **2013,** *25* (5), 777-782.

195. Xie, F.; Zhou, X.; Fang, M.; Li, H.; Su, P.; Tu, Y.; Zhang, L.; Zhou, F. J. A. S., Extracellular Vesicles in Cancer Immune Microenvironment and Cancer Immunotherapy. **2019**, 1901779.

196. Gao, X.; Ran, N.; Dong, X.; Zuo, B.; Yang, R.; Zhou, Q.; Moulton, H. M.; Seow, Y.; Yin, H., Anchor peptide captures, targets, and loads exosomes of diverse origins for diagnostics and therapy. *Science translational medicine* **2018,** *10* (444), eaat0195.

197. Qu, X.; Qiu, P.; Zhu, Y.; Yang, M.; Mao, C., Guiding nanomaterials to tumors for breast cancer precision medicine: from tumor-targeting small-molecule discovery to targeted nanodrug delivery. *NPG Asia materials* **2017,** *9* (12), e452.

198. Logozzi, M.; De Milito, A.; Lugini, L.; Borghi, M.; Calabro, L.; Spada, M.; Perdicchio, M.; Marino, M. L.; Federici, C.; Iessi, E., High levels of exosomes expressing CD63 and caveolin-1 in plasma of melanoma patients. *PloS one* **2009,** *4* (4), e5219.

199. Simpson, R. J.; Jensen, S. S.; Lim, J. W., Proteomic profiling of exosomes: current perspectives. *Proteomics* **2008,** *8* (19), 4083-4099.

200. Pols, M. S.; Klumperman, J., Trafficking and function of the tetraspanin CD63. *Experimental cell research* **2009,** *315* (9), 1584-1592.

201. Petersen, S. H.; Odintsova, E.; Haigh, T. A.; Rickinson, A. B.; Taylor, G. S.; Berditchevski, F., The role of tetraspanin CD63 in antigen presentation via MHC class II. *European journal of immunology* **2011,** *41* (9), 2556-2561.

202. McBride, J. D.; Rodriguez-Menocal, L.; Guzman, W.; Candanedo, A.; Garcia-Contreras, M.; Badiavas, E. V. J. S. c.; development, Bone marrow mesenchymal stem cell-derived CD63+ exosomes transport Wnt3a exteriorly and enhance dermal fibroblast proliferation, migration, and angiogenesis in vitro. **2017,** *26* (19), 1384-1398.

203. Qu, X.; Qiu, P.; Zhu, Y.; Yang, M.; Mao, C. J. N. A. m., Guiding nanomaterials to tumors for breast cancer precision medicine: from tumor-targeting small-molecule discovery to targeted nanodrug delivery. **2017,** *9* (12), e452.

204. Gonda, A.; Kabagwira, J.; Senthil, G. N.; Wall, N. R., Internalization of exosomes through receptor-mediated endocytosis. *Molecular Cancer Research* **2019,** *17* (2), 337-347.

205. Sun, D.; Zhuang, X.; Xiang, X.; Liu, Y.; Zhang, S.; Liu, C.; Barnes, S.; Grizzle, W.; Miller, D.; Zhang, H.-G., A novel nanoparticle drug delivery system: the anti-inflammatory activity of curcumin is enhanced when encapsulated in exosomes. *Molecular Therapy* **2010,** *18* (9), 1606-1614.

206. Yang, T.; Martin, P.; Fogarty, B.; Brown, A.; Schurman, K.; Phipps, R.; Yin, V. P.; Lockman, P.; Bai, S., Exosome delivered anticancer drugs across the blood-brain barrier for brain cancer therapy in Danio rerio. *Pharmaceutical research* **2015,** *32* (6), 2003-2014.

207. Qu, X.; Qiu, P.; Zhu, Y.; Yang, M.; Mao, C., Guiding nanomaterials to tumors for breast cancer precision medicine: from tumor-targeting small-molecule discovery to targeted nanodrug delivery. *NPG Asia materials* **2017,** *9* (12), e452-e452.

208. Liu, P.; Liu, W.; Wang, W. J.; Li, B. G.; Zhu, S., A Comprehensive Review on Controlled Synthesis of Long-Chain Branched Polyolefins: Part 1, Single Catalyst Systems. *Macromolecular Reaction Engineering* **2016,** *10* (3), 156-179.

209. Bae, Y. H.; Park, K., Targeted drug delivery to tumors: myths, reality and possibility. *Journal of controlled release* **2011,** *153* (3), 198.

210. GRAHAM, E. G.; MACNEILL, C. M.; LEVI-POLYACHENKO, N. H., Review of metal, carbon and polymer nanoparticles for infrared photothermal therapy. *Nano Life* **2013,** *3* (03), 1330002.

211. Sancho-Albero, M.; Navascués, N.; Mendoza, G.; Sebastián, V.; Arruebo, M.; Martin-Duque, P.; Santamaria, J., Exosome origin determines cell targeting and the transfer of therapeutic nanoparticles towards target cells. *Journal of nanobiotechnology* **2019,** *17* (1), 16.

Appendix: List of Copyrights and Permission

JOHN WILEY AND SONS LICENSE

TERMS AND CONDITIONS

Apr 27, 2020

This Agreement between University of Oklahoma -- Mengmeng Zhai ("You") and John Wiley and Sons ("John Wiley and Sons") consists of your license details and the terms and conditions provided by John Wiley and Sons and Copyright Clearance Center.

License Number: 4817250383202

License date: Apr 27, 2020

Licensed Content Publisher: John Wiley and Sons

Licensed Content Publication: Small

Licensed Content Title: Self-Assembly of Drug-Loaded Liposomes on Genetically Engineered Target-Recognizing M13 Phage: A Novel Nanocarrier for Targeted Drug Delivery

Licensed Content Author: Pascaline Ngweniform, Gopal Abbineni, Binrui Cao, et al

Licensed Content Date: Aug 26, 2009

Licensed Content Volume: 5

Licensed Content Issue: 17

Licensed Content Pages: 7

Type of use Dissertation/Thesis: Requestor type University/Academic

Format Electronic: Portion Figure/table

Number of figures/tables: 2

Will you be translating: No

Title: graduate student

Institution name: University of Oklahoma

Expected presentation date: May 2022

Portions: Figure 2

Requestor Location: University of Oklahoma,101 Stephenson Pkwy, NORMAN, OK 73019, United States

Attn: university of Oklahoma

Publisher Tax ID EU826007151

Annual Reviews, Inc. - License Terms and Conditions

Apr 27, 2020

This is a License Agreement between Mengmeng Zhai ("You") and Annual Reviews, Inc. ("Publisher") provided by Copyright Clearance Center ("CCC"). The license consists of your order details, the terms and conditions provided by Annual Reviews, Inc., and the CCC terms and conditions.

All payments must be made in full to CCC.

Order Date: 27-Apr-2020

Order license ID: 1031263-1

ISSN: 1530-8995

Type of Use: Republish in a thesis/dissertation

Publisher; ANNUAL REVIEWS

Portion: Chart/graph/table/figure

LICENSED CONTENT

Publication Title: Annual review of cell and developmental biology

Author/Editor: ANNUAL REVIEWS, INC.

Date: 12/31/1994

Language: English

Country: United States of America

Rightsholder: Annual Reviews, Inc.

Publication Type: e-Journal

URL: http://arjournals.annualreviews.org/loi/cellbio

REQUEST DETAILS

Portion Type: Chart/graph/table/figure

Number of charts / graphs / tables / figures requested: 1

Format (select all that apply): Electronic

Who will republish the content: Academic institution

Duration of Use: Life of current and all future editions

Lifetime Unit Quantity: Up to 499

Rights Requested: Main product and any product related to main product

Distribution: United States

Translation: Original language of publication

Copies for the disabled? No

Minor editing privileges? No

Incidental promotional use? No

NEW WORK DETAILS

Title: graduate student

Instructor name: Chuanbin Mao

Institution name: University of Oklahoma

Expected presentation date: 2022-05-08

ADDITIONAL DETAILS

Order reference number: N/A

The requesting person / organization to appear on the license: Mengmeng Zhai

REUSE CONTENT DETAILS

Title, description or numeric reference of the portion(s): exosome biogenesis

Editor of portion(s): N/A

Volume of serial or monograph: N/A

Page or page range of portion: 5-6

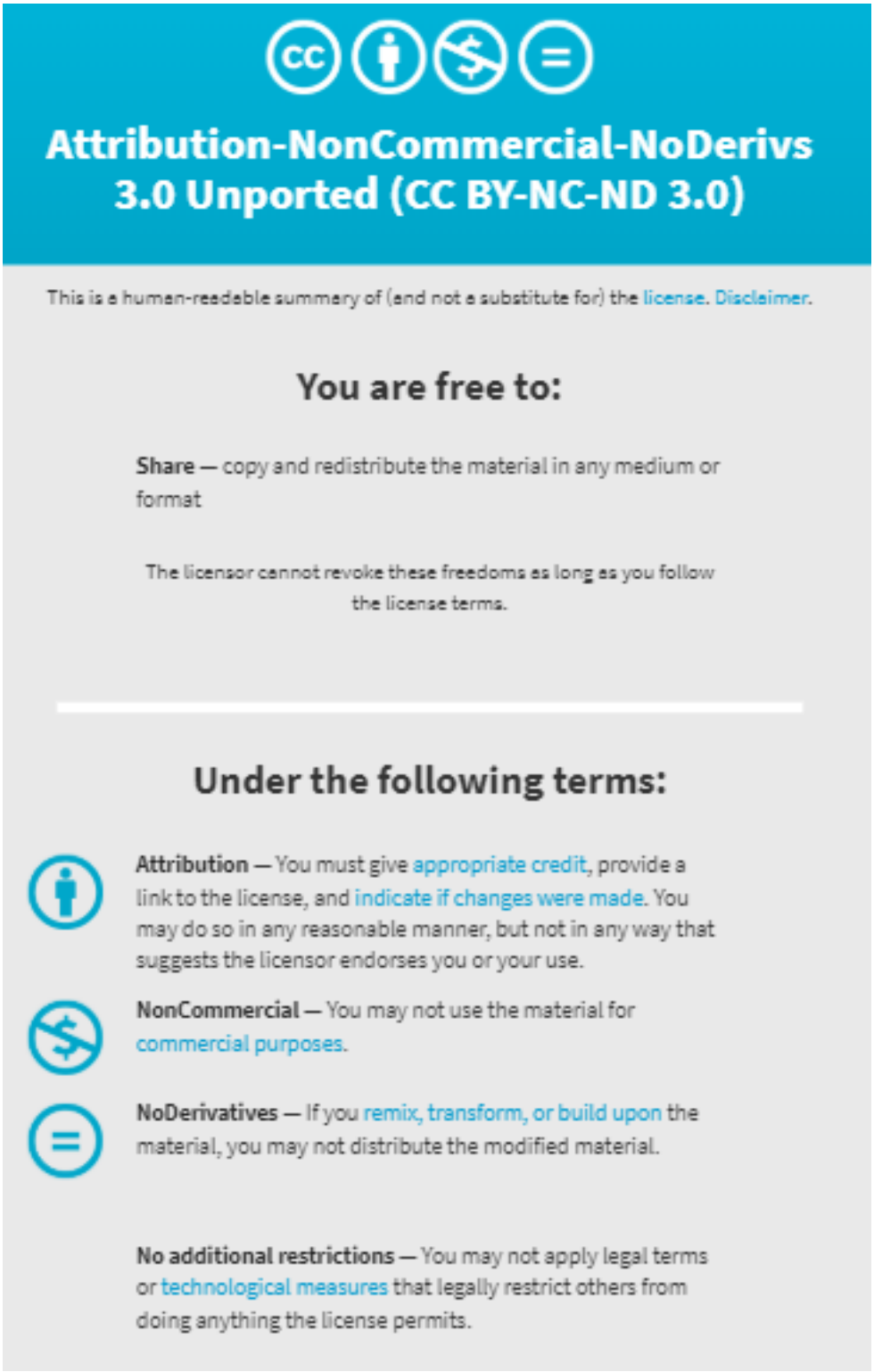
Title of the article/chapter the portion is from: N/A

Author of portion(s): ANNUAL REVIEWS, INC.

Issue, if republishing an article from a serial: N/A

Publication date of portion: 2020-04-27

Creative commons terms and conditions



Attribution-NonCommercial-NoDerivs 3.0 Unported (CC BY-NC-ND 3.0)

This is a human-readable summary of (and not a substitute for) the license. Disclaimer.

You are free to:

Share — copy and redistribute the material in any medium or format

The licensor cannot revoke these freedoms as long as you follow the license terms.

Under the following terms:

Attribution — You must give appropriate credit, provide a link to the license, and indicate if changes were made. You may do so in any reasonable manner, but not in any way that suggests the licensor endorses you or your use.

NonCommercial — You may not use the material for commercial purposes.

NoDerivatives — If you remix, transform, or build upon the material, you may not distribute the modified material.

No additional restrictions — You may not apply legal terms or technological measures that legally restrict others from doing anything the license permits.